SOL-GEL DERIVED NANOCOMPOSITES FOR BIOSENSOR DEVELOPMENT

PREPARATION AND CHARACTERIZATION OF PROTEIN-DOPED SOL-GEL DERIVED NANOCOMPOSITE FILMS FOR BIOSENSOR DEVELOPMENT

By

GILLIAN LOUISE GRACE GORING, B.Sc.H., M.Sc.

BSc. Honours Queen's University (Environmental Chemistry)

M.Sc. Queen's University

A Thesis

Submitted to the School of Graduate Studies

In Partial Fulfillment of the Requirements

For the Degree

Doctor of Philosophy.

McMaster University

Doctor of Philosophy (2007)
(Chemistry)

McMaster University
Hamilton, Ontario

Title: Preparation and Characterization of Biologically Doped Sol-Gel Derived Nanocomposite Films Suitable for Biosensor Development

Author: Gillian Louise Grace Goring B.Sc.H., M.Sc. (Queen's University)

Supervisor: Professor John D. Brennan

Number of Pages: xix, 172

ABSTRACT

The entrapment of biomolecules within TEOS-based sol-gel derived organic/inorganic nanocomposite materials has proven to be a viable platform for the development of biosensors and solid-phase biocatalysts. In this thesis, a series of organically modified silica materials were prepared by a two-step aqueous processing method that was suitable for biomolecule entrapment, and were formed as submicron thick films by dipcasting. Dispersed additives, such as polymers (Class I materials) and covalently bound additives, such as organically modified silanes (Class II materials), were used to modify the internal environment compared to the undoped matrices and to correlate the properties of entrapped enzymes.

The morphology of organically modified silica materials could be modified through the use of either separate or co-hydrolysis of the silane precursors, with the later method generating optically transparent materials. Fluorescence microscopy revealed chemical heterogeneity in materials that appeared to be homogeneous by brightfield or SEM.

Fluorescence emission studies of a solvatochromic dye entrapped within the film confirmed that the internal chemical environment of the films was strongly affected by doping with polymers and organosilanes. The films showed a rapid initial change in chemical properties owing to solvent evaporation, followed by a much slower evolution over several months owing to continued condensation reactions within the film.

A reagentless biosensor was designed based on co-entrapment of an enzyme and a fluorescently labeled polymer. The enzymes urease and lipase were selected for this

study as both catalyze reactions that alter the local pH. By co-entrapping pH sensitive fluorophores (SNARF-1 and fluorescein) bound to a high molecular weight polymer, it was possible to detect the analytes urea and glyceryl tributyrate using changes in the fluorescence intensity (fluorescein) or emission ratio (SNARF-1). By tuning the polarity of the matrix it was possible to optimize the sensitivity of the sensing film for both the polar and non-polar analyte.

ACKNOWLEDGEMENTS

The completion of a Ph.D thesis requires the support and contribution of a network of individuals. First and foremost, I must acknowledge my supervisor Dr. John D. Brennan who inspired me through the sharing of his invaluable insights and expertise, and for being so generous with his time. My two supervisory committee members, Dr. Harold D. H. Stöver and Dr. Brian E. McCarry, were also very supportive in their aid, patience and scientific knowledge.

I would also like to thank the members of the Brennan, McCarry, Stöver, and Dalnoki-Veress groups, as well as members of the BIMR, including many fourth year, summer and graduate students, who have made the experiments and the long hours spent in the lab more enjoyable. I would particularly like to mention past and present Brennanites including Tracey, Kulwinder, Donna, Adam, Hitesh, Yujing, Jai, Roger, Erica, Julie and Liang as well as Stacey, Lisa, Andrew, Mike, and Paul. Training, assistance and humour was provided by many of the BIMR staff including Andy Duft (AFM), Fred Pierce, and Dr. Steve Koprich (SEM) and by Marnie Timleck (confocal fluorescence microscopy) in the HSC. Other members of the department that also must be thanked include Mike Palmer, the glass blower; Paul Bray, technical shop; Christina Gulewitsh of Chem Stores, Mike Mallot for computer assistance and the ladies of the chemistry office: Carol, Lynda, Josie, Barbra, Tammy and Sheila.

Finally I would like to express my sincere gratitude to the people in my personal life who have helped support me through the research process. My parents, Norma and James Goring, my aunt, Frances Goring-Koch and my in-law family, Marilyn and Marvin

Baer, Sandra Hannah and Jennifer, Allison, Emily and Marcus Walsh have provided vital emotional support and encouragement. My husband, Dr. Andrew Baer, has been my calming force, allowing me time to vent but always encouraging me to continue in the pursuit of this thesis. I realize that without family support my life and accomplishments would be so much more difficult. My final thanks are directed to my friends, Kris, Christine, Gayle, David, Theresa, Paul and Karen for making me laugh during the frustrating periods of this research thesis.

TABLE OF CONTENTS

LIST OF FIGURES AND SCHEMES

Chapter 2.0

Chapter 4.0

Chapter 5.0

LIST OF TABLES

LIST OF IMAGES

Chapter 3

Chapter 4

LIST OF ABBREVIATIONS

AFM	Atomic force microscopy
BTMS	n-butyltrimethoxysilane
DMDMS	Dimethyl dimethoxysilane
F	Fluorescein
FD	Fluorescein-dextran
F5M	Fluorescein-5-maleimide
FITC	Fluorescein isothiocyanate
GTB	Glycerol tributyrate
HSA	Human Serum Albumin
LOD	Level of detection
MSQ	Methylsilsesquioxane
MTES	Methyl triethoxysilane
ε	Molar extinction coefficient
PMT	Photomultiplier tube
PDMS	Polydimethylsiloxane
PEG	Poly(ethylene glycol)
PVA	Polyvinyl alcohol
PRODAN	6- propionyl-2-dimethylamino naphthalene
R.S.D.	Relative standard deviation
R6G	Rhodamine 6G
SEM	Scanning electron microscopy

SNARF	5,6-Seminaphtharhodafluor-1
S	5,6-Seminaphtharhodafluor-1 (SNARF)
SD	SNARF-dextran
SS	Sodium Silicate
TEOS	Tetraethylorthosilicate or tetraethoxysilane
TMOS	Tetramethylorthosilicate or tetramethoxysilane
Trp	Tryptophan

This thesis is dedicated to three very important ladies.

Grace Bailey
1910-1984

Nana introduced me to the beauty of art.
She taught me that obstacles can be overcome,
proving that everything is possible in this world.

Elizabeth Goring Halama
1934-2001

Auntie Elizabeth reinforced the 'Go Girl' attitude.
She encouraged me to believe in myself, to strengthen
my abilities and regain balance in all aspects of my life.

Vera Mae Hannah
1911-2006

Grandma Vera taught me to appreciate the small things in life,
encouraged my artistic side and to take things one day at a time.

I love and miss you all very much.

1 Introduction

1.1 Thesis overview and goals

Biologically doped sol-gel derived silica matrices have become a significant area of interest since the early 1990s. Many different biomolecules (soluble and membrane bound proteins, DNA aptamer and DNAzymes) and even whole cells have been entrapped within sol-gel derived silica, and such materials have been used for a variety of applications, including affinity chromatography, solid-phase extraction, biocatalysis and the development of biosensors.

Soon after the initial studies describing the entrapment of proteins within sol-gel derived silica, a number of studies appeared that investigated the effect of organically modified silica (ORMOSIL) matrixes on the properties of entrapped proteins. A series of studies by Reetz and others have shown that different silane precursors, such as alkyl-modified silanes,[1,2,3] and the co-entrapment of compounds such as polymers and surfactants along with the protein, can modulate material properties and/or protein stability.[4,5,6,7,8] However, while there are now a number of studies describing protein-doped ORMOSILs, key aspects including the distribution of environments (polarity, morphology, charge), the evolution of these environments, and the effects of such environments on protein performance are not well understood. In the present study, we have aimed to understand the effects of organic functionality on the physicochemical properties of sol-gel derived materials and have attempted to correlate this to protein activity by encapsulating the biocatalysts urease and lipase into bioglasses of various compositions. Lipase was chosen owing to its applicability to the development of an

optical biosensor for triglycerides, which are a key indicator of overall health. The organic functionality has been incorporated into the matrices in two ways. Firstly, Class I materials were formed by the inclusion of uncharged polymeric dopants, PEG and PVA. Secondly, Class II materials were prepared by the use of organosilane precursors in the form of the monoalkyl and dialkyl silanes such as tetraethylorthosilicate (TEOS), methyltriethoxysilane (MTES) and dimethyldimethoxysilane (DMDMS). Lastly, hybrid Class I/II materials were formed using both organosilane precursors and polymer dopants. The material properties that were examined included phase distribution from the nanometer to the micron scale using various microscopy methods, the internal environment, as probed using the polarity sensitive fluorescent probe 6-propionyl-2(dimethylamino)naphthalene (PRODAN), and the physical properties of the materials. These properties were related to the activity of entrapped proteins (human serum albumin, urease and lipase), and the latter enzymes were further utilized for the development of fluorescence based biosensors for urea and triglycerides.

An important aspect of the work presented in this thesis is the use of thin (submicron thick) films that were dipcast onto glass substrates. Up to this point, the majority of studies on either protein-doped or organically modified silica materials have involved glasses that were formed either as blocks (often referred to as monoliths) or thick films. However, the use of such formats is impractical for biosensor development for several reasons. Both monoliths and thick films age slowly over a period of several weeks or even months, resulting in alterations in the analytical response characteristics over time.[9,10] In addition, the long diffusional path for entry of analytes into the

monoliths produces long response times, ranging from several minutes up to hours.[11] Monoliths are also fragile and are prone to cracking due to hydration stress.[12] Finally, it is difficult to interface monoliths to devices based on optical fibers in order to allow remote analysis to be done. In this study, all data presented was obtained from thin films, and efforts are made to compare the evolution and properties of such films to those of monolithic materials.

1.2 Outline of thesis

The goals of this thesis include analysis of: (1) the physical properties of sol-gel derived thin films to factors that influence phase separation; (2) the chemical properties of sol-gel derived thin films to understand the internal environment of these matrices and how it evolves; (3) the activity of proteins immobilized within a series of organically modified sol-gel derived thin films; and (4) the development of prototypical biosensors using hydrophilic (urease) and hydrophobic (lipase) model enzymes coupled to fluorescence signaling methods. To achieve these goals, a series of composites are investigated that include TEOS as a base material, methyltriethoxysilane (MTES), dimethyldimethoxysilane (DMDMS) or iso-butyltrimethoxysilane (BTMS) as organosilanes and poly(ethyleneglycol) (PEG 600) or poly(vinylalcohol) as polymer additives. The data provide new insights into the methods that can be used to form nanocomposite films, the range of additives and processing conditions that can be used to

form such films, and the effects of various films on protein stability and sensor performance.

Chapter 2 provides a detailed literature review that describes the background to biosensor development, protein immobilization, sol-gel processing and development of protein-doped silica materials, methods for forming organically modified silica materials and thin sol-gel derived films, and the various methods used in this thesis for the characterization of sol-gel derived thin films.

In Chapter 3, a study of phase separation within organically modified silica materials is presented. Separate and co-hydrolysis was performed on various silane precursors of varying numbers and lengths of methyl-based organic functional groups, including sodium silicate (SS), tetraethylorthosilicate (TEOS), MTES, DMDMS and BTMS. The resultant sol was mixed in a one-to-one ratio with buffer containing either the polymer polyethylene glycol and/or the cationic fluorophore Rhodamine 6G. These sol-gel dip cast thin films were analyzed by different microscopic and nanoscopic imaging techniques such as brightfield microscopy, scanning electron microscopy, atomic force microscopy, and fluorescence microscopy to analyze the presence and distribution of film morphology, heterogeneity and chemical distribution within the interior of these matrices.

In Chapter 4, a subset of thin films were further studied to understand the impact of casting rate on film thickness and the evolution of the chemical environment of the films based on changes in the maximum of the emission peak of the solvent sensitive probe 6-propionyl-2-dimethylamino naphthalene (PRODAN) by fluorescence

spectroscopy. The ligand binding behavior of HSA was also explored by monitoring the binding of salicylate to provide a correlation between the chemical properties of the films and the properties of the protein.

In Chapter 5, the Class I and Class II films investigated in Chapter 4 were used to develop two prototypical biosensors for urea and triglycerides. In both cases pH changes arising from the reaction of the analyte with its cognate enzyme were detected using co-entrapped pH sensitive fluorophores.

Finally, Chapter 6 provides overall conclusions and discusses implications for the development of appropriate materials for fluorimetric biosensors. Future studies in this area are also discussed.

1.3 References

1. Brennan, J.D.; Hartman, J.S.; Ilnicki, E.I. and M. Rakic. *Chem. Mater.* **11** (1999): 1853.

2. Reetz, M.T.; Zonta, A. and J. Simpelkamp. *Biotech. Bioeng.* **49** (1996): 527.

3. Kauffmann, C. and R.T. Mandelbaum. *J. Biotechnol.* **62** (1998): 169.

4. Baker, G.A.; Jordan, J.A. and F.V. Bright. *J. Sol-Gel Sci. Technol.* **11** (1998): 43.

5. Baker, G.A.; Pandey, S.; Maziarz III, E.P. and F.V. Bright. *J. Sol-Gel Sci. Technol.* **15** (1999): 37.

6. Lesot, P.; Chapuis, S.; Bayle, J.P.; Tault, J.; Lafontaine, E.; Campero, A. and P. Judeinstein, *J. Mater. Chem.* **8** (1998): 147.

7. Chen, Q.; Kenausis, G.L. and A. Heller. *J. Am. Chem. Soc.* **120** (1998): 4582.

8. Heller, J. and A. Heller. *J. Am. Chem. Soc.* **120** (1998): 4586.

9. Flora, K. and J.D. Brennan. *Anal. Chem.* **70** (1998): 4505.

10. Edmiston, P. L.; Wambolt, C. L.; Smith, M. K. and S. S. Saavedra. *J. Colloid Interface Sci.***163** (1994): 395.

11. Braun, S.; Rappoport, S.; Zusman, R.; Avnir, D. and M. Ottolenghi. *Mat. Lett.* **10 (1990)**: 1.

12. Flora, K.; Dabrowski, M.A.; Musson, S.P. and J.D. Brennan. *Can. J. Chem.* **77** (1999): 1617.

Chapter 2: Literature Review

2.1 Protein immobilization for biosensing

Proteins are often used as selective biorecognition elements for biosensor development as they generally have selective interactions with one particular chemical compound or a class of compounds, such as biological ligands or inhibitors. However, other compounds of similar shape and/or composition may also interact with a given protein, which in some cases may generate a similar response to that of the cognate ligand. For biosensor development, the ligand or an inhibitor may be the desired analyte, while non-target ligands can act as interferants. In some cases, these species may also bind irreversibly to the active site of the protein, resulting in the loss of function and hence fouling of the biosensor.

The selective binding of an analyte to a particular biomolecule typically involves a series of weak interactions such as Van der Waals forces, hydrophobic interactions, hydrogen bonding and ionic bonding.[1] However, the binding itself does not usually generate a signal that can be utilized for biosensing. In order to develop a signal and ultimately detect it, the immobilization of the biomolecule to a suitable surface (electrode, piezoelectric crystal, thermistor, optical fiber, etc) becomes necessary. The potential for fouling or degradation of the protein (i.e., by proteases) also makes it desirable to immobilize the protein within a protective barrier to isolate it from interfering or degradative species in the surrounding environment.[2]

Ideally, detection of an analyte within a complex matrix can be performed rapidly by unskilled personnel, making it much more amenable to applications which do not

require specialized knowledge, such as home testing of glucose levels or the pregnancy hormone, or rapid screening of analytes of interest in prenatal screening. However, the success of such methods requires the selection of an immobilization method that results in the retention of a high level of the biological activity of the biomolecule, as well as a stable environment to allow long-term stability of the immobilized biomolecule.

When designing an immobilization protocol, it is important to consider several factors. These factors include the density and activity of the biomolecules, the orientation of the biomolecule on the surface, the long-term stability of the biological agent, the accessibility of the analyte to the biomolecule, fast response times and the ability to reduce leaching or fouling of the immobilized biomolecules. As all of these factors may be interrelated and their dependence varies between biomolecules, there is no one immobilization method that is suitable for all biomolecules. Some biomolecules will aggregate at high concentrations, may be immobilized in an orientation that blocks their active site, or may interact with the surface in a manner which causes unfolding, all of which can lead to a reduction or loss in signal for a biosensor.

There are several different methods by which biomolecules can be immobilized for biosensing. The most common methods include physical adsorption,[3,4] chemisorption (covalent binding),[5] affinity based techniques,[6,7] entrapment within semi-permeable membranes,[8] and microencapsulation within porous polymeric materials.[9,10] Physical adsorption involves the use of weak interactions such as hydrogen bonding, hydrophobic interactions or electrostatic interactions between the biomolecule and the surface. While physical adsorption is relatively easy to perform, there is little control over protein

orientation, proteins may undergo undesirable conformational changes upon absorption, and minor alterations in solvent conditions or temperature can lead to desorption of the biomolecule. Chemisorption involves the formation of covalent bonds between the biomolecule and the substrate, normally involving reactive groups such as cysteines (thiols) or lysines (amines) at the surface of the folded protein and a suitably activated surface (normally iodoacetoxy or aldehyde modified surfaces, respectively).[11] A limitation of this method is that most biomolecules can contain multiple cysteine or lysine residues, making it difficult to control the orientation of the biomolecule. Indeed, it is possible to tether the biomolecule to the surface through either an essential residue or a residue adjacent to the active site, which will result in inaccessibility to analytes.

In some cases, it is possible to utilize residues that are common to a class of biomolecules to control the orientation of the protein on a substrate surface. For example, the Fab fragment of antibodies have a free cysteine at the end opposite to the Fab binding site. In this case, it is possible to use site specific binding through the cysteine to control the orientation.[12,13] However, the wide diversity in the tertiary and quaternary structure of proteins does not permit this form of oriented immobilization to be uniformly used for all proteins.

Affinity-based immobilization techniques make use of natural biomolecular binding interactions to tether the biomolecule to a suitably modified substrate. Examples include biotin-avidin interactions, aptamer capture, antibody capture, His_6 tags to bind to Ni(II)nitrilo triacetic acid (NiNTA) derivatized surfaces and glutathione-S-transferase tags to bind to glutathione modified surfaces.[14,15,16] These affinity methods often allow

for some control over orientation but require recombinant proteins and are not amenable to intrinsic or extrinsic membrane proteins or highly hydrophobic proteins such as lipases, which tend to aggregate upon immobilization.

The use of physical barriers such as dialysis tubing or polymer microcapsules for entrapment of biomolecules provides a generic method to locate biomolecules in close proximity to the surface of analytical devices without requiring contact between the biomolecule and the surface. The size exclusion properties of the membrane or microcapsule allow small analyte molecules to approach and interact with the biomolecule while retaining the biomolecule near the surface of the analytical device. The key difficulty with this immobilization approach is the minimal control over the properties of the membranes and films (i.e. pore size, polarity) and the fragility of such materials, making the prevention of protein leaching difficult[4] and limiting the variety of proteins that are amenable to this immobilization method.

2.2 The sol-gel process

Although the methods of immobilization described above have proven to be successful for the entrapment of some biomolecules, the lack of tuneability of the biomolecule environment and the inability to immobilize all classes of biomolecules reduces the potential of such methods for diverse classes of biomolecules. The use of inorganic polymer matrices which can be formed via the sol-gel process is an alternative method by which biomolecules can be immobilized while providing small molecule analytes access to the biomolecule from all directions.[17,18] The general process by which

proteins are entrapped in sol-gel derived materials is shown in Figure 2.1. The general protocol involves hydrolysis of an alkoxysilane precursor followed by condensation to form an inorganic gel (see Figure 2.2), which is then further processed to form a silica material. The ease with which sol-gel derived materials can be prepared and modified makes it one of the best generic immobilization methods currently available.

The sol-gel process has been known since the mid 1800's, and typically utilized alcohol or other harsh solvents as an aid in the dissolution of inorganic precursors and high temperatures to aid in the curing of the resultant gels, rendering these materials non-biocompatible. Several metal precursors can be used in the sol-gel process including silicon (Si),[18,19] titanium (Ti),[20] aluminum (Al),[21] and zirconium (Zr).[22,23,24,25] The end use of the sol-gel derived matrix dictates the precursor and the processing route under which the sol-gel process can occur.

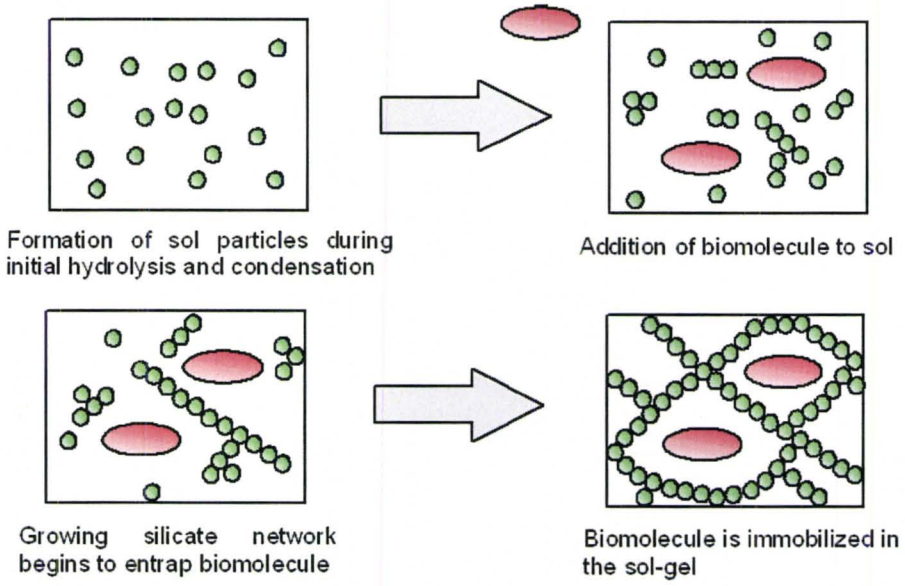

Figure 2.1: Representation of the process by which a biomolecule is immobilized in a sol-gel matrix.

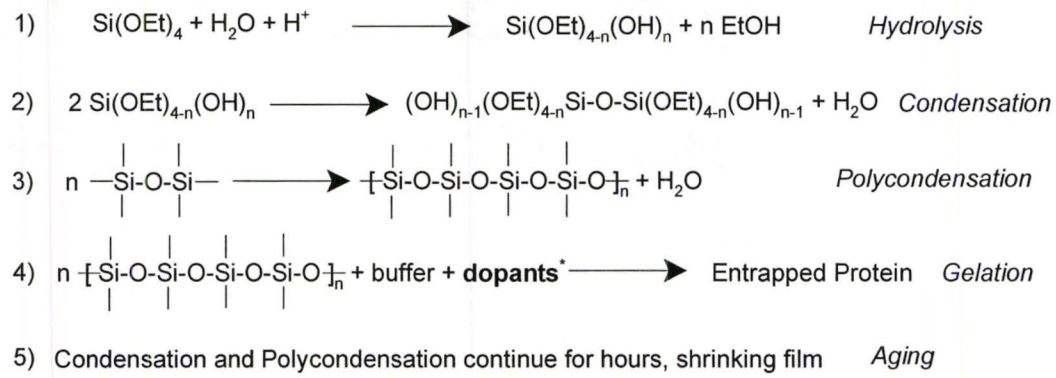

Figure 2.2: The acid-catalyzed sol-gel processing method for tetraethoxysilane (TEOS). **Dopants*** can include polymers, organically modified silanes or biomolecules.

While traditional sol-gel methods were not compatible with entrapment of biomolecules, work in the early 1990's showed that it was possible to produce these materials at low temperatures and in aqueous environments using a two step sol-gel process, which made them amenable to the entrapment of functional biomolecules. The typical steps in the biocompatible silane-based sol-gel process are shown in Figure 2.2. The first main step involved acid or base catalyzed hydrolysis of alkoxysilane precursors in forming the sol solution. This sol could be aged for several days to allow for a certain degree of condensation and continued growth of silica nanoparticles. The second key step involved the addition of a buffered solution of protein, which diluted the alcohol produced in the hydrolysis step and adjusted the pH to the physiologically range, providing an environment that was suitable for biomolecules.[2,19,26,27,28] The increase in pH and ionic strength leads to a significant increase in the rate of condensation, and produces rapid gelation, resulting in biomolecule entrapment. Aging and partial drying of the biogel results in the formation of a mesoporous silicate glass, with typical pore

diameters of 2-20 nm. Such materials retain proteins by size-exclusion while allowing small molecule analytes to penetrate the material and react with the immobilized biomolecule.[18,29]

Protein immobilization in sol-gel derived matrices

In 1990, Avnir et al. published a seminal paper, in which a two-step sol-gel processing method was used to physically entrap biomolecules (in particular, alkaline phosphatase) within an inorganic silica matrix.[30] This was soon followed by a key paper by Dunn, Zink and co-workers wherein oxygen binding biomolecules (cytochrome c and myoglobin) were entrapped within a tetra-alkoxysilane derived silica matrix and shown to retain O_2 binding ability.[31] The primary breakthrough demonstrated in these two papers was the ability to prepare sol-gel based materials without the use of additional alcohol to aid in the solubility of the tetra-alkoxysilane precursors. Instead, the sol-gel derived material was prepared in two steps: (1) low temperature hydrolysis of alkoxysilane precursors in an aqueous solvent system; and (2) addition of buffer containing the protein to initiate gelation of the matrix around the biomolecules (Figure 2.2). Since this time there has been a large number of reports on protein entrapment within sol-gel derived materials, as described in several recent reviews.[19,32,33,34]

Protein doped sol-gel derived matrices have been used in a variety of applications, however, the most prevalent of these has been the development of biosensors. A large variety of optical and electrochemical sensors have been developed using sol-gel entrapped enzymes, antibodies and regulatory proteins, and this area has been extensively

reviewed.[35,36,37] Examples include absorbance, fluorescence and electrochemical based sensors for enzyme substrates such as glucose, lactate, glutamate and urea, various enzyme inhibitors (i.e., organophosphate inhibition of acetylcholinesterase), and a wide variety of small molecules (toxins, explosives, small hormones, etc) which have been detected using entrapped antibodies. However, it should be noted that the size exclusion properties of sol-gel materials generally prevents access of large analytes to entrapped proteins. Hence, there are few reports on the sensing of species, such as full size proteins which cannot enter the mesoscale pores of typical sol-gel materials.

2.3 Influence of additives to sol-gel derived matrices

The majority of the early research on biomolecule entrapment within sol-gel derived glasses primarily focused on bulk monolith compositions derived from pure alkoxysilanes such as TEOS (tetraethylorthosilicate) and TMOS (tetramethylorthosilicate).[2,18,29] Such materials have highly polar and anionic interior environments, shrink substantially and crack easily.[18,29,38] While these materials have been used successfully for the entrapment of various soluble proteins,[2] the polarity of the internal environment and the evolution of alcohol during processing is not ideal for the immobilization of many biological molecules, including several enzymes[39] and membrane-associated proteins.[32]

Since biomolecules exist in a variety of unique *in vivo* environments, it is important to attempt to reproduce these optimal conditions within the internal environment of the sol-gel derived matrix in order to maintain optimal performance for

the entrapped biomolecule.[40,41,42,43,44] There are two general approaches to modifying sol-gel derived silica materials: (1) the use of non-covalently bound components (i.e. hydrophobic or hydrophilic polymers), which result in Class I organically modified silanes;[42,43,44,45,46] and (2) the use of covalently bound compounds (i.e. organically modified silanes) to produce Class II organically modified silanes.[43,45,47,48] Incorporation of both dispersed and anchored organic groups is also possible, leading to the formation of Class I/II materials. These materials have been extensively studied for applications such as superhydrophobic materials,[49] hydrophobic coatings,[25,50] and more recently have been examined as platforms for biomolecule immobilization.[51]

Examples of biomolecule entrapment in ORMOSILs include: the entrapment of atrazine chlorohydrolase into methyltrimethoxysilane-based materials;[52] lipase into polymer-doped materials formed from organically modified silanes (which produced an 8800% enhancement of activity compared to free lipase for esterification reactions, but only 40% for hydrolysis reactions involving emulsified oils);[53,54,55] lipase and human serum albumin in organically modified silicates, with lipase showing up to 50% activity for the hydrolysis of glyceryl tributyrate (GTB);[46] glucose oxidase and horseradish peroxidase in the presence of a graft copolymer of polyvinylimidazole and polyvinylpyridine;[56,57] and acetylcholinesterase and butyrylcholinesterase in the presence of polyethylene glycol.[58] In each case, the addition of organosilane precursors or polymers resulted in improved function for the entrapped protein. However, in many cases the resulting materials were not suitable for spectroscopic studies (owing to

extensive cracking and light scattering),[15] and often they were not fully characterized in order to better determine the origin of the stabilization effect.

As noted above, examples of typical species used for organic derivatization of silica materials are manifold, but for the purposes of this study a selection of key modifiers will be highlighted. Non-covalently bound additives, which can be used to enhance the stability of the immobilized biomolecule and to modify the morphology or polarity of the internal environment, normally consist of hydrophilic, hydrophobic or charged polymers. The two polymer Class I additives used in this thesis are shown in Figure 2.3.

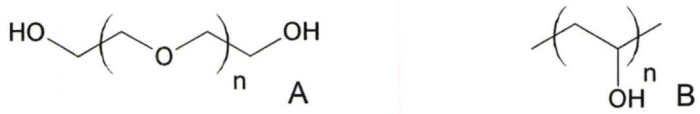

Figure 2.3: Structures of A) polyethylene glycol (PEG) and B) polyvinyl alcohol (PVA) (87% hydrolyzed).

The presence of additives with alkyl, aryl, amino or other organofunctional groups, that are capable of forming bonds with the silica gel, modify the internal environment and the degree of crosslinking within these materials. These covalently bound additives also alter the polarity of the material, and can have specific effects such as enhancing the conductivity or the plasticity of the final matrix. However, a significant increase in the concentration of these organically modified silanes can result in undesirable properties, such as macroscopic phase separation, cracking or unduly long gelation times.[18] Examples of the organically modified silanes used in this thesis are

shown in Table 2.1. Such materials were chosen to provide a series of model compounds that could allow an investigation of the effects of alkyl chain length, number of alkyl chains, and the effects of alcohol generating (TEOS) and non-alcohol generating (SS) species.

Table 2.1: Monomer structures of undoped silanes and organically modified silanes used in thesis.

Silane monomer structure	Name	Abbreviation
$Na_2Si_3O_7$	Sodium Silicate	SS or S
$Si(OCH_2CH_3)_4$	Tetraethoxysilane	TEOS or T
$(CH_3)Si(OCH_2CH_3)_3$	Methyl triethoxysilane	MTES or M
$(CH_3)_2Si(OCH_3)_2$	Dimethyl dimethoxysilane	DMDMS or D
$CH_3(CHCH_3)CH_2Si(OCH_3)_3$	Isobutyl trimethoxysilane	BTMS or B

It is also possible to include, both types of additives, which may produce materials that are capable of enhancing the properties of biomolecules immobilized in the material.[45] These materials are known as Class I/II materials and may have additive or unique properties relative to their respective precursor components. In addition to changes in polarity and crosslinking, the hardness, homogeneity, transparency and morphology of the final material can be dramatically altered upon addition of Class I or Class II additives. Such changes in the material can have significant effects on their utility for biosensor development, particularly in cases where optical signals are used to

report on analyte concentration. Thus, it is important to understand the various effects that specific precursors have on the physical and chemical properties of materials that are used for biomolecule entrapment.

2.4 Methods of hydrolysis

The method used for hydrolysis influences the manner in which the monomers in the sol will undergo condensation. Using acid catalyzed hydrolysis the terminal silicon atoms are most reactive, and this causes monomers to form long linear chains, leading to the formation of a highly crosslinked three-dimensional network with relatively low porosity.[18] In base catalyzed hydrolysis, the central silicon atoms are most reactive, and thus the sol consists of colloidal particles, which continue to grow in size as they undergo polycondensation. The materials formed by this route tend to be more porous and in some cases can grow sufficiently large in diameter that they do not remain suspended in the sol and instead flocculate. The lower porosity obtained using acid catalyzed hydrolysis leads to materials that have better protein retention and better optical clarity. Thus, in this thesis, only acid catalyzed hydrolysis was used for the formation of sol-gel derived thin films. This process is shown in Figure 2.4.

$$Si(OEt)_4 + n\ H_2O \xrightarrow{H^+} Si(OEt)_{4-n}(OH)_n + n\ EtOH$$

Figure 2.4: Hydrolysis of tetraethoxysilane.

In general, the alkoxy functional group (for TEOS it is OCH_2CH_3) undergoes hydrolysis to form a hydroxyl group and an alcohol byproduct. Organically modified alkoxysilane precursors, which are discussed below, will undergo similar hydrolysis reactions to that shown in Figure 2.4; however, the presence of the organic group increases the isoelectric point of the silicon and tends to result in a more rapid rate of hydrolysis. Hence, the degree of hydrolysis of organosilanes will be greater than that of tetra-alkoxysilanes under the same reaction conditions.[18]

When sol-gel materials are formed with both organosilanes and tetra-alkoxysilanes, it is possible to separately hydrolyze the silanes prior to mixing, or to mix the silanes followed by co-hydrolysis. In separate hydrolysis, each silane precursor can react for a desired length of time to form sols composed of a single type or narrow range of materials (silica, methylsilsesquioxane, polydimethylsiloxane) prior to mixing. This method allows different conditions of pH, water:silicon ratio, or hydrolysis time to be used for each silane, providing a larger variety of possible reaction conditions. Once hydrolyzed, the individual sols are mixed to form a composite sol, which is then mixed with a buffered protein solution to form the final material. Depending on the extent of hydrolysis for each component and the relative molar ratio of each silane, a significant heterogeneity in the composition of material may be obtained.

In co-hydrolysis reactions, all the silane precursors are mixed together with the appropriate catalyst and solvent(s) prior to agitation. The individual silanes are thus hydrolyzed under identical conditions, and reactions between different silanes occur

immediately, generating oligomers with mixed silane compositions. This sol is then mixed with a buffered protein solution to form the final material.

In addition to alkoxysilanes, both silicic acid and sodium silicate solutions can also be used as silane precursors; however, these species can be considered to be fully hydrolyzed, and thus there is essentially no need for a hydrolysis step.[59] However, in the case of sodium silicate solutions, the very high amount of sodium and the very high pH (ca. pH 13) can lead to rapid gelation of the sol, and may also result in pH or salt-induced denaturation of entrapped proteins. For this reason, the sodium silicate solution is mixed with a pretreated acidic cation-exchange resin, which lowers the pH of the mixture to 4.0 while simultaneously reducing the sodium ion concentration by several orders of magnitude. The resultant sol is vacuum filtered to remove the resin, and is passed through a syringe to remove any large silicate particles which may be present in the original sodium silicate solution. This sol is then mixed with a buffered solution containing the desired dopants or biomolecules.[59] The complete hydrolysis and lack of alcohol byproducts make this sol significantly different from those derived from TEOS, and make it useful as an undoped reference material to monitor the influence of the diluted alcohol byproducts from separate or co-hydrolysis processes on the dopants.

Condensation and polycondensation reactions of the sol-gel reaction scheme

Once the hydrolysis of alkoxysilane precursors is initiated, the condensation reaction will begin to occur. Hydroxyl groups will form siloxane bonds (Si – O – Si) between two silicon atoms and release water as a byproduct (Figure 2.5). These water

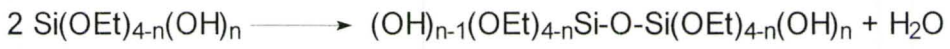

Figure 2.5: Condensation reaction occurring during the sol-gel process.

molecules further promote the hydrolysis reaction, however, it should be noted that not all alkoxysilane molecules become fully hydrolyzed; many residual alkoxy groups can remain in the material long after gelation. The polycondensation reaction will also begin to occur resulting in the formation of the three dimensional silicate network (Figure 2.6). For those alkoxysilane molecules that may contain an alkyl functional group, there will a reduction in the degree of crosslinking within the sol-gel derived matrix.

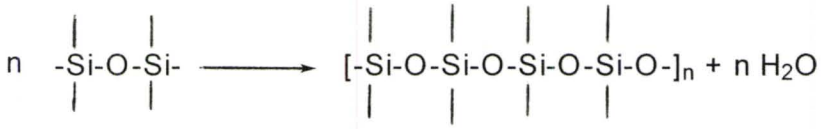

Figure 2.6: Polycondensation reactions leading to formation of the three-dimensional structure. Dashes from the silicon atoms represent bonds to oxygen atoms, which in turn are bound to further silicon atoms, leading to a three-dimensional network.

After gelation, the material will continue to evolve for a significant period of time.[38,47,60] The key process at this stage is the continued dissolution and reprecipitation of the silica material (syneresis), which is driven by water molecules present within the pores of the material. The syneresis process tends to result in larger and smoother pores and significantly enhanced mechanical properties, such as elasticity, binding and mechanical strength, of the final material.[18] This process also results in a decrease in

hydroxyl group density and increases in the number of siloxane bonds,[38] which will alter the polarity of the internal environment and the overall charge of the silica surface.

The degree of syneresis can be controlled by varying the method by which the sol-gel material is aged. Sol-gel derived materials can be aged either in water (wet-aged) or in air (dry aged), or can be washed extensively after gelation to remove alcohol and increase water content followed by dry-aging.[38] Wet-aging is potentially useful for biologically doped materials as the alcohol byproduct is rapidly removed from the matrix and the protein remains fully hydrated. However, the material must be given sufficient time to form a stable gel prior to addition of aging buffer, which tends to preclude this method for aging of thin films, since thin films will dry very rapidly as they gel.[61,62] In cases where materials are aged in air, it is important to slowly rehydrate samples before use by exposing them to a minimal amount of buffer or water in the bottom of their sealed container. Otherwise upon insertion into a buffer solution, these thin films often will crack due to hydration stress, resulting in a loss of matrix integrity.[18]

Phase separation

The distribution of chemical compositions with sol-gel derived matrices is very important with respect to their desired applications. Through variations in the concentration of the silane precursors, their relative ratios and the concentration of other additives, the morphology of these gel materials can be controlled or tuned for a specific purpose. In some cases, a homogeneous distribution of the silane precursors and other additives will offer the ideal chemical composition for a desired application (such as

optical sensing),[63] while other applications, such as the development of highly porous chromatographic columns, may require a heterogeneous distribution of chemical environments (polarity, charges and crosslinking) to drive macroscale phase separation.[64,65,66,67] As well, issues such as immiscibility between any of the modifying agents, such as silane precursors, additives or solvents, can lead to the possibility of phase separation.

The presence of alkyl functional groups on silane precursors strongly influences the morphology of the final gels. When bulky or long chain functional groups (such as butyl or propyl groups) are exposed to an aqueous environment, they may interact amongst themselves to form micellar structures during condensation reactions.[18,66] This restricted distribution of silane precursors can generate regions within the silica matrix which are purely of one chemical composition. At elevated concentrations of the modified silane precursors, these regions can either remain as isolated clusters or form the predominant (continuous) structure of the final material. In binodal decomposition, the clusters are irregularly shaped islands distributed throughout a continuous gel structure and there is no contact between the individual clusters.[18] However in spinodal decomposition, the different phases arrange within the sol to reduce the interfacial or overall energy of the mixture.[68,69] As a result, there is a continuous structure that stretches across the entire gel network. It should be noted that during the mixing of separately hydrolyzed silanes and buffer, there is a limited window in which this rearrangement can occur prior the structure being "locked in" upon gelation. Furthermore, for dipcast thin films, gelation and solvent loss can occur quickly during the

dip casting of sol-gel derived thin films, which can restrict further rearrangements, and thus produce highly phase separated films.[69,70,]

Microscale domains that are less than two nanometers in diameter generate optically transparent glasses. Increasing the size of the domains to diameters between two nanometers and 50 nm results in mesoscale size regions that can be seen by AFM or SEM but not by optical techniques. Macroscale domains (clusters which are greater than 50 nm in diameter), which usually result from phase separation created by spinodal decomposition, will result in an opaque glass matrix. [71] Such phase separation is easily observed by standard optical microscopy or SEM methods.

Phase separation may also be observed in materials that have been doped with polymers of high molecular weight, as these additives can interact with growing silica particles to produce a material that is immiscible with the solvent phase.[69,72] Such materials have been widely used as the basis for fabricating monolithic sol-gel derived columns. More recently, biocompatible processing methods were employed to produce macroporous sol-gel derived bioaffinity columns, which had large macropores to allow passage of eluent with low backpressure and a large proportion of mesopores (< 20 nm diameter) to allow entrapment of a significant fraction of protein.[64]

While there have been many previous studies of phase separation within sol-gel materials, most of these involved materials formed with high alcohol levels and processing conditions that were not suitable for protein entrapment. [73,74,75,76,77,78,79,80,81,82,83] In this thesis, phase separation behavior within organic-inorganic nanocomposite materials was investigated using protein compatible aqueous processing

methods. Our interest in investigating phase separation in these materials is the significant impact of heterogeneity on the mechanical properties of the material, the optical clarity, protein performance, and the potential for solid phase extraction into the film.

2.5 Preparation of sol-gel derived thin films

Most studies of protein doped materials done up to the late 1990s utilized sol-gel derived bulk materials, with thicknesses on the order of several hundred micrometers up to one centimeter.[45,46,47,53,54,55,84] Such a format allows high amounts of protein to be loaded, making spectroscopic and other studies of protein properties straightforward. However, in terms of biosensor development there were some significant disadvantages to these monolithic matrices. Bulk materials require large volumes of starting materials (silane precursors, additives and biomolecules),[85] have long aging and curing times,[45] require diffusion of analytes over large distances, which increases the response time of the sensing material,[45] and can undergo significant shrinkage and cracking, which makes it difficult to maintain calibration.

In order to reduce the response times, bulk materials can be crushed into powders, thus increasing the surface area over which biomolecular interactions could occur. However, this solution is not practical for all analytical applications, and tends to dramatically increase light scattering when used for optical sensing. As well, the cost of some biomolecules is very expensive, particularly for those that are not commercially available, due to the processes required for acquisition and purification of rare varieties of

biomolecules of interest. Therefore, it is generally agreed that thin films (ie. submicron thickness) are most appropriate for the development of analytical devices, such as biosensors, biocatalysts or coatings for capillary columns.[61,84,86,87,88] Thin films tend to age rapidly (limiting drifts in calibration),[89] offer faster response times[63] and can be interfaced to standard fiber-optic based biosensors[90,91] or columns.[64,67,92]

There are several different methods by which sol-gel derived thin films can be applied to a variety of substrates. These methods include dipcasting, [25,89,93] spin casting,[94] aerosol spraying,[95,96,97] or the sandwich technique.[96] In spin casting, a substrate is attached to a platform, a small volume of sol is placed or dropped onto the substrate surface and the platform is rotated at a set speed over a given length of time. Although this is a quick method of preparing thin films, the majority of the sol sample is lost as it is expelled during the rotation. In aerosol spraying, the substrate is also attached to a platform and the sol mixture is vaporized and then sprayed over the entire surface of the substrate. This method is suitable for flat surfaces, but is less amenable to the curved surface of an optical fiber. The sandwich technique offers the ability to place several different layers on one substrate with different sol compositions, additives or biomolecules being present in each layer. This method results in a biomolecule layer "sandwiched" between two sol-gel layers, the thickness of which can be varied to allow rapid diffusion through a thin top layer, and thus faster response times, while having a thicker bottom layer to protect the biomolecule from the substrate surface.

The dip casting technique (Figure 2.7), is the final method for preparing thin films, and provides a versatile platform for coating substrates with a variety of shapes or

sizes. The sol is placed in a casting well and several different samples can be cast from the same well, with the speed of the casting and the sol viscosity controlling the thickness of the thin film.

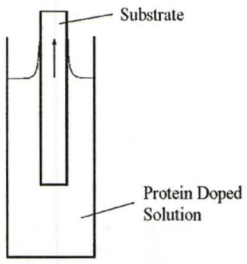

Figure 2.7: Schematic of dip casting process for preparation of sol-gel derived films.

Film thickness in the dip casting method is dependent on the coating solution and the rate at which the film is removed from the casting well. This correlation between these parameters is given in Equation 2.1:

$$t = 0.944\left(\frac{\eta U}{\sigma}\right)^{1/6}\left(\frac{\eta U}{\rho g}\right)^{1/2} \qquad \text{Equation 2.1}$$

where t is the film thickness, η is the solution viscosity, σ is the surface tension of the solution, ρ is the density of the solution, U is the withdrawal speed and g is the gravitational acceleration constant. This equation indicates that film thickness increases as solution viscosity or withdrawal speed increases.[85]

2.6 Analysis of sol-gel derived matrices

There are a large number of methods that have been used to characterize the physical and chemical properties of sol-gel derived materials, ranging from spectroscopic methods (NMR, FTIR, Raman, fluorescence) which give useful information on chemical properties to physical methods (stress-strain measurements, porosimetry, light scattering, etc) which give information on the morphology and physical properties of such materials. Characterization of thin sol-gel derived films significantly reduces the number of methods available for analysis, owing to the very small sample volumes and the need to employ methods which are surface sensitive. Given these constraints, fluorescence and imaging methods have emerged as among the most useful for characterization of the properties of thin films.

Several researchers, including Higgins and Collinson,[76,77,78,79,80,81,82,83] Brennan[61,84,98,99,100] and Yip[101,102,103,104,105,106] have utilized both fluorescence and imaging methods to investigate the properties of thin films. Higgins and Collinson have used atomic force microscopy, scanning electron microscopy and single molecule fluorescence methods to probe the physical and chemical properties of sol-gel derived films. Their work focused on the evolution of the internal environment of sol-gel derived dip-cast thin films containing mixtures of TEOS and organosilanes which were either separately or co-hydrolyzed. Their studies have shown that inclusion of organic functional groups can dramatically alter the phase distribution in sol-gel films, as well as the interaction of small molecules with the silica (or ORMOSIL) skeleton.[76,77,78,79,80,81,82,83] Yip and co-workers have reported several studies that use single molecule fluorescence spectroscopy

to monitor the chemical heterogeneity within sol-gel derived matrices. Single molecule polarization experiments were performed to assess the degree of rotational motion experienced by fluorophores of different charge when entrapped in an anionic sol-gel derived silica film. This work demonstrated that electrostatic interactions between cationic dyes and the silica surface result in a dramatic reduction in probe mobility, which can be partially overcome by increasing ionic strength. Yip's group has also examined the changes in emission wavelength under single molecule conditions to provide information about the presence or absence of heterogeneity within these matrices.[101,102,103,104,105,106]

Our group has previously used fluorescence methods to examine the accessibility and conformational flexibility of the protein HSA within sol-gel derived thin films[63] and demonstrated that the protein retained significant conformational freedom and was fully accessible to external analytes. The response time for interacting with a model analyte was up to 600-fold faster than was observed for monolithic silica materials, and detection limits were similar to those obtained in solution. This study clearly demonstrated that detailed information on proteins could be obtained using the thin film format.[45,60,63]

In this thesis thin films were characterized by both physical and chemical methods, predominantly based on imaging of fluorescence. Imaging methods included brightfield microscopy, scanning electron microscopy (SEM) and atomic force microscopy (AFM), which provided detailed information on the heterogeneity and morphology of thin films. Fluorescence microscopy was also employed to provide chemically relevant information on phase separation within thin films.

Fluorescence methods were employed both to characterize the chemical environment within sol-gel derived films and to assess the properties of the model protein human serum albumin upon entrapment into a range of different film compositions. This method was also used as a platform for the development of reagentless enzymatic sensors for urea and triglycerides, again using the thin film format to maximize sensor response times. An outline of these methods is provided in the following sections.

2.6.1 Imaging methods

Brightfield microscopy: Microscopic analysis of sol-gel derived thin films offers information about the distribution of precursor components within the final matrix, through changes in the appearance of the material. Brightfield microscopy can be used for the analysis of optically transparent thin films, because changes in the refractive index cause changes in the passage of light through material. Such changes in refractive index typically provide information on change in the chemical composition of the matrix on the micrometer scale. The larger field of view (ca. 1 mm^2) can provide information about the macroscale morphology of the matrix, which can provide evidence of bimodal or spinodal decomposition. Furthermore, this method provides information on cracking and the uniformity of the film edges over a large area. However, the resolution of brightfield imaging is diffraction limited to ca. 200 nm, and thus mesoscale structures cannot be observed. Furthermore, the chemical information that can be obtained from brightfield imaging is limited, and thus other imaging methods are required to aid in the interpretation of such images.

SEM: Scanning electron microscopy has been widely used to examine sol-gel derived matrices, particularly those that have been used for the development of chromatographic stationary phases.[107,108,109,110,111] This method makes use of the backscattering of electrons from the surface of a sol-gel material to produce images with a resolution that can approach the nanometer scale. Typically, SEM is used to image macroscale porosity or heterogeneity in sol-gel materials, with features > 50 nm in diameter being detected. Materials to be analyzed by this technique do not need to be optically transparent in nature, however, they must be conductive. For sol-gel derived materials, which are typically non-conductive, this is achieved through the application of a thin gold coating of approximately 15Å to allow the beam of electrons to interact with the surface of the silane matrix.

The operation of a SEM is shown in Figure 2.8. In this method a beam of electrons is focused onto the surface of the sample. Since the wavelength of an electron is much smaller than that of light, it is possible to focus the electrons to a very small area to increase resolution. Upon interaction with the sample the primary electron beam is backscattered in a manner that depends on the density of the material. The secondary electrons are detected using an electron multiplier and the intensity of the secondary electron beam is recorded as the primary electron beam is rastered over the sample surface, generating an image of the surface. The SEM method is ideal for imaging macropores in sol-gel materials, and can also provide useful images in cases where the density of the material changes over the 0.1 – 10 mm scale, which makes it useful for imaging large scale phase separation within nanocomposite films.

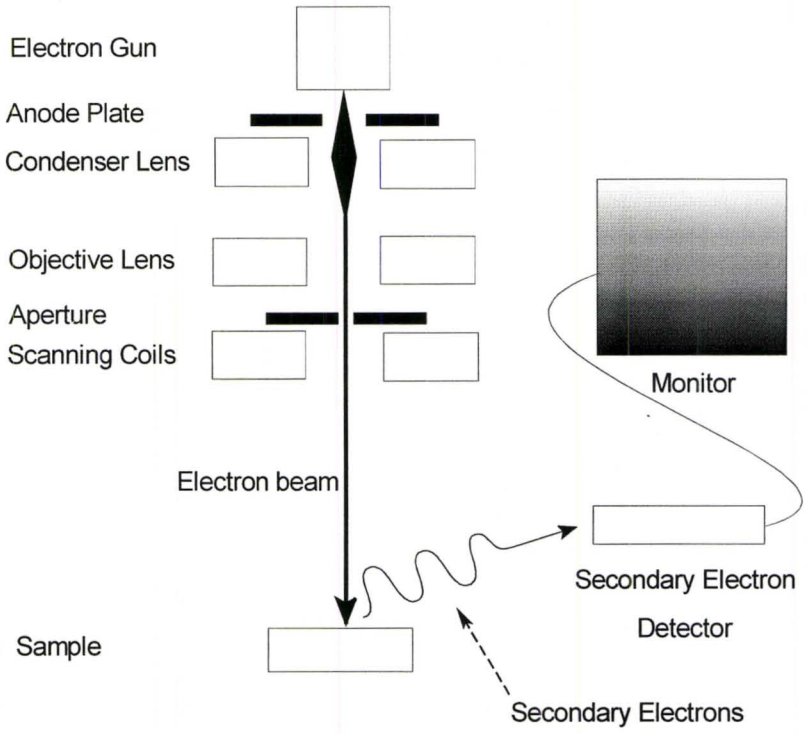

Figure 2.8: A schematic diagram of a scanning electron microscope.

AFM: High resolution analysis of film heterogeneity can be done by atomic force microscopy and the resultant images can be on the order of a few hundred nanometers to tens of microns wide. AFM imaging is based on the interaction of the repulsive forces that occur between the tip and the sample.[112] A sol-gel derived thin film sample is centered on a sample plate that is placed underneath an atomically sharp tip usually etched from Si_3N_4 and mounted at one end of a silicon cantilever.[113] The tip is mounted into a holder which is placed at the bottom of the piezo-ceramic tube, which controls the lateral and vertical movement of the tip through a series of compressions and expansions

that are related to the interactions occurring between the electrodes located on the inner and outer compartments of this tube.[114,115,116] When the appropriate voltages are applied to the piezo-ceramic tube, the tip can be rastered over the surface of the sample in either a contact or tapping mode of operation (see Figure 2.9).[114]

In this thesis, tapping mode was the method of operation, in which the tip was oscillating at a frequency of approximately 100 kHz between the sample and the surrounding media. In this mode, the tip-sample interactions will affect the amplitude of the oscillating amplitude and the height is kept constant in the feedback loop cycle.[113,115] All of the images obtained by AFM in this thesis depict the tip displacement in the z-direction that is the result of constant interaction, force or oscillation, depending on the mode that is in use. There are several different ways in which the images can be plotted using height, phase or amplitude data. A series of different methods of analysis (for example height and phase modes) can be collected for a region of the sample during one passage of the tip. By comparing changes between these different modes, information can be gained about the composition of the matrix, the distribution of the morphology and surface roughness.[113,116] From topography images, it is possible to determine if the surface is relatively smooth (little change in height in the Z-direction), and if the surface appears to be of a uniform morphology or if there are regions of heterogeneity.[117] Phase images are based on the delay in phase between the input signal to cause tip oscillation and phase lag in cantilever oscillation at a given point over the surface.[118] Hard materials will not alter the phase of the tip, resulting in a phase shift of zero. Softer materials interact differently with the tip due to adhesive and viscoelastic forces, and causing the

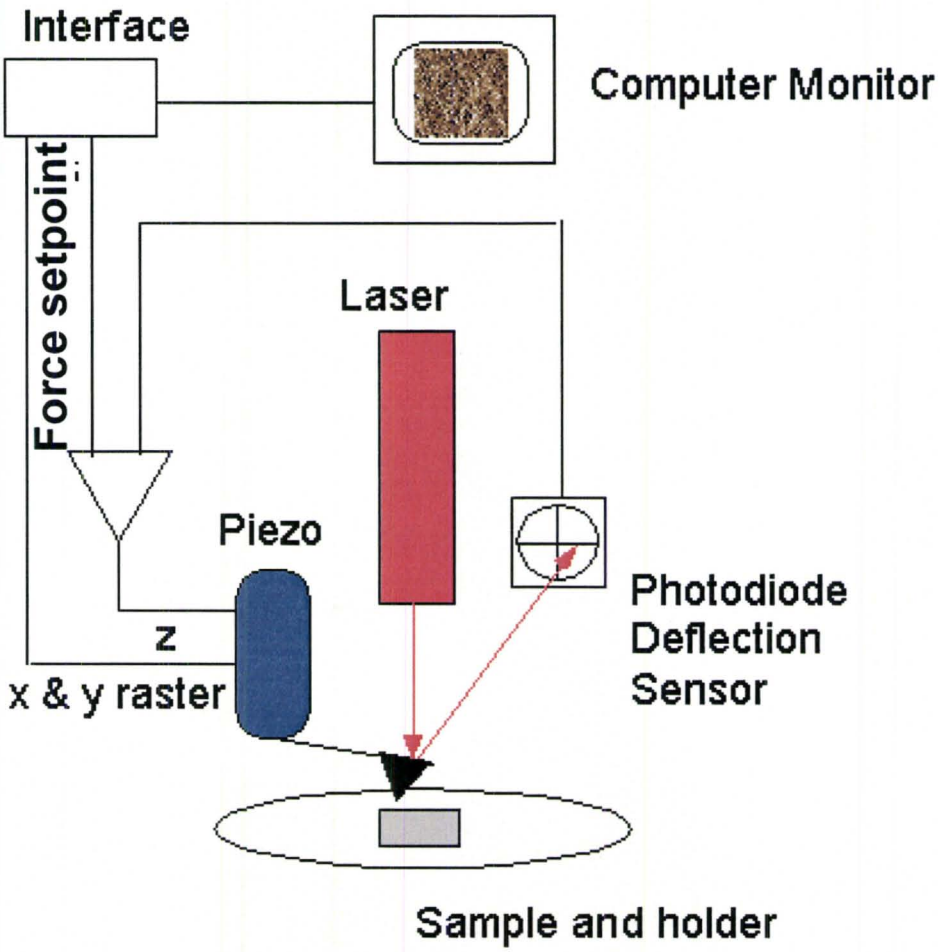

Figure 2.9: A schematic diagram of an atomic force microscope.

phase to shift by up to several 10's of degrees. This mode of imaging provides useful information on the variation in the mechanical properties of nanocomposite films, which in turn reflect variations in chemical properties. By comparing differences in appearance between height and phase mode images of the same sample area, collected at the same time, it is possible to see if changes in topography are related to alterations in the mechanical properties of the film.[66,112]

2.6.2 Fluorescence methods:

Fluorescence Overview: Fluorescence measurements can also be used to investigate sol-gel derived materials provided that they are optically clear. Fluorescence techniques can range from steady-state emission spectra to monitor changes in the polarity or pH of the internal environment[119,120] of a sol-gel material to advanced time resolved fluorescence anisotropy measurements to probe the rotational dynamics of species entrapped within sol-gel materials.[100,119,121,122,123] In all cases a fluorophore, which is a molecule capable of undergoing electronic transitions, is either doped by itself or bound to a biomolecule within the buffer solution prior to the mixing of the buffer with the sol to initiate gelation.

Fluorescence has been widely used to probe the properties of proteins within sol-gel materials. Intrinsic protein fluorescence occurs from amino acid residues (tryptophan, tyrosine or phenylalanine, as shown in Figure 2.10). The indole group of the tryptophan offers the strongest signal with a molar extinction coefficient of 5600 $M^{-1}.cm^{-1}$ at 280 nm and a quantum yield of ~ 0.14, with emission normally in the range of 320 - 340 nm. Tryptophan emission is extremely sensitive to the local

environment, which makes it useful for studies of protein conformation and ligand binding.[119] For those proteins which contain only one tryptophan, such as human serum albumin (HSA), monitoring changes in protein configuration or biochemical interactions are very simple as there is no overlapping fluorescence signals from other residues.[124,125]

Extrinsic fluorescence occurs from fluorophores that are bound to specific reactive residues within proteins (normally lysine or cysteine). The advantage of extrinsic labeling is the ability to use longer excitation and emission wavelengths, which may help to avoid interferences, and the ability to change the nature of the probe to allow different kinds of information to be obtained (polarity, dynamics, etc).[119] Care must be taken when labeling biomolecules with fluorophores to ensure that all free dye residue is removed from the labeled product to ensure that the results are only due to the bound dye.[119,126]

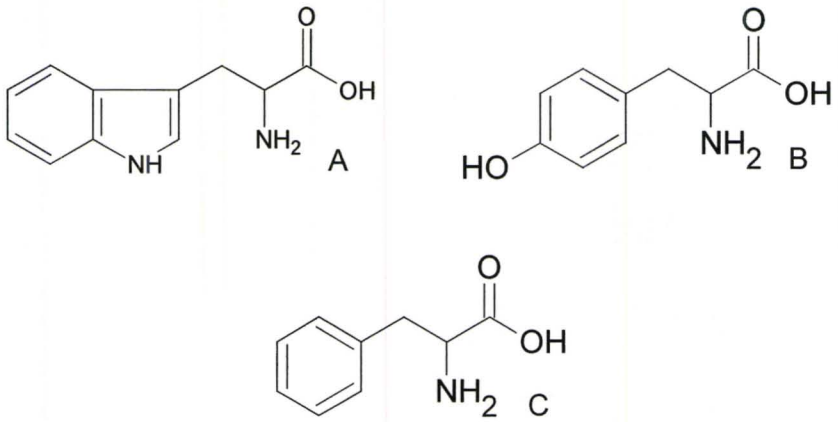

Figure 2.10: The three naturally fluorescent amino acid residues found in proteins. (A) tryptophan, (B) tyrosine and (C) phenylalanine.

The intensity of fluorescence emission, F(λ), is dependent on several factors including the excitation power, P_o; a wavelength dependent instrument correction factor, *k*; the molar extinction coefficient of the fluorophore, ε; the optical path length, *b*; the molar concentration of the fluorophore, *c*, and s the wavelength independent quantum yield of the probe, Φ, which is the ratio of radiative photons to absorbed photons and is a measure of the probability of fluorescence. These factors are related in Equation 2.2:

$$F(\lambda) = 2.303P_o k\varepsilon bc\Phi \qquad \text{Equation 2.2}$$

In many cases, the values P_o, k, ε, b and c are constant, and thus the fluorescence intensity is directly proportional to Φ, which is common for most protein studies.[119]

In addition to protein fluorescence, it is possible to use free fluorophores to probe various aspects of sol-gel materials. Many fluorophores are sensitive to the polarity of the solvent within sol-gel materials. Generally fluorophores exhibit red shifts as solvent polarity increases. These shifts result from interactions of the dipole moment of the fluorophore with that of the solvent molecules. In addition, shifts can occur due to specific chemical interactions between the fluorophore and solvent molecules or the silica matrix itself.[119] Interactions between the solvent and fluorophore can affect changes in the energy difference between the absorption and emission bands. These differences can be approximated by the Lippert equation (Equation 2.3):

$$\nu_a - \nu_f = \frac{2}{hc}\left(\frac{\varepsilon - 1}{2\varepsilon + 1} - \frac{n^2 - 1}{2n^2 - 1}\right)\frac{(\mu^* - \mu)^2}{a^3} + \text{constant} \qquad \text{Equation 2.3}$$

where ν_a is the absorbance maximum, ν_f is the emission maximum, and the difference between them is a function of the refractive index (*n*, a measure of electronic polarizability) and the dielectric constant (ε, a measure of orientational polarizability) of the solvent. In this equation *h* is Planck's constant; *c* is the speed of light; *a* is the radius of the cavity in which the fluorophore resides, μ is the dipole moment of the fluorophore in its ground state configuration, μ^* is the dipole moment of the fluorophore in its excited state configuration and the constant is the inherent Stokes' shift. From this equation, it can be seen that higher values of *n* or ε will result in larger shifts in wavenumbers and consequently greater red shifts in emission wavelength.[119]

In order to gain a better understanding about the effect of solvent on specific fluorophores, an examination of the Lippert equation is necessary. The effects of solvent can be divided into two different categories: general solvent effects and specific solvent effects.[119] General solvent effects, which are described by the Lippert equation, are always present while specific solvent effects such as those arising from chemical interactions between solvents and probes are more specific to a given solvent. The reorientation of a dipolar solvent around the excited state dipole moment of a fluorophore will lower the excited state energy, causing the emission wavelength to shift to the red. This is the general solvent effect, and is the predominant effect controlling the emission properties of probes such as PRODAN.[127] On the other hand, protonation of a

fluorescent molecule, either in the ground or excited state, leads to a large alteration in the electronic configuration of the molecule and can lead to very large changes in emission wavelength which do not reflect solvent polarity. This is the basis of the wavelength shifts observed for the fluorescent probe SNARF -1 (see below), and provides a convenient method for monitoring changes in pH within sol-gel derived materials.

Probes used in this study: A variety fluorophores can be doped into sol-gel derived materials to probe various aspects of the materials. In this study, (6-propionyl-2-dimethylaminonaphthalene (PRODAN)) was used to probe the internal polarity of sol-gel materials,[60] while fluorescein and carboxy seminaphtharhodafluor-1 (SNARF-1) were used to probe the pH within sol-gel materials. Another fluorophore, Rhodamine 6G, (R6G), was used for fluorescence microscopy studies, as it is known to partition strongly to unmodified silica surfaces, which can provide a means to image chemical heterogeneticy within sol-gel materials.[100,128,129] The structures of these four fluorophores, which are used in this thesis, are shown in Figure 2.11.

PRODAN was selected as the fluorophore of choice to monitor changes in the solvent polarity within the pores of the sol-gel derived matrix. PRODAN undergoes significant emission spectral shifts depending on its surrounding solvent environment, ranging from 401 nm in a non-polar environment such as cyclohexane to 530 nm in a polar solvent such as water.[127] As the solvent evaporates from within the pores, it is

possible to monitor the change in solvent polarity, which in turn can have a dramatic influence on entrapped biomolecules.

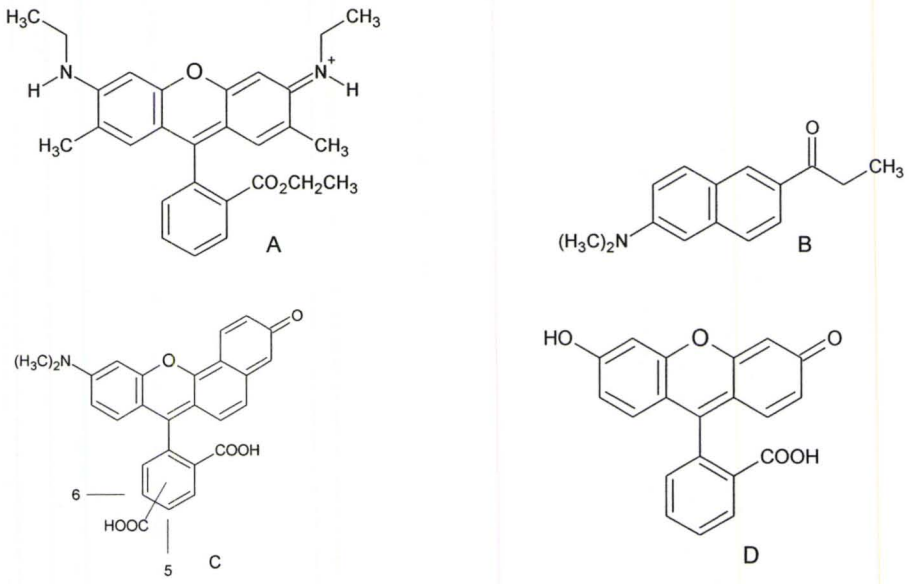

Figure 2.11: Fluorophores used within this thesis. (a) Rhodamine 6G, (b) PRODAN, (c) SNARF-1 and (d) Fluorescein.

Two fluorophores which are influenced by changes in internal pH were selected to observe changes in pH within sol-gel materials; fluorescein and SNARF-1. Fluorescein is an anionic probe which undergoes an increase in emission intensity as the pH becomes more basic owing to changes in the quantum yield of this fluorophore.[130] At elevated pH, the monoanionic form of fluorescein is converted to its dianionic form causing a change of quantum yield from 0.37 to 0.93 respectively. SNARF-1 is a

cationic pH sensitive probe,[131] and has two emission maxima, one corresponding to the acidic form of the probe and the other to the basic form. An advantage of this probe is the ability to use the ratio of intensity of the acidic and basic emission maxima to measure pH of the surrounding solution, which can avoid issues with leaching or photobleaching of the probe.

2.7 Biological assays in sol-gel derived materials

Many different biomolecules can be entrapped within sol-gel derived matrices to allow for detailed biophysical studies of the effects of entrapment on protein performance, or to develop biologically selective sensors.[2,19,26,27,28] Among the many proteins that have been examined for sensor development are three that were chosen for study in this thesis. Human Serum Albumin (HSA), as well as the related bovine serum albumin, has been widely studied in solution and sol-gel materials,[84,125,132] and there is significant background information on the conformation, dynamics, thermodynamic stability, ligand binding properties and long-term stability of the protein when entrapped in sol-gel silica materials.[38,63,120,125] However, there is only one previous study describing the behavior of this protein when entrapped in sol-gel derived organic-inorganic materials[47] and no studies of this protein in nanocomposite films. The presence of a single Trp residue, along with the availability of a simple fluorescence-based ligand binding assay, make this a useful model protein to derive information on the effects of different organically modified materials on protein properties.

For the development of prototypical biosensors, the model enzymes urease and lipase were chosen. Both of these enzymes have been widely studied in a variety of sol-gel materials,[96,133,134,135] and both catalyze well understood reactions that can be monitored using a variety of methods. In this present work, fluorescence is used to monitor pH changes that result from hydrolysis of the substrates urea (urease) or glyceryl tributyrate (lipase). In the case of urease, the reaction results in the formation of ammonium carbonate, and a resultant shift toward basic pH. In the case of lipase, the reaction produces glycerol and butyric acid, causing a shift toward acidic pH. The reaction schemes of both the urease and lipase are shown in Figure 2.12.

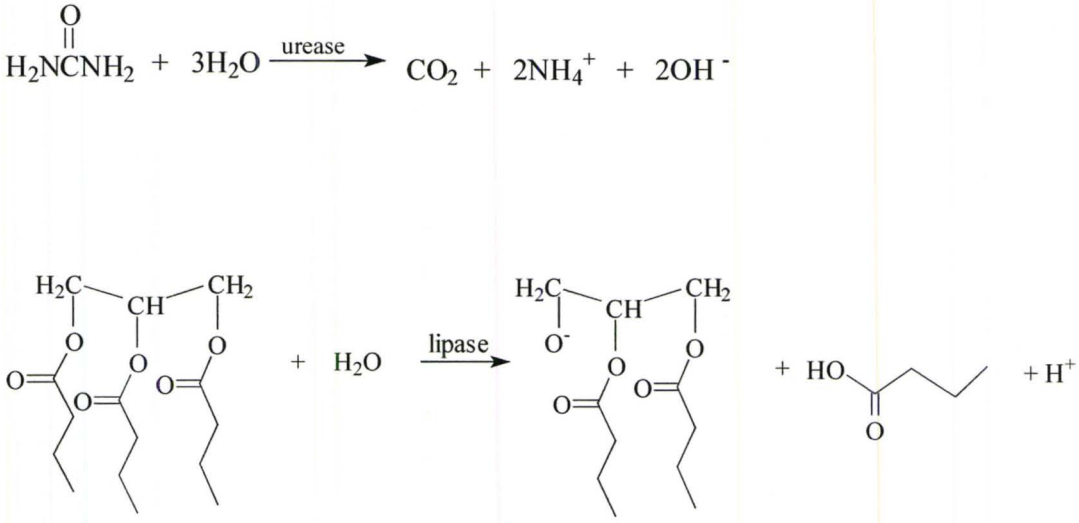

Figure 2.12: The reactions catalyzed by urease and lipase.

These two enzymes also provide the ability to assess the effects of the sol-gel materials on a hydrophilic protein (urease) relative to a lipophilic enzyme (lipase). Through changes in the internal polarity of sol-gel derived materials, it should be possible to determine if more hydrophobic environments enhance the activity of more lipophilic proteins, and if other factors, such as partitioning of substrates or the response of the pH dependent probes, are affected by the presence of organic dopants.

2.8 References

1. Lehninger, A. L., Nelson, D. L., and M. M. Cox. *Principles of Biochemistry* 2nd ed. New York: Worth Publishers, **1993**, Chapters 3, 6-8.

2. Jin, W. and J. D. Brennan. *Anal. Chim. Acta* 461 (2002): 1.

3. Collings, A. F. and F. Caruso. *Rep. Prog. Phys.* (1997): 1397.

4. Andrade, J.D.; Hlady, V. and A. P. Wei. *Pure Appl. Chem.* **64** (1992): 1777.

5. Weetall, H.H. *App. Biochem. Biotechnol.* **41** (1993): 157.

6. Turkova, J. *J. Chromat. B.* **722** (1999): 11.

7. Cox, C. J.; Hayhurst, A.; Hesselberth. J.; Bayer, T. S.; Georgiou, G.; and A. D. Ellington. *Nucleic Acids Research.* **30** (2002): e108.

8. Doretti, L., Ferrara, D., and S. Lora. *Biosens.Bioelectron.* **8** (1993): 443.

9. O'Driscoll, K.F. *Meth. Enzymol.* **44** (1976): 169.

10. Scouten, W.H. *Meth. Enzymol.* **135** (1987): 30.

11. Trevan, M. D. in *Immobilized Enzymes: An Introduction and Applications in Biotechnology*. New York: John Wiley and Sons, **1980**, 1.

12 Ingersoll, C.M. and F.V. Bright. *Anal. Chem.* **69** (1997): 403A.

13. Holthoff, E. L. and F.V. Bright. *Acc. Chem. Res.* **40** (2007): 756.

14. Tozzi, C.; Anfossi, L. and G. Giraudi. *J. Chromat. B.* **797** (2003): 289.

15. Turkova, J. *J. Chromat. B.* **722** (1999): 11.

16. Allard, L.; Cheynet, V.; Oriol, G.; Mandrand, B.; Delair, T. and F. Mallet. *Biotechnol. Bioeng.* **80** (2002): 341.

17. Dave, B. C.; Dunn, B.; Valentine, J. S. and J. I. Zink. *Anal. Chem.* **66** (1994): 1120A.

18. Brinker, C. J., and G. W. Scherer. *Sol- Gel Science: The Physics and Chemistry of Sol-Gel Processing*. New York: Academic Press Inc, **1990**.

19. Gill, I. *Chem. Mater.* **13** (2001): 3404.

20. Doong, R., and H. Shih. *Biosens. Bioelectron.* **22** (2006): 185.

21. Sampanthar, J. T. and H.C. Zeng. *Chem. Mat.* **13** (2001): 4722.

22. Anast, M.; Jamting, Å.; Bell, J.M. and B. Ben-Nissan. *Thin Solid Films* **253** (1994): 303.

23. Niesen, T.P.; De Guire, M. R.; Bill, J.; Aldinger, F.; Rühle, M.; Fischer, A.; Jentoft, F. C. and R. Schlögl. *J. Mater. Res.* **14** (1999): 2464.

24. Xagas, A.P.; Androulaki, E.; Hiskia, A. and P. Falaras. *Thin Solid Films* **357** (1999): 173.

25. Quinet, M.; Neveu, B.; Moutarlier, V.; Audebert, P. and L. Ricq. *Progress in Organic Coatings* **58** (2007): 46.

26. Pierre, A.C. *Biocat. Biotrans.* **22** (2004): 145.

27. Avnir, D.; Coradin, T.; Lev. O. and J. Livage. *J. Mater. Chem.* **16** (2006): 1013.

28. Coradin. T.; Boissiere, M. and J. Livage. *Curr. Med. Chem.* **13** (2006): 99.

29. Hench, L. L. and J, K. West *Chem. Rev.* **90** (1990): 33.

30. Braun, S.; Rappoport, S.; Zusman, R.; Avnir, D. and M. Ottolenghi *Mater. Lett.* **10** (1990): 1.

31. Ellerby, L. M.; Nishida, C.R.; Nishida, F.; Yamanaka, S.A.; Dunn, B.; Valentine, J.S.; and J. I. Zink. *Science* **255** (1992): 1113.

32. Besanger T.R. and J.D. Brennan. *J. Sol-Gel Sci. Tech.* **40** (2006): 209.

33. Gupta R. and N.K. Chaundrey. *Biosens. Bioelectron.* **22** (2007): 2387.

34. J.D. Brennan. *Acc. Chem. Res.* **40** (2007): 827.

35. Avnir, D.; Coradin, T.; Lev, O. and J. Livage. *J. Mat. Chem.* **16** (2006): 1013.

36. Gill, I. and A. Ballesteros. *Trends Biotechnol.* **18** (2000): 469.

37. Gill, I. and A. Ballesteros. *Trends Biotechnol.* **18** (2000): 282.

38. Flora, K.K.; Dabrowski, M.A.; Musson, S.P. and J.D. Brennan. *Can. J. Chem.* **77** (1999): 1617.

39. Cruz-Aguado, J.; Chen, Y.; Zhang, Z.; Elowe, N.; Brook, M.A. and J.D.Brennan. *J. Am. Chem. Soc.* **126** (2004): 6878.

40. Chen, Q.; Kenausis, G.L. and A. Heller. *J. Am. Chem. Soc.* **120** (1998): 4582.

41. Heller, J. and A. Heller. *J. Am. Chem. Soc.* **120** (1998): 4586.

42. Baker, G.A.; Jordan, J.D. and F.V. Bright. *J. Sol-Gel Sci. Technol.* **11** (1998): 43.

43. Baker, G.A.; Pandey, S.; Maziarz III, E.P. and F.V. Bright. *J. Sol-Gel Sci. Technol.* **15** (1999): 37.

44. Lesot, P.; Chapuis, S.; Bayle, J.P.; Tault, J.; Lafontaine, E.; Campero A. and P. Judeinstein. *J. Mater. Chem.* **8** (1998): 147.

45. Keeling-Tucker, T.; Rakic, M.; Spong, C. and J.D. Brennan. *Chem. Mater.* **13** (2000): 3695.

46. Reetz, M.T.; Zonta, A. and J. Simplekamp. *Biotechnol. Bioeng.* **49** (1996): 527.

47. Brennan, J.D.; Hartman, J.S.; Illnicki, E.I. and M. Rakic. *Chem. Mater.* **11** (1999): 1853.

48. Wittouck, N.; De Schryver, F. and I. Snijkers-Hendrickx, *J. Sol-Gel Sci. Technol.* **8** (1997): 895.

49. Avci, G.G. and D. Abanoz. *Key Engineering Materials* **264-268** (2004): 387.

50. Tang, Y.; Finlay, J.A.; Kowalke, G.L.; Meyer, A.E.; Bright, F.V.; Callow, M.E.; Callow, J.A.; Wendt, D.E. and M.R. Detty. *Biofouling* **21** (2005): 59.

51. Harada, Y. *Bio Industry* **22** (2005): 66.

52. Kauffmann, C. and R.T. Mandelbaum. *J. Biotechnol.* **62** (1998): 169.

53. Reetz, M.T.; Zonta, A.; Simpelkamp, J.; and W. Konen. *Chem. Commun.* (1996): 1397.

54. Reetz, M.T.; Zonta, A.; and J. Simpelkamp. *Agnew. Chem. Int. Ed. Engl.* **34** (1995): 301.

55. Kuncova, G.; Guglielmi, M.; Dubina, P.; and B. Safar *Collect. Czech. Chem. Commun.* **60** (1995): 1573.

56. Wang, B.; Li, B.; Deng, Q.; and S. Dong. *Anal. Chem.* **70** (1998): 3170.

57. Wang, B.; Li, B.; Wang, Z.; Xu, G.; Wang, Q.; and S. Dong. *Anal. Chem.* **71** (1999): 1935.

58. Altstein, M.; Segev, G.; Aharonson, N.; Ben-Aziz, O.; Turniansky, A. and D. Avnir. *J. Agric. Food Chem.* **46** (1998): 3318.

59. Bhatia, R.B.; Brinker, C.J.; Gupta, A.K. and A.K. Singh. *Chem. Mater.* **12** (2000): 2434.

60. Flora, K.K. and J.D. Brennan. *J. Phys. Chem. B.* **105** (2001): 12003.

61. Goring, G.L.G. and J.D. Brennan. *J. Mater. Chem.* **12** (2002): 3400.

62. Huang, M.H.; Dunn, B.S.; Soyez, H. and J.I. Zink. *Langmuir* **14** (1998): 7331.

63. Flora, K.K. and J.D. Brennan. *Analyst* **124** (1999): 1455.

64. Hodgson, R.; Chen, Y.; Zhang, Z.; Tleugabulova, D.; Long, H.; Zhao, X.; Organ, M.G.; Brook, M.A. and J.D. Brennan. *Anal. Chem.* **76** (2004): 2780.

65. Kovarik, P.; Hodgson, R.J.; Covey, T.; Brook, M.A. and J.D. Brennan. *Anal. Chem.* **77** (2005): 3340

66. Striova, J.; Higgins, D.A. and M.M. Collinson. *Langmuir* **21** (2005): 6137.

67. Besanger, T.R.; Hodgson, R.J.; Guillon, D.and J.D. Brennan. *Anal. Chim. Acta* **561** (2006): 107.

68. Nakanishi. K.; Kaji, H. and S. Naohiro. *Ceram. Transactions* **31** (1993): 51.

69. Nakanishi, K. *J. Porous Mat.* **4** (1997): 67.

70. Nishida, F.; McKiernan, J.M.; Dunn, B.; Zink, J.I.; Brinker, J.C. and A.P. Hurd. *J. Am. Ceram. Soc.* **78** (1995): 1640.

71. Kanamori, J.; Nakanishi, K.; Hirao, K. and H. Jinnai. *Coll. Surf. A* **241** (2004): 215.

72. Hara, T.; Kobayashi, H.; Ikegami, T.; Nakanishi, K. and N. Tanaka. *Anal. Chem.* **78** (2006): 7632.

73. Wang, H.; Bardo, A. M.; Collinson, M. M. and D.A. Higgins. *J. Phys. Chem. B.* **102** (1998): 7231.

74. Makote, R. and M.M. Collinson. *Anal. Chim. Acta* **394** (1999): 195.

75. Wei, H. and M.M. Collinson. *Anal. Chim. Acta* **397** (1999): 113.

76. Mei, E.; Bardo, B. A.; Collinson, M.M. and D.A. Higgins. *J. Phys. Chem. B* **104** (2000): 9973.

77. Howells, A.R.; Zambrano, P.J. and M.M. Collinson. *Anal Chem.* **72** (2000): 5265.

78. Bardon, A.M.; Collison, M.M. and D.A. Higgins. *Chem. Mater.* **13** (2001): 2713.

79. Higgins, D.A.; Collinson, M.M.; Saroja, G. and A.M. Bardo. *Chem. Mater.* **14** (2002): 3734.

80. Fu, Y.; Collinson, M.M. and D. A. Higgins *J. Am. Chem. Soc.* **126** (2004): 13838.

81. Wetzel, D.L.; Striova, J.; Higgins, D.A. and M.M. Collinson. *Vibrat. Spectr.* **35** (2004): 153.

82. Martin-Brown, S.A.; Fu, Y.; Saroja, G.; Collinson, M.M. and D.A. Higgins. *Anal. Chem.* 77 (2005): 486.

83. Striova, J.; Higgins, D.A. and M.M. Collinson. *Chem. Mater.* **21** (2005): 6137.

84. Gulcev, M.D.; Goring, G.L.G.; Rakic, M. and J.D. Brennan. *Anal. Chim. Acta*, **457** (2002): 47.

85. Guglielmi, M; Colombo, P.; Peron, F. and L. M. D. Esposti. *J. Mat. Sci.* **27** (1992): 5052.

86. Battisha, I.K.; Afify, H.H. and Y. Badr. *J. Sol-Gel Sci. Technol.* **25** (2002): 5.

87. Gupta, R.; Mozumdar, S. and N.K. Chaudhury. *Biosens. Bioelectron.* **20** (2005) 1358.

88. Gupta, R.; Mozumdar, S. and N.K.Chaudhury. *Biosens. Bioelectron.* **21** (2005): 549.

89. Huang, M.H.; Soyez, H.; Dunn, B.S. and J.I. Zink. *Chem. Mater.* **12** (2000): 231.

90. Butler, T.M.; MacCraith, B.D. and C. McDonagh. *J. Non-Cryst. Solids* **224** (1998): 249.

91. Rughini, G.C. and S.J. Pelli. *J. Sol-Gel Sci. Technol.* **8** (1997): 991.

92. Hodgson, R.J.; Brook, M.A. and J.D. Brennan. *Anal. Chem.* 77 (2005): 4300.

93. Nashida, F.; NcKiernan, J. M.; Dunn, B.; Zink, J. I.; Brinker, C. J. and A. J. Hurd. *J. Am. Ceram. Soc.* **78** (1995): 1640.

94. Dunawila, D. D.; Torgerson, B. A.; Chang, C. K. and K. A. Berglund. *Anal. Chem.* **66** (1994): 2739.

95. Narang, U.; Prasad, P.N.; Bright, F.V.; Kumur, A.; Kumur, N.D.; Malhotra, B. M.; Kamalasanan, M.N. and S. Chandra. *Chem. Mater.* **6** (1994): 1596.

96. Narang, U.; Prasad, P.N.; Bright, F.V.; Ramanathan, K.; Kumar, N.D.; Malhotra, B.D.; Kamalasanan, M.N. and S. Chandra. *Anal. Chem.* **66** (1994): 3139.

97. Jordan, J.D.; Dunbar, R.A. and F.V. Bright. *Anal. Chim. Acta* **332** (1996): 83.

98. Dong, H. and J.D. Brennan. *Chem. Mat.* **18** (2006): 4176.

99. Dong, H. and J.D. Brennan. *Chem. Mat.* **18** (2006): 541.

100. Tleugabulova, D.; Duft, A.M.; Zhang, Z.; Chen Y.; Brook, M.A. and J.D. Brennan. *Langmuir* **20** (2004): 5924.

101. Gilliliand, J.W.; Yokoyama, K. and W. T.Yip. *J. Phys. Chem. B* **109** (2005): 4816.

102. Martyn, T.A.; Moore, J.L.; Halterman, R.L. and W.T. Yip. *J. Am. Chem. Soc.* **129** (2007): 10338.

103. Gilliland, J.W.; Yokoyama, K. and W.T. Yip. *Chem. Mat.* **17** (2005): 6702.

104. Viteri, C.R.; Gilliland, J. W. and W.T. Yip. *J. Am. Chem. Soc.* **125** (2003): 1980.

105. Li, Y. and W.T. Yip. *Langmuir* **20** (2004): 11039.

106. Gilliland, J.W., Yokoyama, K. and W.T. Yip. *Chem. Mat.* **16** (2004): 3949.

107. Cabreara, K.; Lubda, D.; Eggenweiler, H.-M.; Minakuchi, H. and K. Nakanishi. *J. High Resolut.* **23** (2000): 93.

108. Nakanishi, K.; Shikata, H.; Ishizuka, N.; Koheiya, N. and N. Soya. *J. High Resolut.* **23** (2000): 106.

109. Ishizuka, N.; Minakuchi, H.; Nakanishi, K.; Soga, N. and N. Tanaka. *J. Chromatogr. A.* **797** (1998): 133.

110. Tanaka, N.; Nagayama, H.; Kobayashi, H.; Ikegami, T.; Hosoya, K.; Ishizuka, N.; Minakuchi, H.; Quirino, J.P.; Dulay, M.T. and R.N. Zare. *Anal. Chem.* **73** (2001): 5557.

111. Motokawa, M.; Kobayashi, H.; Ishizuka, N. Minakuchi, H. Nakanishi, K. Jinnai, H.; Hosoya, K.; Ikegami, T. and N. Tanaka. *J. Chromatogr. A.* **961** (2002) 53.

112. Magonov, S.N. and M.-H. Whangbo. *Surface Analysis with STM and AFM Experimental and Theoretical Aspects of Imaging Analysis*; VCH Publishers, Inc.: New York, 1996, Chapter 1.

113. Tersoff, J. In *Scanning Tunning Microscopy and Spectroscopy: Theory Techniques and Applications* (Bonnell, D.A.,ed.); VCH Publishers, Inc.: New York, 1993; Chapter 3.

114. Magonov, S.N. and M.-H. Whangbo. *Surface Analysis with STM and AFM Experimental and Theoretical Aspects of Imaging Analysis*; VCH Publishers, Inc.: New York, 1996, Chapter 2.

115. Burnham, N.A. and R.J. Colton. In *Scanning Tunning Microscopy and Spectroscopy: Theory Techniques and Applications* (Bonnell, D.A.,ed.); VCH Publishers, Inc.: New York, 1993; Chapter 7.

116. Amrein, M. In Procedures in Scanning Probe Microscopies(Coltron, R.J.; Engel, A.; Frommer, J.E.; Gaub, H.E.; Gewirth, A.A.; Gukenberger, R.; Rabe, J.; Heckl, W.M.; Parkinson, B. eds.) John Wiley & Sons: Chichester, 1998; Chapter 1.

117 Digital Instruments. *Scanning Probe Microscopy Training Notebook*, 1999.

118. Babcock, K.L. and C.B. Prater. *Phase Imaging: Beyond Topography*. Veeco Instruments Inc.
Website address: Http.www.google.com
Search: Phase Imaging: Beyond Topography [last checked12/19/07].

119. Lakowicz, J.R. Principles of Fluorescence Spectroscopy 2nd edition, Plenum Publishers, New York, 1999.

120. Flora, K.K.; Brennan, J.D.; Baker, G.A.; Moody, M.A. and F.V. Bright. *Biophysical J.* **75** (1998): 1084.

121. Geddes, C.D. and D.J.S. Birch. *J. Non-Cryst. Solids* **270** (2000): 191.

122. Birch, D.J.S. and C.D. Geddes. *Phys. Rev. E.* **62** (2000): 2977.

123. Geddes, C.D.; Karolin, J. and D.J.S. Birch. *J. Fluoresc.* **12** (2002): 113.

124. Zheng, L. and J.D. Brennan. *Analyst* **123** (1998): 1735.

125. Flora, K.K. and J.D. Brennan. *Chem. Mat.* **13** (2001): 4170.

126. Brennan. J.D. *Appl. Spectroscopy* **53** (1999): 106A.

127. Weber, G. and F. J. Ferris. *Biochem.* **18** (1979): 3075.

128. Tleugabulova, D.; Zhang, Z.; Chen, Y.; Brook, M.A. and J.D. Brennan. *Langmuir* **20** (2004): 848.

129. Tleugabulova, D.; Zhang, Z. and J.D. Brennan. *J. Phys. Chem. B.* **107** (2003) 10127.

130. Sjöback, R.; Nygren, J. and M. Kubista. *Spectrochim. Acta A* **51** (1995): L7.

131. Whitaker, J.E.; Haugland, R.P. and F.G. Prendergast. *Anal. Biochem.* **194** (1991): 330.

132. Sui, X.; Cruz-Aguado, J.A.; Chen, D.Y.; Zhang, Z.; Brook, M.A. and J.D. Brennan. *Chem. Mater.* **17** (2005): 1174.

133. Lee, W. Y.; Kim, S. R.; Kim, T. H.; Lee, K. S.; Shin, M.C. and J. K. Park. *Anal. Chim. Acta.* **404** (2000): 195.

134. Lee, W. Y.; Lee, K. S.; Kim, T. H.; Shin, M. C. and J. K. Park. *Electroanalysis* **12** (2000): 78.

135. Ogura, K; Nakaoka, K; Nakayama, M; Kobayashi, M. and A. Fujii. *Anal. Chim. Acta.* **384** (1999): 219.

Chapter 3: Effect of Ormosil and Polymer Doping on the Morphology of Separately and Co-hydrolyzed Silica Films Formed by a Two-Step Aqueous Processing Method

The following chapter has been accepted in the scientific journal *Chemistry of Materials* under the following citation:

Goring, Gillian L.G. and John D. Brennan. "Effect of Ormosil and Polymer Doping on the Morphology of Separately and Co-hydrolyzed Silica Films Formed by a Two-Step Aqueous Processing Method." *Chemistry of Materials* **19(22)** (2007): 5336-5346.

I was responsible for all experimental design, data collection, analysis and interpretation. I wrote the first draft of the manuscript and Dr. Brennan provided editorial input to generate the final draft of the paper.

3.0 Abstract

The entrapment of biomolecules within organic/inorganic nanocomposite materials derived by the sol-gel method has proven to be a viable route for development of biosensors and biocatalysts. However, the phase separation behaviour within nanocomposite materials formed by a protein compatible two-step aqueous processing method is not well understood. In this study, a range of imaging methods were used to assess the degree of heterogeneity in a series of dipcast thin films formed with different types and levels of ormosils in the presence and absence of polyethylene glycol (PEG), using both separate and co-hydolysis of precursors. Both microscopic (brightfield and fluorescence microscopy) and nanoscale (atomic force microscopy and scanning electron microscopy) imaging demonstrate that short chain monofunctional ormosils such as methyltriethoxysilane do not lead to significant heterogeneity when mixed with TEOS, while disubstituted (dimethyldimethoxysilane) or longer chain (isobutyltrimethoxysilane) ormosils show significant heterogeneity at the microscopic and nanoscopic scale when prepared by the separate hydrolysis method. Addition of PEG can improve homogeneity in some materials, likely due to the coating of silica sol particles which reduces microscopic phase separation, however co-hydrolysis of precursors provides a more general route to create homogeneous materials. Interestingly, the heterogeneity observed by brightfield microscopy, which reflects variations in refractive index, did not fully

correlate to fluorescence microscopy images of entrapped fluorophores and proteins, suggesting that chemical heterogeneity exists even when samples appear to be homogeneous. The implications of these findings for biosensor development will be discussed.

3.1 Introduction

The sol-gel processing method provides a facile route for fabrication of a range of materials, including organic-inorganic nanocomposites[1,2,3] and biologically doped composite materials.[4,5,6,7,8] In particular, there has been significant progress in the development of organically-modified silica materials that can be used to entrap lipophilic enzymes such as lipase,[9,10,11,12,13,14,15] or ligand binding proteins such as urease[15] and human serum albumin.[16,17,18] Such materials are typically formed from a mixture of one or more organosilanes with a tetraalkoxysilane, and often include one or more polymer additives to aid in protein stability. Such materials are generally prepared using a two-step processing method involving the addition of a buffered aqueous protein solution to a preformed silica sol, which helps to dilute alcohol formed during silane hydrolysis and also adjusts the pH to physiologically acceptable levels.[4,5,6,7,8] Although more recent methods utilize protein compatible precursors such as sodium silicate[19] or glycerated silanes[20,21,22] to avoid the production of alcohol during processing, such materials are

generally restricted to the formation of polar silica materials. Glycerated ormosils have been utilized for the fabrication of mesostructured materials,[23] but have not been utilized to form organic-inorganic biocomposites.

While significant progress has been made on the development of biologically-doped nanocomposites, one issue that has not been widely examined for such materials is the potential for phase separation of the organic and inorganic components as a result of poor miscibility of organic and inorganic silanes, differences in hydrolysis and condensation rates for organosilanes relative to tetraalkoxysilanes, and the solubility of polymer additives. Previous studies of phase separation within organic/inorganic silica composites have typically involved materials formed with high alcohol levels using processing conditions that were not suitable for protein entrapment.[24,25,26,27,28,29,30,31,32,33,34] These studies utilized fluorescence-based imaging methods and atomic force microscopy (AFM) to image phase separation within Class II ormosils, and showed that the type and loading of organosilane and the method used to process the material can have a dramatic affect on phase separation. These studies have inspired us to use similar methods to investigate the phase separation behaviour within Class I, Class II and Class I/II composite materials that are formed using protein compatible aqueous processing methods.

Our interest in investigating phase separation in protein-compatible nanocomposite materials arises from the impact of heterogeneity on a number of factors, such as: the mechanical properties of the material; the optical clarity of protein-doped materials (which can be important in the development of optical biosensors); protein performance (i.e., the local environment of protein, which can affect protein stability or interfacial activation of membrane-associated proteins); and the potential for solid-phase extraction of hydrophobic analytes into the film. The key differences between our materials and those studied previously by other groups are: 1) the use of a much higher water:silicon ratio during processing; 2) the use of a two-step acid/base processing method; 3) the sonication of silane precursors to accelerate hydrolysis; 4) the use of neutral pH conditions to perform the condensation reaction and; 5) the use of polymer additives to manipulate the phase separation process. Taken together, significant differences are expected in the phase separation behaviour in our materials relative to those examined previously.

In this study, we focus on the effect of the number and type of substituents on the organically modified silane, the organosilane doping level, the processing method (separate or co-hydrolysis of silanes), and the effect of low molecular weight polyethylene glycol additives on the phase separation within composite materials formed by a two-step aqueous processing method. All materials are formed as dipcast thin

films[35,36,37,38] and are examined by a range of imaging methods, including brightfield optical microscopy, scanning electron microscopy, phase contrast atomic force microscopy and confocal fluorescence microscopy of fluorophore-doped materials. The thin-film format was chosen owing to its relevance to the formation of optical sensors,[15,17,39,40,41] and because it is amenable to the various imaging methods. The imaging data are used to provide an overall picture of the factors influencing the phase separation process, the scale of the heterogeneity for different films, and the methods for controlling phase separation in protein compatible nanocomposite materials.

3.2 Experimental

Chemicals

Sodium silicate solution (SS, technical grade, 9% Na_2O, 29% silica, 62% water), tetraethyl orthosilicate (TEOS, 99.999+%), poly(ethylene glycol) (PEG, MW 600), methyltriethoxysilane (MTES, 98%), dimethyldimethoxysilane (DMDMS, 98%)], isobutyltrimethoxysilane (BTMS, Fluka 95%) and rhodamine 6G (R6G) were from Sigma Aldrich (Oakville, Ontario, Canada). Fisherbrand glass microscope slides were obtained from Fisher Scientific (Toronto, Canada), while glass microscope coverslips (12 mm diameter) were purchased from Ernest F. Fullam, Inc. (Lantham, NY, USA). All water was purified by reverse osmosis and deionized using a 4-stage Milli-Q water

purification system. All other chemicals and solvents used were of analytical grade and were used without further purification.

Procedures

Preparation of sol-gel derived films: Films are denoted based on the type of silane (Sodium silicate (S); TEOS (T), MTES (M); DMDMS (D); BTMS (B)), volume percent of ormosil (0 - 50%) in TEOS, amount of PEG 600 (0 – 8% v/v) and type of hydrolysis (separate (S) or co-hydrolysis (C)). Thus, a film denoted as B5P3-S refers to a film containing 5% (v/v) butyltrimethoxysilane in TEOS with 3% (v/v) of PEG 600 prepared using separately hydrolyzed silanes. Separately hydrolyzed materials were prepared by first generating sols from pure silane solutions (TEOS, MTES, DMDMS or BTMS), which were prepared by combining 4.5 mL of silane with 1.4 mL of water and 0.1 mL of 0.1 N HCl, followed by sonication at 0 °C for ~1 h until the mixture was visibly homogeneous. These silane solutions were stored on ice and used immediately in the preparation of dip-cast films. Appropriate amounts of the organosilanes were mixed with TEOS to form sols with organosilane:TEOS volume ratios ranging from 5% to 50%. Based on the results obtained from imaging studies of separately hydrolyzed materials, co-hydrolyzed precursor solutions containing MTES, DMDMS or BTMS were formed by adding an appropriate amount of organosilane to TEOS to provide organosilane:TEOS molar ratios of 50% MTES/TEOS, 15% DMDMS/TEOS, 5% BTMS/TEOS or 50%

BTMS/TEOS. 4.5 mL of the silane mixture was combined with 1.4 mL of water and 0.1 mL of 0.1 N HCl and sonicated at 0 °C until the mixture was visibly homogeneous. Sols were also prepared from sodium silicate to provide a control material with no potential for phase separation. In this system, 0.9 mL of sodium silicate was mixed with 4 mL of distilled deionized water and 2.2 g of Dowex resin (monosphere 650C) and allowed to stir for one minute. The mixture was then immediately filtered using a Büchner funnel and then passed through a 0.45 μm syringe-filter to remove large particles. All sols were stored on ice and used immediately to prepare sol-gel derived thin films.

For sodium silicate, separately and co-hydrolyzed sols, 0.5 mL of the sol solution was mixed with an equal volume of 10 mM Tris buffer (pH 7.2; with 100mM KCl) containing 0%, 6.0% or 16.0% (v/v) of PEG 600 (and optionally 2 μM R6G) and was placed into a Teflon casting well. A clean glass cover slip or microscope slide (8 x 32 mm) was mounted on a motorized dipcaster (Kibron Layer-X filmlift, Helsinki, Finland) with a vertically moving arm and was cast into the solution at 10 $mm \cdot min^{-1}$ and then withdrawn at a rate of 4 $mm \cdot min^{-1}$.[17] The cast films were suspended in air at room temperature for 10 minutes, and then placed into a disposable cuvette that was sealed with Parafilm and stored in the dark for 72 hr at 4 °C before testing, unless otherwise stated.

Instrumentation

Microscopy: Optical micrographs were obtained in brightfield mode using an Olympus microscope (BX51) with a 5x objective. A minimum of five images per sample was obtained from at least three independent samples and the most representative image is provided for each sample.

Samples imaged by scanning electron microscopy (SEM) were sputter-coated with gold (layer thickness 15 Å) to avoid charging effects prior to SEM imaging. A Philips SEM 515 with an operating voltage of 20kV was used to obtain images of the sol-gel derived films present on microscope slides, with a minimum of three images obtained per sample.

A Nanoscope III digital instruments scanning probe microscope was used in the tapping mode to obtain both low resolution (15 μm x 15 μm) and high resolution (500 nm x 500 nm) AFM images of sol-gel derived films dipcast onto circular microscope cover slips. Images were obtained using SiN_3 tips with a stiffness of 42N.m^{-1} and an average frequency of 300 kHz, and a set point ratio of 1.0 V. Tips were periodically checked against a sample of known structure in order to ensure that the obtained images were due to the sample and not a defective tip. The images were analyzed using NanoscopeIII v. 5.1r4 and SSIP software. Topography and phase images were obtained simultaneously for thin film samples in order to be able to compare changes in height and/or hardness

features within these samples. All images underwent auto plane fitting and flattening procedures.

Fluorescence microscopy was performed with a LSM 510 confocal fluorescence microscope (Carl Zeiss, Jena, Germany). The 488 nm output of an Argon ion laser was used to excite R6G-doped samples and a 505-550 nm band pass filter was used to collect the fluorescence emission. A 20x objective lens was used during the collection of the fluorescence micrographs, providing an image field of ca. 400 μm x 400 μm. Images were processed using false coloring to highlight the distribution of fluorescent species within the films.

3.3 Results and Discussion

Film preparation and physical properties

Film compositions were selected based on: 1) the size of the alkyl chain; 2) the number of organic groups on the silicon center; 3) the amount of polymer and; 4) separate or co-hydrolysis of silanes. This series of compositions allows us to examine the miscibility of the organosilane with TEOS, solvent, and polymer components, and to determine how the factors listed above contribute to the heterogeneity of the resulting films. Use of separate and co-hydrolysis of silanes also allows us to test if the pre-condensation of MTES or DMDMS to form methylsilsesquioxane (MSQ)[42,43,44,4546] or

polydimethylsiloxane (PDMS),[47] respectively, may influence the phase separation and/or aggregation behaviour relative to co-hydrolyzed systems, and if addition of low MW PEG influences this process (note that PEG 600 will not cause macroscopic phase separation in sol-gel materials). A control sample was also produced consisting of silica derived from sodium silicate. SS sols undergo rapid hydrolysis and contain neither alcohol hydrolysis products nor organic functional groups, and thus are expected to be able to produce highly homogeneous materials, unlike TEOS which could potentially undergo some phase separation owing to immiscibility of partially hydrolyzed silica oligomers with fully hydrolyzed and condensed silica species.

A particularly important aspect of our synthetic method relative to previously reported studies of silica nanocomposites is the use of "low alcohol" processing, which is often used to improve protein stability in sol-gel derived bioglasses.[19,20,21,22] Typically, our samples use a water:silicon (*R*-value) of ~4 for hydrolysis and *ca.* 20 for condensation. While alcohol is not added as a co-solvent, significant levels of alcohol are generated during hydrolysis, which can reach levels of up to 35% (v/v) for TEOS derived materials formed by the two-step processing method (assuming complete hydrolysis of the precursor).[48] Thus, there is still a significant amount of alcohol to aid in solubilizing separately hydrolyzed organosilanes. Other differences relative to previous studies include the use of sonication, which will accelerate the initial hydrolysis reaction, and the

addition of buffer to the hydrolyzed silane(s), which results in gelation over a period of 30 – 60 min, and thus does not allow significant time for separately hydrolyzed components to mix.

The physical properties of separately and co-hydrolyzed films prepared from the various precursors is provided in Table 3.1. The majority of the films were optically clear, as judged by eye. However, films containing the highest levels of ormosils (50% MTES, DMDMS or BTMS) were generally translucent, regardless of whether the samples were separately or co-hydrolyzed or whether they contained PEG. A similar trend was observed for monolithic samples prepared from the same compositions, the only exceptions being cases where samples with the highest ormosil levels often did not gel, particularly for co-hydrolyzed samples. The hardness of the films, as judged by the ability to scratch the film with a needle, also decreased as ormosil level increased, and again had no dependence of the hydrolysis method or presence of PEG. Most samples were not tacky, with the exception of samples containing high levels of MTES or BTMS, which also tended to be the softest samples. Taken together, the physical properties suggest that samples with the highest ormosil content, and thus the lowest degree of crosslinking, produce softer films and also produce the least optically clear materials, indicative of local phase separation, which leads to variations in refractive index within the material.

Table 3.1: Properties of separately and co-hydrolyzed films.

Composition	Optical Quality	Hardness	Tackiness	Wettability (Contact Angle)	Appearance of Monolith
SSP0	Clear	Hard	Not tacky	70°	Clear
SSP3	Clear	Hard	Not tacky	60°	Clear
TP0	Clear	Hard	Not tacky	60°	Clear
TP3	Clear	Hard	Not tacky	70°	Clear
20MP0-S	Clear	Hard	Not tacky	120°	Clear
20MP3-S	Clear	Hard	Slightly	115°	Clear
50Mp0-S	Clear	Semi hard	Slightly	90°	White/DNG
50MP3-S	Translucent	Soft	Not tacky	70°	Translucent
2.5DP0-S	Clear	Hard	Not tacky	60°	Clear
2.5DP3-S	Clear	Hard	Not tacky	75°	Clear
15DP0-S	Clear	Semi hard	Not tacky	90°	Clear/ trans
15DP3-S	Clear	Hard /	Not tacky	75°	Translucent
50DP0-S	Translucent	Soft	Not tacky	60°	Translucent
50DP3-S	Translucent	Hard	Not tacky	70°	Translucent
5BP0-S	Clear	Hard	Not tacky	70°	Clear
5BP3-S	Clear	Soft	Not tacky	60°	Clear
50BP0-S	Translucent	Semi hard	Not tacky	90°	Translucent
50BP8-S	Translucent	Hard	Not tacky	70°	Translucent
20MP0-C	Clear	Hard	Not tacky	125°	Clear
M20P3-C	Clear	Soft	Not tacky	140°	Clear
50MP0-C	Translucent	Soft	Not tacky	120°	Translucent
50MP3-C	Translucent	Soft	Not tacky	140°	Translucent
2.5DP0-C	Clear	Hard	Not tacky	160°	Clear
2.5DP3-C	Clear	Hard	Not tacky	135°	Clear
15DP0-C	Clear	Hard	Not tacky	135°	Trans / white
15DP3-C	Clear	Semi hard	Not tacky	95°	Trans / white
50DP0-C	Translucent	Semi hard	Not tacky	140°	Did not gel
50DP3-C	Translucent	Hard	Not tacky	110°	Did not gel
5BP0-C	Clear	Hard	Not tacky	90°	Clear
5BP3-C	Clear	Semi hard	Not tacky	90°	Clear
50BP0-C	Clear	Soft	Slightly	135°	Did not gel
50BP8-C	Translucent	Soft	Slightly	120°	Did not gel

Brightfield optical microscopy

Brightfield optical micrographs of the various sol-gel derived films were obtained to determine how the presence of organically modified silanes and PEG affected the homogeneity of films at the microscopic level. This method images the entire film (not only the surface) and provides information on refractive index changes, which are assumed to reflect underlying variations in chemical properties and thus phase separation. Image 3.1 shows images of films prepared either from single precursors (TEOS or SS) with or without polymer or by mixing different proportions of separately hydrolyzed TEOS and MTES in the presence and absence of PEG. Both SS and TEOS samples are relatively homogeneous, with only a few small features on the <50 μm scale evident in TEOS films. Addition of PEG to either material did not lead to an observable change in film homogeneity, consistent with good miscibility of PEG 600 with the silica. The slightly more heterogeneous appearance of TEOS based films may relate to the presence of a mixture of partially and fully hydrolyzed/condensed ethoxysilane species, which may not be fully miscible with each other.

Addition of low levels of MTES (up to 20%) to TEOS via the combination of separately hydrolyzed silanes did not lead to an increase in heterogeneity of the film. Although such films did show some small features that may be due either to dust particles or gas bubbles, the latter of which could be formed as a result of the heat of mixing the

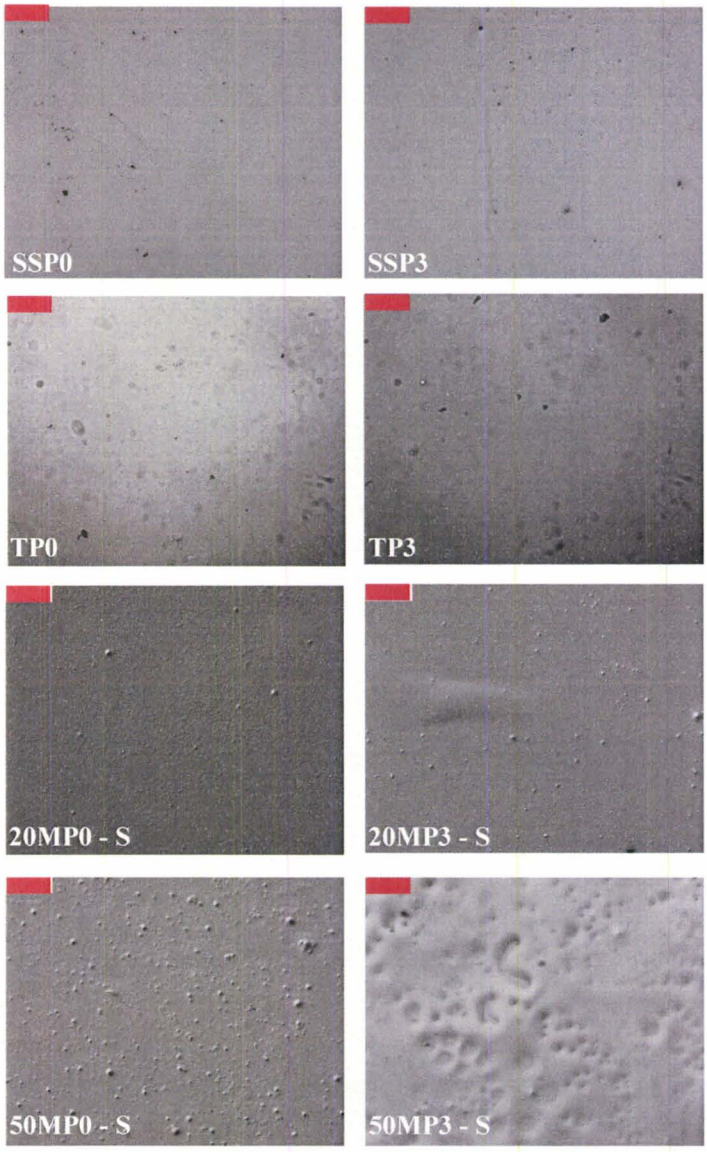

Image 3.1: Optical micrographs of separately hydrolyzed silane compositions containing either 0 (SS or T) or 1 (M) methyl functional group per silane molecule. Scale bars are 30 μm.

two silanes. Addition of PEG to films formed with 20% MTES did not appear to significantly alter the film morphology. Inclusion of higher levels of MTES (50%) led to a small but clearly increased level of phase separation, with further addition of polymer providing further phase separation. In this latter system it is likely that a range of MSQ species, including linear and cyclic oligomers, are present in the MTES sol,[49,50] while small linear and branched silica species with an average radius of *ca.* 1 nm are present in the TEOS sol prior to mixing of the components.[51] Upon mixing and addition of water, it is expected that the cyclic MSQ materials will be immiscible with the polar solvent, and should phase separate. However, this process is relatively slow (based on the fact that the bulk MTES:TEOS material does not show rapid phase separation or precipitation), and thus minimal phase segregation is observed prior to casting of the film. As the film undergoes very rapid loss of solvent (< 5 min),[17,52] the initial morphology of the film is locked in almost at the point of casting, leading to a relatively homogeneous film. The increase in film heterogeneity upon addition of PEG may relate to poorer miscibility of MSQ with the PEG loaded solvent, or possibly with PEG coated silica nanoparticles.[53]

Image 3.2 shows images obtained for films obtained by mixing separately hydrolyzed sols formed from TEOS and either DMDMS or BTMS, and then mixing the resulting two component sol with aqueous buffer with and without PEG. The optical images demonstrate that phase separation increases as the level of DMDMS increases,

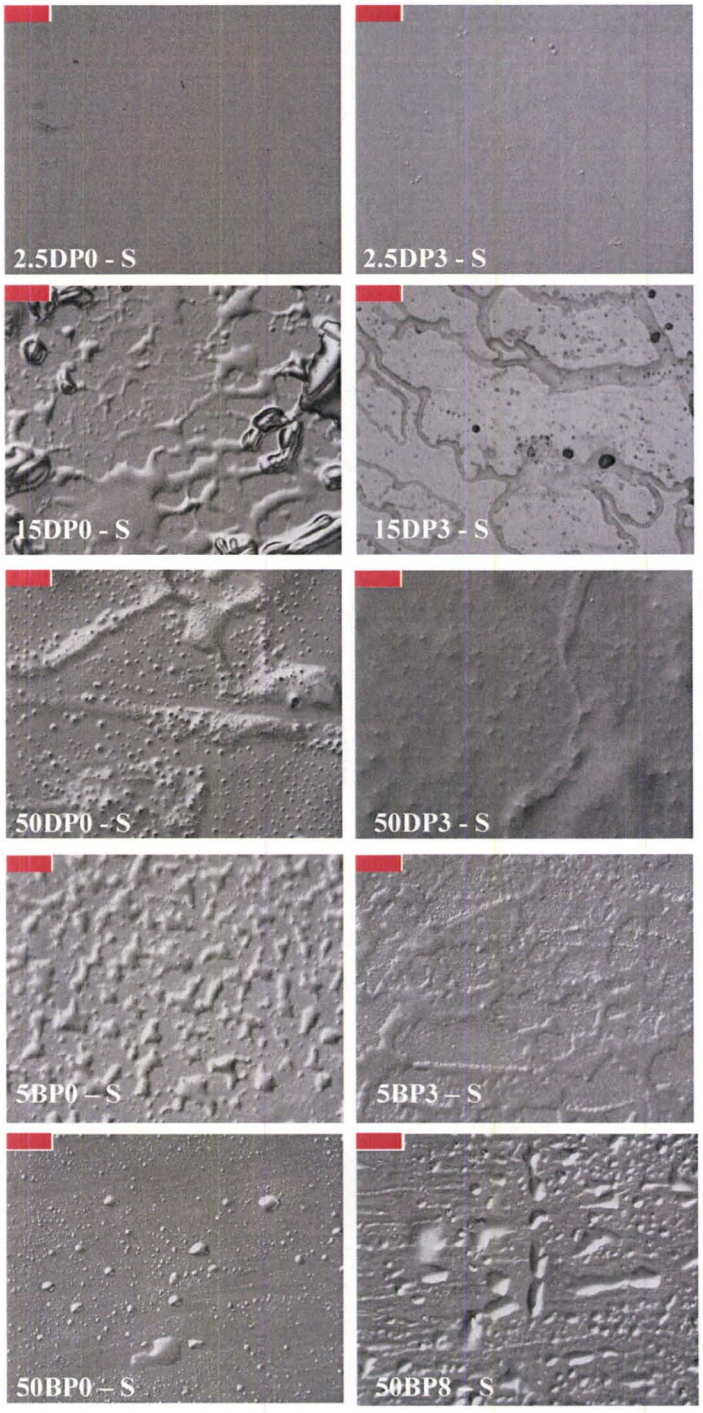

Image 3.2: Optical micrographs of separately hydrolyzed silane compositions containing either two methyl functional groups (D) or a butyl chain (B). Scale bars are 30 μm.

consistent with poor miscibility of linear PDMS with silica nanoparticles. However, it is interesting to note that addition of even low levels of PEG results in an apparent improvement in film homogeneity, particularly for samples containing an intermediate level of DMDMS. This observation suggests that PEG may be able to aid in co-solubilization of silica and PDMS, perhaps owing to the known ability of low MW PEG to coat the highly polar silica particles[53] and thus prevent immiscibility of PDMS with the silica.

Samples containing either low or high levels of BTMS show a different morphology than DMDMS doped samples, consisting mainly of small, well separated domains in BTMS doped films rather than a more continuous phase separated system in DMDMS doped materials. The longer alkyl chain in BTMS is more likely to form micellar structures in the aqueous solvent system[34] and may thus produce an emulsion upon mixing with TEOS derived sols that is then transferred onto the slide during casting. Increased levels of BTMS appear to produce a more homogeneous system (perhaps reflecting the dominance of the BTMS at higher levels, and thus less formation of an emulsion), while addition of PEG does not significantly reduce the heterogeneity in the material, suggesting that the polymer cannot solubilize the BTMS micelles within the silica/water system. It is noted that the significant level of phase separation in the separately hydrolyzed BTMS/TEOS materials is in agreement with earlier findings by

Higgins et al,[34] who observed heterogeneity in such materials using both single molecule fluorescence spectroscopy and tapping mode AFM.

Image 3.3 shows selected images of materials formed by co-hydrolysis of TEOS and an ormosil. Only those systems that showed significant phase separation under separate hydrolysis conditions are shown; all samples that were homogeneous using separate hydrolysis conditions were also homogeneous when co-hydrolyzed, as expected. An interesting finding was that all films formed by co-hydrolysis of silane precursors showed significantly improved homogeneity relative to the separately hydrolyzed counterparts, with some materials, such as the 15DP0-C and 5BP0-C compositions, appearing to be almost completely homogeneous except for pinhole defects, which likely arose due to bubble formation in the sol. These results agree with previous single molecule fluorescence and tapping mode AFM studies, which have demonstrated improved homogeneity for co-hydrolyzed materials relative to separately hydrolyzed materials, but show that this situation holds even in cases where biocompatible two step processing is used with high amounts of water. Thus, it should be possible to produce protein-doped films with a specific level of ormosil and generate either macroscopically heterogeneous or homogeneous films, depending on the specific requirements.

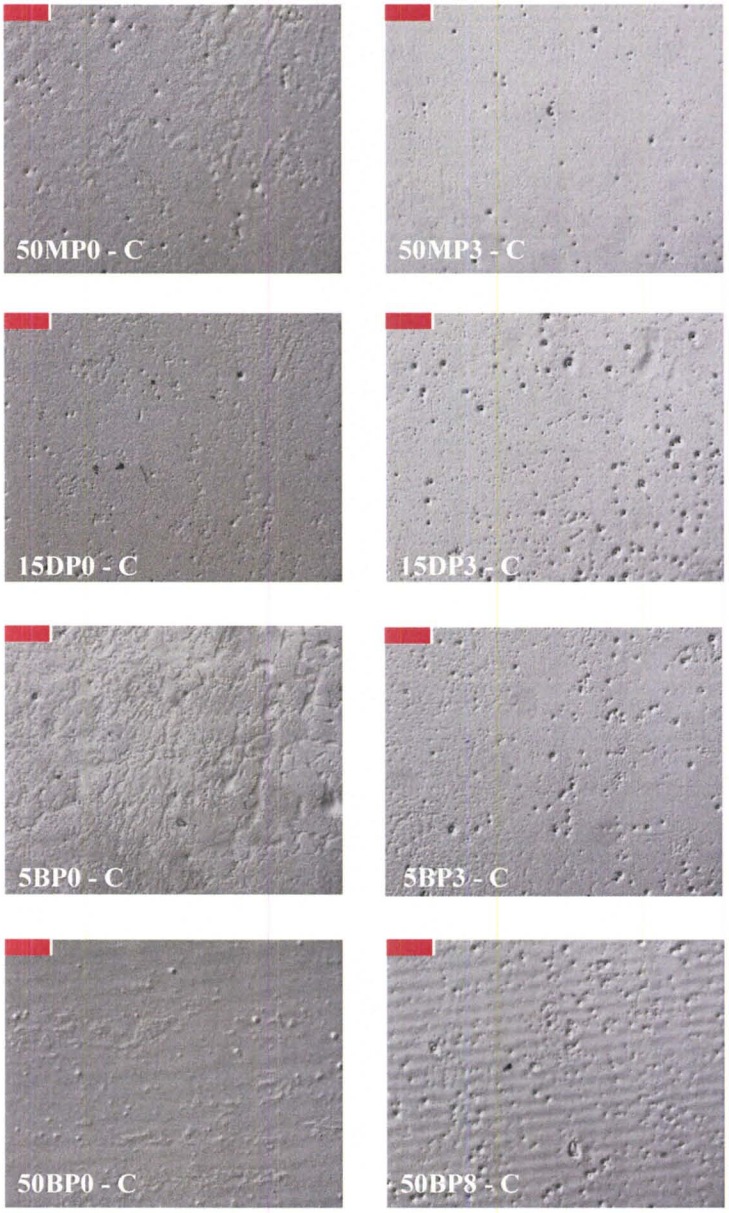

Image 3.3: Optical micrographs of co-hydrolyzed systems containing one (M) or two (D) methyl groups or a butyl group (B). Scale bars are 30 μm.

Fluorescence microscopy of entrapped R6G

While brightfield microscopy can give an indication of phase separation based on physical properties (i.e., variations in refractive index), it is of interest to determine if such phase separation is also manifested in a chemically relevant way based on partitioning of a fluorescent probe within the materials. Several previous studies, many based on single molecule spectroscopy, have shown that probes are distributed more heterogeneously in films that are derived from mixtures of silanes relative to those derived from a single silane.[24,25,26,27,28,29,30,31,32,33,34,54] R6G was chosen for our imaging study as it is now well established that in aqueous solution this cationic probe has a strong tendency to adsorb to anionic silica surfaces, and that modification of silica with either ormosils or PEG leads to partitioning of the probe to the solvent phase.[53.,55,56] Since R6G is added to the evolving sol, it should bind to silica nanoparticles and thus partition preferentially into the silica-rich phase. Images of pure TEOS or SS derived films showed a homogeneous brightfield (images not shown), indicative of the presence of a single chemical environment in such films. The presence of polymer did not produce an increase in heterogeneity of the probe distribution, indicating that PEG 600 did not induce any observable phase separation in TEOS or SS derived materials, consistent with brightfield images.

Image 3.4 shows fluorescence images of the R6G distribution in a variety of films derived by separate hydrolysis of silanes. The larger images show a wide field (1.3 mm x 1.3 mm), while the inset images show a higher magnification (80 μm x 80 μm). In general, the extent of phase separation observed by fluorescence is in good agreement with that observed by brightfield imaging. Films containing MTES show relatively good homogeneity, with the addition of polymer causing an increase in phase separation; films containing DMDMS show extensive phase separation at intermediate DMDMS levels (particularly the D15P0-S film) and somewhat improved homogeneity at higher DMDMS levels; while films containing BTMS show evidence of small "micellar" structures similar to those observed by brightfield imaging. The addition of PEG600 does not appear to alter the extent of phase separation to a significant degree. For example, a comparison of D15P0-S with D15P3-S shows almost no improvement in homogeneity upon addition of polymer, even though brightfield images show an apparent improvement in homogeneity upon addition of the polymer. These data indicate that the fluorescence images of the distribution of R6G are better able to report on heterogeneity within nanocomposite films.

Image 3.5 shows fluorescence images of nanocomposite films derived from co-hydrolysis of silane components. As was the case for brightfield images, the fluorescence images generally show an improvement in film homogeneity, and the

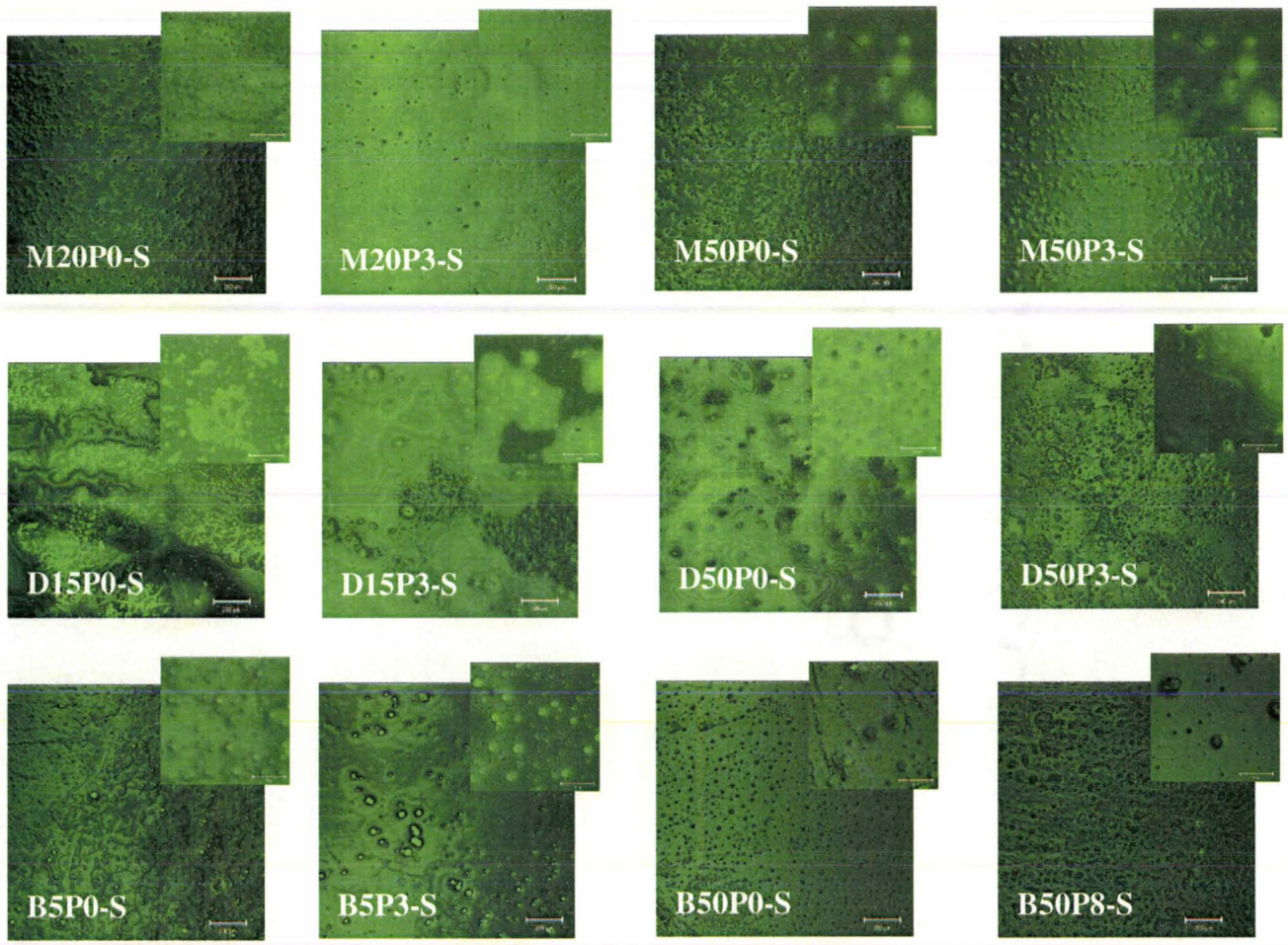

Images 3.4: Fluorescence micrographs of R6G doped within sol-gel derived films prepared with separately hydrolyzed silane components. Large images are 1.3 mm x 1.3 mm; inset images are 80 μm x 80 μm.

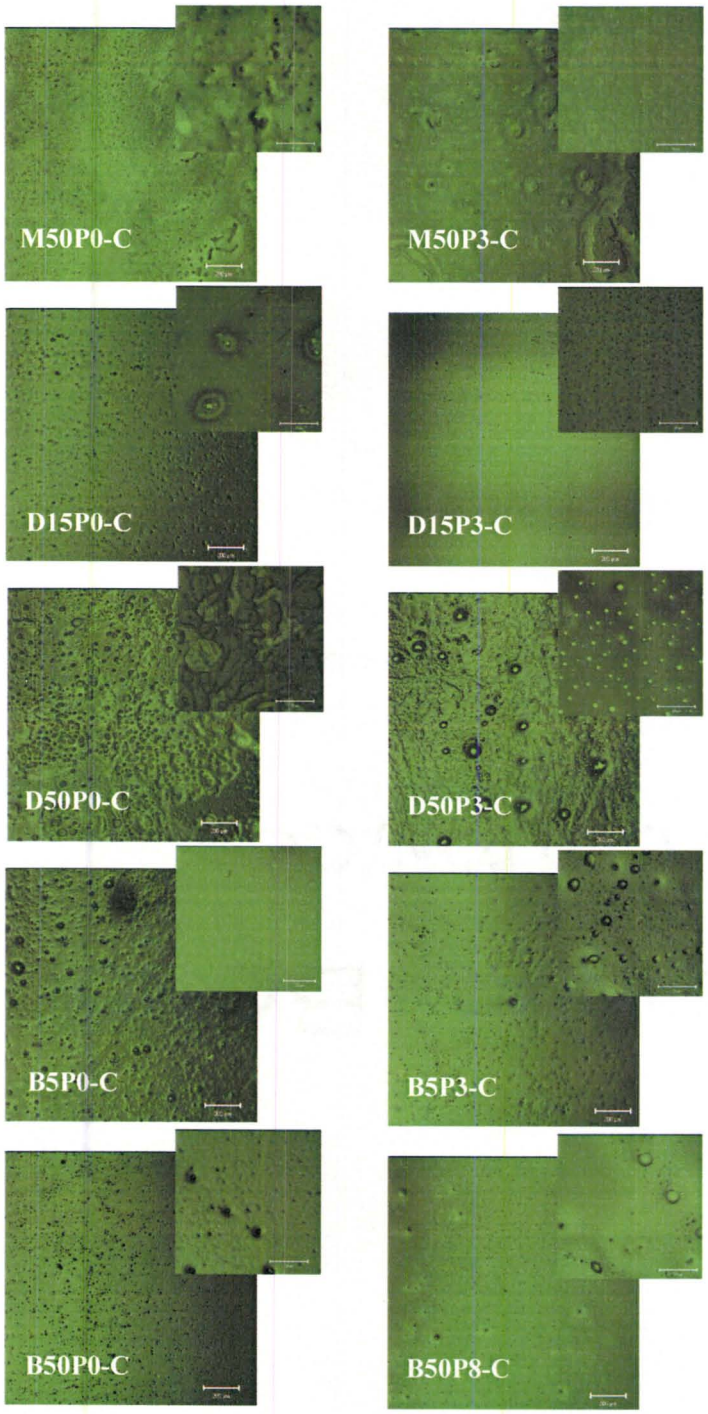

Image 3.5: Fluorescence micrographs of R6G doped within co-hydrolyzed systems containing one (M) or two (D) methyl groups or a butyl group (B). Large image is 1.3 mm x 1.3 mm; inset images are 80 μm x 80 μm

features observed by the two imaging methods are quite similar for the different silane compositions. However, the fluorescence images demonstrate that high levels of ormosils (50% v/v) still produce some observable phase separation within the sol-gel films, which is not easily observed using brightfield imaging. Hence, the fluorescence based imaging is more sensitive to phase separation within the sol-gel films. In general, low levels of ormosils (20% MTMS or 15% DMDMS) produce completely homogeneous films, while addition of 50% (v/v) of these components still produces some phase separation. The use of BTMS results in more heterogeneous films, consistent with the poor miscibility of the longer alkyl chain with the aqueous solvent system.

Scanning electron microscopy:

SEM imaging was performed to evaluate whether any of the materials displayed submicron scale alterations in morphology as a result of phase separation, and to determine if the phase separation process led to the formation of macropores, as has been observed previously for TEOS/PEG[57,58] and MSQ materials. A significant number of films did not show any obvious features when imaged by SEM (data not shown), indicative of a homogeneous material at the micron scale. The homogenous samples included those derived from pure TEOS and SS (with or without polymer), separately hydrolyzed thin films containing MTES, and co-hydrolyzed thin films containing either DMDMS or MTES. In general, the homogeneity observed by SEM was in agreement

with observations from brightfield and fluorescence images, with the exception of separately hydrolyzed samples containing 50% MTES, which did appear to have some phase separation by brightfield and fluorescence microscopy, but not by SEM.

Image 3.6 shows SEM images of films derived by separate hydrolysis of DMDMS and TEOS, and various films containing BTMS at different levels and produced under different processing conditions. Interestingly, separately hydrolyzed DMDMS samples prepared in the absence of PEG had macroporous morphologies that were consistent with spinodal decomposition. The SEM images correlate well with the brightfield and fluorescence images, which also showed significant phase separation. SEM images also indicated that the inclusion of PEG caused the film to become more homogeneous at the micron-scale, although the fluorescence images show that some heterogeneity is still evident at the millimeter scale. The appearance of macropores within the separately hydrolyzed DMDMS based materials was not initially expected, as previous reports have indicated that generation of such morphologies typically requires the presence of a high molecular weight hydrophilic polymer (i.e., 10 kDa PEG). The use of separately hydrolyzed DMDMS/TEOS composites may lead to the formation of high molecular weight PDMS, which can then graft onto silicate nanoparticles formed from TEOS and initiate phase separation under conditions that allow spinodal decomposition to occur. Importantly, addition of PEG or use of co-hydrolysis for film

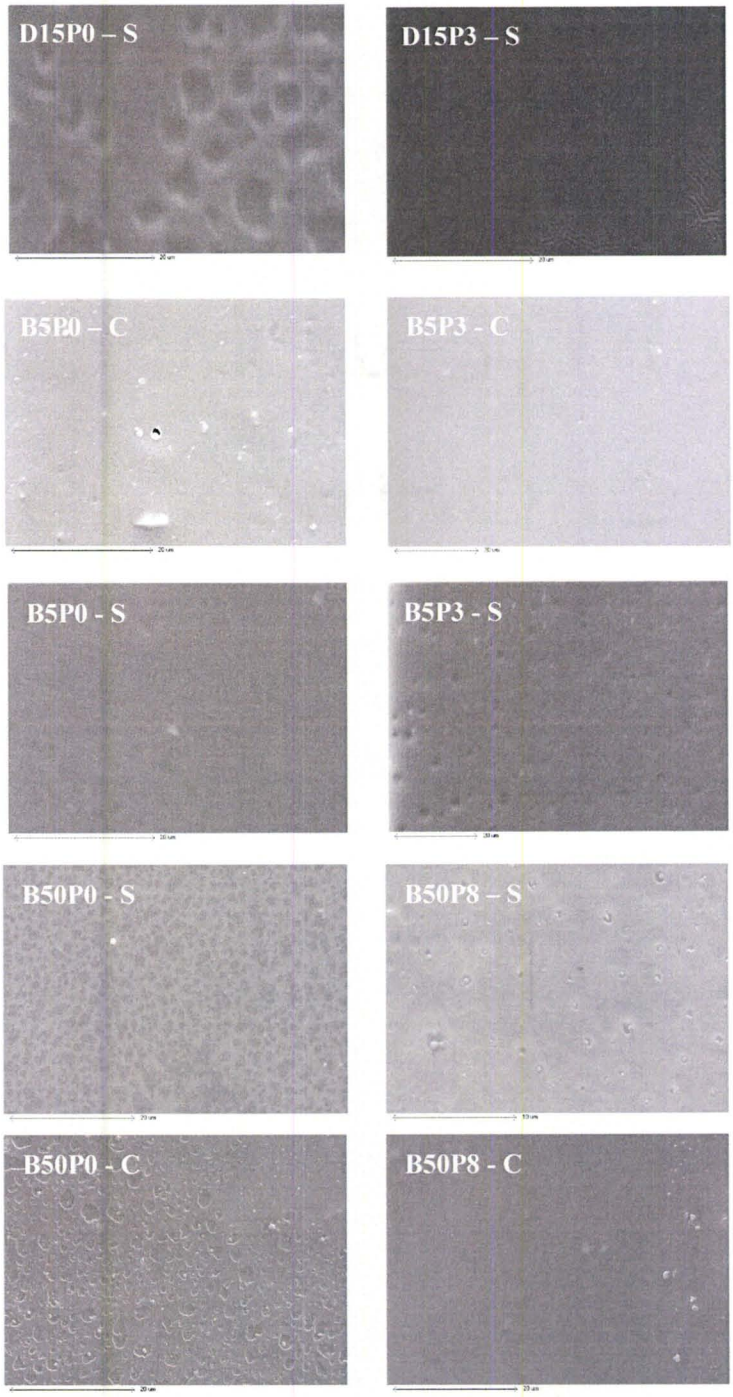

Image 3.6: SEM Images of sol-gel derived thin films that are either separately or co-hydrolyzed for D15, B5 and B50 film sets. Scale bars are 20 μm.

processing leads to a loss of the macroporous morphology. In the former case it is possible that the PEG coats the silica nanoparticles, leading to better miscibility with PDMS or prevention of grafting. In the latter case, co-hydrolysis would be expected to improve miscibility and prevent formation of long PDMS chains. The results thus show that careful tuning of processing conditions can lead to control over material morphology which could be useful for eventual applications such as development of monolithic chromatography columns, where macroporous morphologies are required.

Also shown in Image 3.6 are SEM images of BTMS/TEOS composites. In this case, low levels of BTMS (5%) tended to result in heterogeneous films when samples were prepared by separate hydrolysis of silanes, and more homogeneous films when co-hydrolysis was employed, in agreement with fluorescence images. Higher levels of BTMS generally led to increased heterogeneity in SEM images, while the inclusion of PEG tended to produce more homogeneous images relative to samples without PEG. The phase separation in BTMS/TEOS samples appeared to be similar to that expected for an emulsion, unlike the bicontinuous phase separation observed for DMDMS/TEOS samples, again in agreement with fluorescence images. Overall, the data suggesting that polymer doping can be used to increase the homogeneity of materials at the micron scale, but that the effect does not scale to the millimeter level. Instead, co-hydrolysis of precursors is required to maximize homogeneity within the nanocomposite films.

Atomic force microscopy:

AFM is a nanoscale surface imaging technique where topographical features can be monitored by imaging variations in height across a sample, while differences in mechanical properties can be detected through changes in phase when using an oscillating tip. Both height and phase imaging have been used previously to map phase separated polymer films[59,60,61,62,63,64,65,66,67,68,69,70] and phase separation within sol-gel derived nanocomposites.[34] For the sol-gel derived films, we assume that differences in stiffness from phase imaging translate into variations in chemical properties owing to difference in cross linking, which should occur in cases where phase separation exists.[34,71,72,73,74] It is important to note that this method reports only on the properties of surfaces, and cannot provide information on bulk properties. However, it is still useful for exploring the link between the microscopic and nanoscopic scales in terms of phase separation.

Images 3.7 and 3.8 show both height (left side) and phase (right side) AFM images of the various films examined by brightfield imaging and SEM. Each pair of height and phase images was collected simultaneously, and the image area is 1 μm by 1 μm with a Z-range of 0 - 20 nm for height images and 0° to 60° for phase images. Similar to Higgins, we use low tapping forces, and thus mechanical stiffness dominates

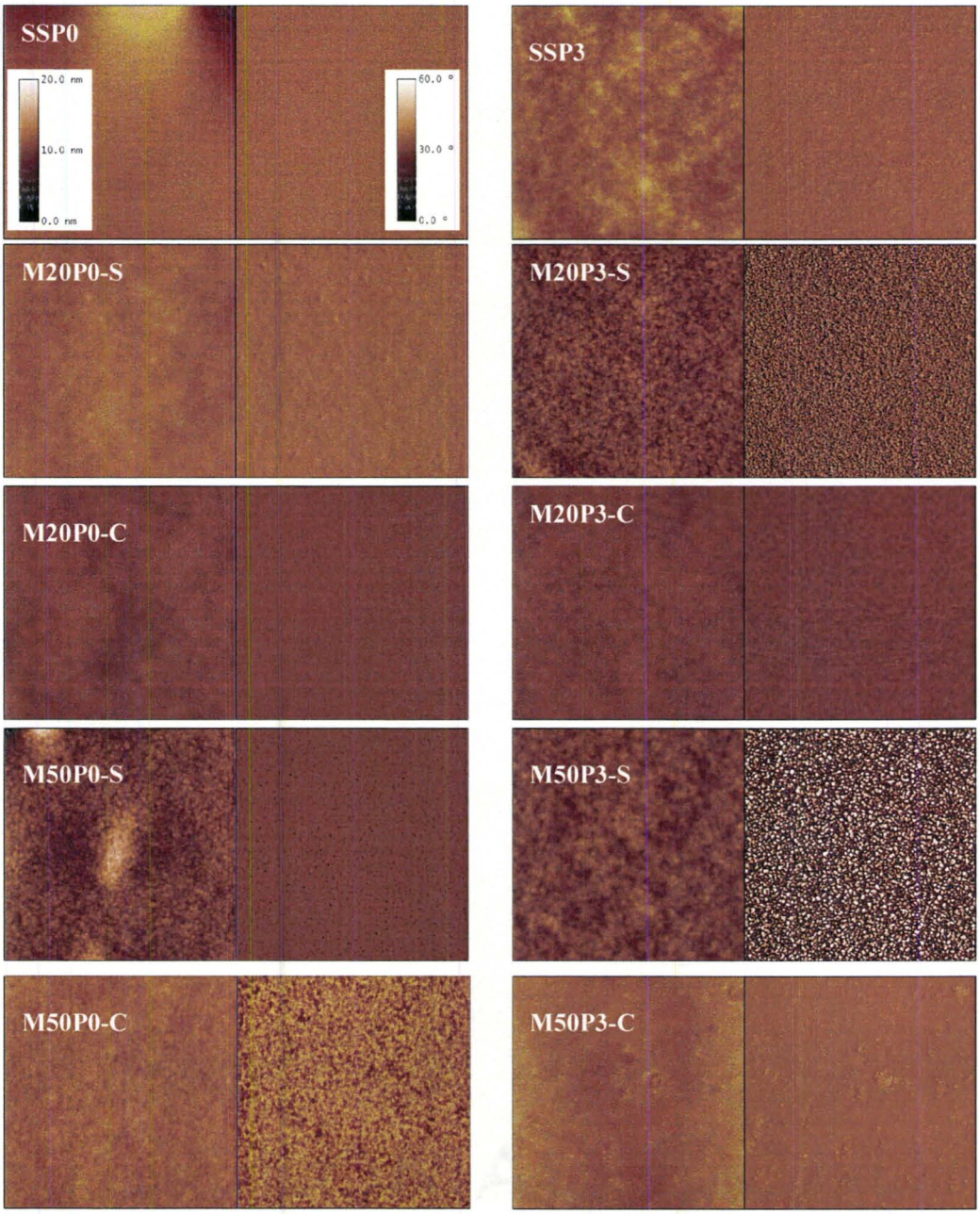

Image 3.7: AFM images of separately and co-hydrolyzed silane compositions containing either 0 (SS or T) or 1 (M) methyl functional group per silane molecule. Height images are on the left of each set of images (Z-range: 0 nm to 20 nm), while the phase images are on the right (Z-range: 0° - 60°). All images are 1 μm x 1 μm and have been manually planefitted and flattened.

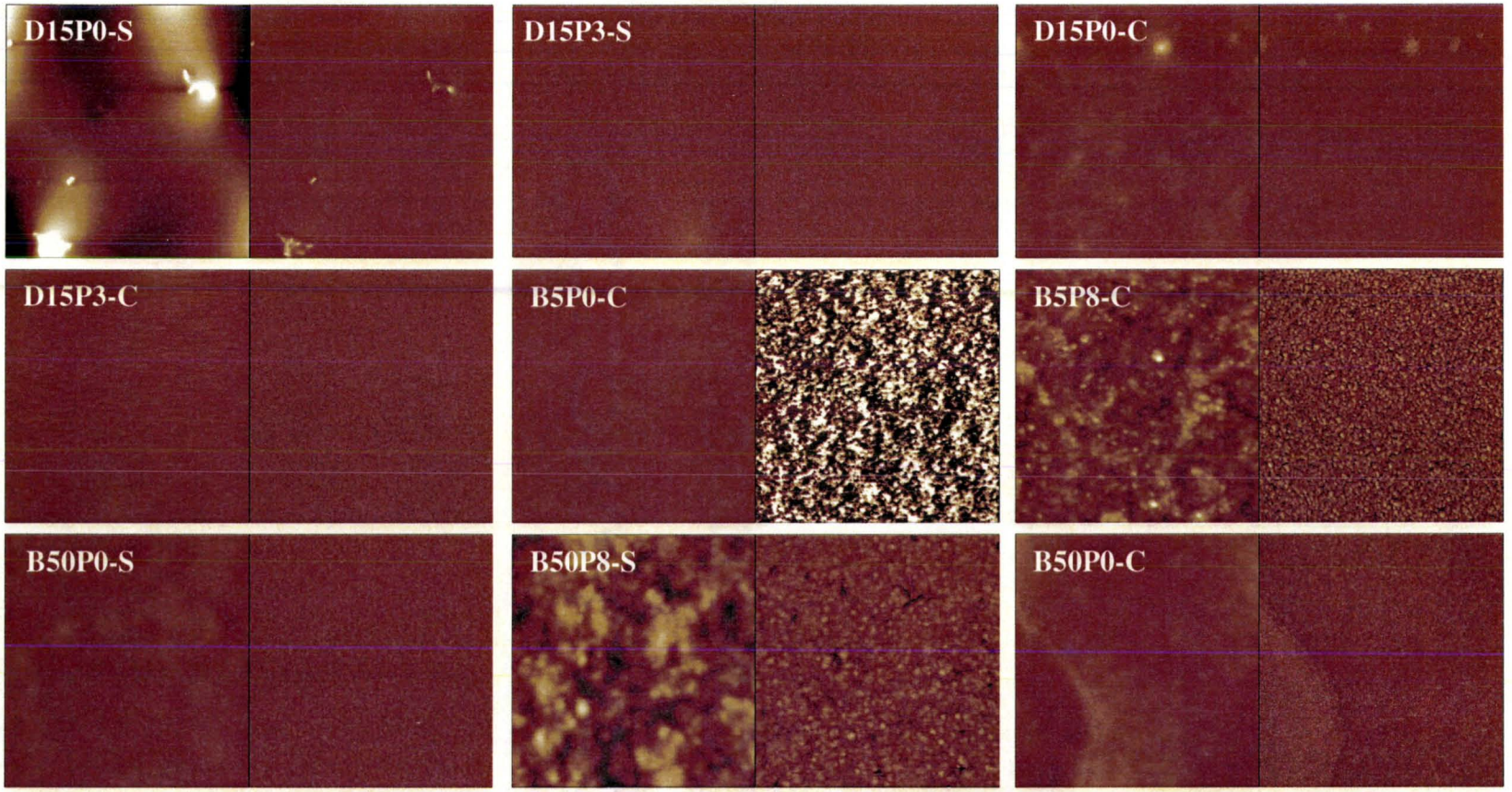

Images 3.8: AFM images of separately and co-hydrolyzed silane compositions containing either 2 methyl functional groups (D) or a butyl chain (B) per silane molecule. Height images are on the left of each set of images (Z-range: 0 nm to 20 nm), while the phase images are on the right (Z-range: 0°- 60°). All images are 1 μm x 1 μm and have been manually planefitted and flattened.

the system – darker domains are less stiff and deemed to be less cross-linked and hence more organic in nature.[34]

In the case of SS and MTES/TEOS samples (Image 3.7), two general trends exist. Firstly, higher levels of MTES generally produce a more heterogeneous film. Secondly, co-hydrolyzed films are generally more homogeneous than separately hydrolyzed films, particularly when PEG is present. These trends are in agreement with data from the other imaging methods, showing that for these samples the nanoscale heterogeneity is ultimately reflected in the microscale morphology. A point to note with MTES based samples is that the increased heterogeneity occurred at a very fine scale - features could be seen at lower Z-ranges (0 nm to 10 nm for height or 0° to 10° for phase images), however the changes in height or phase were uniform throughout the area imaged, indicating that the MTES and TEOS were well mixed even when separately hydrolyzed. In the case of DMDMS/TEOS composites, the AFM images (Image 3.8) reveal that the films are generally more heterogeneous that the MTES/TEOS films, particularly in the case of co-hydrolyzed films. For example, the 15DP0-S sample shows large scale phase separation in the height image (though not in the phase image), while the 15DP3-S is more homogenous, which agrees well with the other imaging methods. The AFM images also show that co- hydrolyzed samples containing DMDMS are more homogenous than

the corresponding samples prepared with separately hydrolyzed silanes, again demonstrating good correspondence between nanoscale and microscale images.

Also shown in Image 3.8 are AFM images of films containing varying levels of BTMS. In this case, the phase separation is much more evident than was the case for MTES or DMDMS doped films. In general, both height and phase images show significant variations across the image field, with features typically being in the range of 50 – 100 nm, particularly when PEG is present (i.e., B5P8-C and B50P8-C films). Most interesting is the B5P0-C film, which showed two distinct phases with sizes of hundreds of nanometers or more. The circular shape of the phase separated region is similar in both size and shape to the image obtained by SEM, indicating that "emulsion-like" phase separation is present. Once again, the inclusion of PEG resulted in a loss of the large-scale phase separation in the AFM image, in agreement with SEM images of the B50P8-C film.

It is interesting to compare our data to that obtained by Higgins et al., who used AFM to study thin spin-coated films prepared with high alcohol levels using either separately or co-hydrolyzed sols.[34] The key conclusion from the work of Higgins et al. was that co-hydrolyzed thin films were more uniform in composition than separately hydrolyzed films, and that films containing smaller functional groups (i.e., methyl) led to more homogeneous films that those containing larger functional groups (i.e., butyl).

These trends were also observed in our work, even though we use a significantly higher level of water and no added alcohol in the sol. In addition, our study suggests that inclusion of PEG can cause some differences in film morphology, although at the low levels tested (3% v/v) the effects are minor. Given that PEG is often used as a stabilizer of entrapped proteins,[14,75] it is worthwhile to note that this species can be added to nanocomposite films without significant alterations in nanoscale or microscale phase separation.

Implications for sensor development:

The data above show that it is possible to prepare sol-gel based organic-inorganic composite films by a two step aqueous processing method using a variety of precursors with extensive control over nanoscale and microscale morphologies. In general, preparation of materials using separate hydrolysis of silane precursors leads to heterogeneous films, while co-hydrolysis of silanes produces more homogeneous films. Addition of polymer species, which are often included to aid in protein stability, is possible, and in most cases either improves homogeneity or does not dramatically alter the morphology of the material. The ability to form films via the two step aqueous processing method has been shown previously to provide a route for entrapment of active proteins into sol-gel derived nanocomposite bulk glasses[9,10,11,12,13,14,15] and thin films.[15,17]

The data shown herein indicate that it should be possible to develop protein doped materials that cover a wide range of polarity with control over the morphology of the material. This can have significant implications in sensor development. For example, in some cases it is desirable to have a relatively homogeneous material so that the partitioning of analytes into the sensing film will be identical across the film. In such a case, the response of the sensing film should be similar regardless of which region of the film is probed. On the other hand, some proteins, such as lipase, are known to be activated upon partitioning to interfaces between hydrophobic and hydrophilic regions.[76,77,78,79,80] In such cases, the use of more heterogeneous films may be advantageous in order to maximize enzyme activity. Future studies will examine the distribution of both hydrophilic and hydrophobic proteins within separately and co-hydrolyzed films and will explore the impact of film morphology on protein activity and sensor performance.

3.4 Conclusions

A range of imaging methods was used to assess the effects of silane types and levels, processing conditions and polymer additives on the morphology of sol-gel films over the millimeter to nanometer length scales. The various imaging methods demonstrated that phase separation increased with both the number and length of alkyl

chains present in ormosils, and with the level of ormosil present in composite materials. Phase separation was more prevalent in materials formed by separate hydrolysis of silane components, although in some cases (particularly for DMDMS based materials) PEG could improve homogeneity. Furthermore the nature of the phase separation depended on the type of ormosil, with DMDMS based materials showing morphologies consistent with spinodal decomposition, while BTMS doped materials showed morphologies consistent with an emulsion of micellar-like structures within the silica matrix. Co-hydrolysis of precursors provided a general route to create more homogeneous materials, although the various imaging methods still displayed evidence of nanoscale and microscale phase separation in materials containing high levels of ormosil species. Interestingly, the heterogeneity observed by brightfield microscopy, which reflects variations in refractive index, did not fully correlate to fluorescence microscopy images of entrapped fluorophores, suggesting that chemical heterogeneity exists even when samples appear to be homogeneous. These results suggest that fluorescence imaging methods are more sensitive to phase separation than are conventional optical imaging methods.

Acknowledgments

The authors thank the Natural Sciences and Engineering Research Council of Canada, MDS-Sciex, the Canadian Foundation for Innovation, and the Ontario Innovation Trust for financial support of this work. JDB holds the Canada Research Chair in Bioanalytical Chemistry.

3.5 References

1. Walcarius, A.; Mandler, D.; Cox, J.A.; Collinson, M. and O. Lev. *J. Mater. Chem.* **15** (2005): 3663.

2. P.V. Braun. *Nanocomp. Sci. Technol.* (2003): 155.

3. Keeling-Tucker, T. and J.D. Brennan. *Chem. Mater.* **13** (2001): 3331.

4. Jin, W. and J.D. Brennan. *Anal. Chim. Acta* **461** (2002): 1.

5. Gill, I. *Chem. Mater.* **13** (2001): 3404.

6. Pierre, A.C. *Biocat. Biotrans.* **22** (2004): 145.

7. Avnir, D.; Coradin, T.; Lev. O. and J. Livage. *J. Mater. Chem.* **16** (2006): 1013.

8. Coradin. T.; Boissiere, M. and J. Livage. *Curr. Med. Chem.* **13** (2006): 99.

9. Reetz, M.T.; Zonta, A. and J. Simpelkamp. *Biotech. Bioeng.* **49** (1996): 527.

10. Reetz, M.T.; Zonta, A.; Simpelkamp, J. and W. Konen. *Chem. Commun.* **(1996)**: 1397.

11. Reetz, M.T.; Zonta, A. and J. Simpelkamp. *Agnew. Chem. Int. Ed. Engl.* **34** (1995): 301.

12. Kuncova, G.; Guglielmi, M.; Dubina, P. and B. Safar. *Collect. Czech. Chem. Commun.* **60** (1995): 1573.

13. Brennan, J.D.; Hartman, J.S.; Ilnicki, E.I. and M. Rakic. *Chem. Mater.* **11** (1999): 1853.

14. Keeling-Tucker, T.; Rakic, M.; Spong, C. and J.D. Brennan. *Chem. Mater.* **12** (2000): 3695.

15. Gulcev, M.D.; Goring, G.L.G.; Rakic, M. and J.D. Brennan. *Anal. Chim. Acta*, **457** (2002): 47.

16. Flora, K.K. and J.D. Brennan. *Chem. Mater.* **13** (2001): 4170.

17. Goring, G.L.G. and J.D. Brennan. *J. Mater. Chem.* **12** (2002): 3400.

18. Sui, X.; Cruz-Aguado, J.A.; Chen, D.Y.; Zhang, Z.; Brook, M.A. and J.D. Brennan. *Chem. Mater.***17** (2005): 1174.

19. Bhatia, R.B.; Brinker, C.J.; Gupta, A.K. and A.K. Singh. *Chem. Mater.* **12** (2000): 2434.

20. Gill, I. and A. Ballesteros. *J. Am. Chem. Soc.* **120** (1998): 8587.

21. Brook, M.A.; Chen, Y.; Guo, K.; Zhang, Z.; Jin, W.; Deisingh, A. and J.D. Brennan. *J. Sol-Gel Sci. Technol.* **31** (2004): 343.

22. Brook, M.A.; Chen, Y.; Guo, K.; Zhang, Z. and J.D. Brennan. *J. Mater. Chem.* **14** (2004): 1469.

23. Hüsing, N.; Brandhuber, D. and P. Kaiser. *J. Sol-Gel Sci. Technol.* **40** (2006): 131.

24. Wang, H.; Bardo, A. M.; Collinson, M. M. and D.A. Higgins. *J. Phys. Chem. B.* **102** (1998): 7231.

25. Makote, R. and M.M. Collinson. *Anal. Chim. Acta* **234** (1999): 195.

26. Wei, H. and M.M. Collinson. *Anal. Chim. Acta* **397** (1999): 113.

27. Mei, E.; Bardo, B. A.; Collinson, M.M. and D.A. Higgins. *J. Phys. Chem. B* **104** (2000): 9973.

28. Howells, A.R.; Zambrano, P.J. and M.M. Collinson. *Anal Chem.* **72** (2000): 5265.

29. Bardon, A.M.; Collison, M.M. and D.A. Higgins. *Chem. Mater.* **13** (2001): 2713.

30. Higgins, D.A.; Collinson, M.M.; Saroja, G. and A.M. Bardo. *Chem. Mater.* **14** (2002): 3734.

31. Fu, Y.; Collinson, M.M. and Higgins, D.A. *J. Am. Chem. Soc.* **126** (2004): 13838.

32. Wetzel, D.L.; Striova, J.; Higgins, D.A. and M.M. Collinson. *Vibrat. Spectr.* **35** (2004): 153.

33. Martin-Brown, S.A.; Fu, Y.; Saroja, G.; Collinson, M.M. and D.A. Higgins. *Anal. Chem.* **77** (2005): 486.

34. Striova, J.; Higgins, D.A. and M.M. Collinson. *Chem. Mater.* **21** (2005): 6137.

35. Nishida, F.; McKiernan, J.M.; Dunn, B.; Zink, J.I.; Brinker, J.C. and A.J. Hurd. *J. Am. Ceram. Soc.* **78** (1995): 1640.

36. Huang, M.H.; Soyez, H.; Dunn, B.S. and J.I. Zink. *Chem. Mater.* **13** (2000): 231.

37. Dave, B.C.; Soyez, H.; Miller, J.M.; Dunn, B.; Valentine, J.S. and J.I. Zink. *Chem. Mater.* **7** (1995): 1431.

38. Dave, B.C.; Miller, J.M.; Dunn, B. Valentine, J.S. and J.I. Zink. *J. Sol-Gel Sci. Technol.* **8** (1997): 629.

39. Battisha, I.K.; Afify, H.H. and Y. Badr. *J. Sol-Gel Sci. Technol.* **25** (2002): 5.

40. Gupta, R.; Mozumdar, S. and N.K. Chaudhury. *Biosens. Bioelectron.* **20** (2005) 1358.

41. Gupta, R.; Mozumdar, S. and N.K.Chaudhury. *Biosens. Bioelectron.* **21** (2005): 549.

42. Baney, R.H.; Itoh, M.; Sakakibara, A. and T. Suzuki. *Chem. Rev.* **95** (1995): 1409.

43. Perry, R.J. and M.E. Adams In *Silicones and Silicone-Modified Materials*, Clarson, S. J.; Fitzgerald, J. J.; Owen, M. J.; Smith, S. D. Ed. American Chemical Society: Washington DC, **728** (2000): p. 533.

44. Nguyen, C.V.; Kenneth, R.C.; Hawker, C.C.; Hedrick, J.L.; Jaffe, R.L; Miller, R.D.; Remenar, J.F.; Rhee, H-W; Rice, P.M.; Toney, M.F.; Trollasa, M. and D.Y. Yoon. *Chem. Mater.* **11** (1999): 3080.

45. Yang, S.; Mirau, P.A., Pai, C-S; Nalamasu, O; Reichmanis, E.; Pai, J.C.; Obeng, Y.S.; Seputro, J.; Lin, E.K.; Lee, H-J.; Sun, J. and D.W. Gidley. *Chem. Mater.* **14** (2002): 369.

46. Xu, J.; Moxom, J.; Yang, S.; Suzuki, R. and T. Ohdaira, T. *Applied Surf. Sci.* **194** (2002): 189.

47. Brook, M.A. *Silicon in Organic, Organometallic and Polymer Chemistry.* John Wiley & Sons, New York, **2000**.

48. Flora, K.K.; Dabrowski, M.A.; Musson, S.P. and J.D. Brennan. *Can. J. Chem.* **77** (1999): 1617.

49. Dong, H.; Brook, M.A. and J.D. Brennan. *Chem. Mater.* **17** (2005): 2807.

50. Dong, H. and J.D. Brennan. *Chem. Mater.* **18** (2006): 541.

51. Geddes, C.D.; Karolin, J. and D.J.S. Birch. *J. Phys. Chem. B* **106** (2002): 3835.

52. Huang, M. H.; Dunn, B. S.; Soyez, H. and J.I. Zink. *Langmuir* **14** (1998): 7331.

53. Tleugabulova, D.; Duft, A. M.; Brook, M. A. and J. D. Brennan. *Langmuir* **20** (2004): 101.

54. Gilliland, J.W.; Yokoyama, K. and W.T. Yip. *J. Phys. Chem. B* **109** (2005): 4816.

55. Tleugabulova, D.; Zhang, Z. and J.D. Brennan. *J. Phys. Chem. B* **107** (2003): 10127.

56. Tleugabulova, D.; Zhang, Z.; Chen, Y.; Brook, M.A. and J.D. Brennan. *Langmuir* **20** (2004): 848.

57. Nakanishi, K. *J. Porous Mater.* **4** (1997): 67.

58. Hara, T.; Kobayashi, H.; Ikegami, T.; Nakanishi, K. and N. Tanaka. *Anal. Chem.* **78** (2006): 7632.

59. Buck, E. and J. Fuhrmann. *Macromolecules* **34** (2001): 2172.

60. Eaton, P. J.; Graham, P.; Smith, J. R.; Smart, J. D.; Nevell, T. G. and J. Tsibouklis. *Langmuir* **16** (2000): 7887.

61. Garrett, J.T.; Runt, J. and J.S. Lin. *Macromolecules* **33** (2000): 6353.

62. Garrett, J.T.; Siedleci, C. A. and J. Runt. *Macromolecules* **34** (2001): 7066.

63. McLean, R.S. and B.B. Sauer. *Macromolecules* **30** (1997): 8314.

64. Paige, M.F. *Polymer* **44** (2003): 6345.

65. Raghavan, D.; Gu, X.; Nguyen, T.; Van Landingham, M. and A. Karim. *Macromolecules* **33** (2000): 2573.

66. Raghavan, D.; Van Landingham, M.; Gu, X. and T. Nguyen. *Langmuir* **16** (2000): 9488.

67. Viswanathan, R.; Tian, J. and D.W.M. Marr. *Langmuir* **13** (1997): 1840.

68. Wang, H. and R. J. Composto. *Macromolecules* **35** (2002): 2799.

69. Woodcock, S. E.; Chen, C. and Z. Chen. *Langmuir* **20** (2004): 1928.

70. Yurekli, K.; Karim, A.; Amis, E. J. and R. Krishnamoorti. *Macromolecules* **36** (2003): 7256.

71. Magonov, S. N.; Elings, V. and M.-H.Whangbo. *Surf. Sci.* **375** (1997): L385.

72. Bar, G.; Brandsch, R. and M.-H. Whangbo. *Langmuir* **14** (1998): 7343.

73. Bar, G.; Thomann, Y.; Brandsch, R.; Cantow, H.-J. and M.-H. Whangbo. *Langmuir* **13** (1997): 3807.

74. Bar, G.; Brandsch, R. and M.-H. Whangbo. *Surf. Sci.* **411** (1998): L802.

75. Luo, T.-J.M.; Soong, R.; Lan, E.; Dunn, B. and C. Montemagno, C. *Nature Mater.* **4** (2005): 220.

76. Turner, N.A.; Needs, E.C.;. Khan, J.A. and E.N. Vulfson. *Biotechnol. Bioeng.* **72** (2001): 108.

77. Grochulski, P.; Li, Y.; Schrag, J.D.; Bouthillier, F.; Smith, P.; Harrison, D.; Rubin, B. and M. Cygler. *J. Biol. Chem.* **268** (1993): 12843.

78. Dodson, G.G.; Lawson, D.M. and F.K. Winkler. *Faraday Disc.* **93** (1992): 95.

79. Shirai, K. and R.L. Jackson. *J. Biol. Chem.* **257** (1982): 1253.

80. Chapus, C.; Semeriva, M.; Bovier-Lapierre, C. and P. Desnuelle. *Biochemistry* **15** (1976): 4980.

Chapter 4: Fluorescence and Physical Characterization of Sol-Gel Derived Nanocomposite Films Suitable for the Entrapment of Biomolecules

The following chapter has been accepted in the scientific journal *Journal of Materials Chemistry* under the following citation:

Goring, Gillian L.G. and John D. Brennan. "Fluorescence and Physical Characterization Sol-Gel Derived Nanocomposite Films Suitable for the Entrapment of Biomolecules." *Journal of Materials Chemistry* **12(12)** (2002): 3400 - 3406.

I was responsible for all experimental design, data collection, analysis and interpretation. I wrote the first draft of the manuscript and Dr. Brennan provided editorial input to generate the final draft of the paper.

4.0 Abstract

Thin films (100 – 500 nm thick) of Class I, Class II and Class I/II organic-inorganic silicates were prepared by casting mixtures of TEOS, MTES and/or DMDMS that were first partially hydrolyzed *via* sonication in the presence of water using acid catalysis, followed by induction of gelation through the addition of buffer solutions containing polymer (0 or 3% weight/volume of PEG). In some cases, the fluorescent probe 6-propionyl-2-dimethylaminonaphthalene (PRODAN) or the protein human serum albumin (HSA) were also added to the buffer solution, which permitted the fluorescence probing of the internal environment and the protein binding capacity of analyte within the various silicate films, respectively. Parameters such as the type and level of organosilane precursor, polymer level, casting speed and aging time were varied to determine how such factors affected the thickness, morphology, and internal environment of the resulting films that were formed by this two-step process. The results show that composite films evolve in two stages: (1) rapid drying during the initial one to two hours after casting of the film, followed by (2) a slower aging process that the final state of the films can be quite different from that obtained for bulk materials. Preliminary studies of HSA-doped films show that the entrapped protein adopts a partially expanded conformation, but in most cases is still able to bind to ligands such as salicylic acid.

4.1 Introduction

The sol-gel process offers a promising route for the development of nanocomposite materials.[1,2,3,4,5,6] Hydrolysis and condensation of tetraalkoxysilanes can be done in the presence of either a dispersed additive such as an organic polymer producing a Class I material,[7,8,9,10,11] or along with an organosilane leading to Class II materials with covalently anchored functional groups.[7,10,12,13] Incorporation of both dispersed and anchored organic groups is also possible, leading to Class I/II nanocomposite materials.

An emerging area that is attracting increased attention is the development of biologically doped nanocomposite materials, which are useful for the development of biosensing devices. Encapsulation of biologicals via the sol-gel process typically involves the hydrolysis of an alkoxysilane precursor in the absence of added alcohol, followed by addition of a buffered solution containing the protein of interest to promote gelation. The addition of the buffer brings the pH to the physiological range of 7.5 ± 1.0 and dilutes the alcohol produced during the hydrolysis. Low temperature aging over a period of several weeks or months results in a durable, optically clear biomaterial which shows good retention of protein activity, as summarized by Avnir *et al.*[14]

Most research describing biologically-doped sol-gel materials has focused on the preparation of bulk glasses (*i.e.* glass blocks or slides) with thicknesses on the order of several hundred micrometers up to 1 cm.[15,16] Bulk glasses allow sufficient amounts of the biomolecule to be entrapped to permit spectroscopic or electrochemical investigations, but suffer from drawbacks such as long aging times and extremely slow

response times.[10] Therefore, it is generally agreed that thin films (*i.e.* submicron thickness) are most appropriate for the development of analytical devices, such as biosensors. Thin films age rapidly, thereby limiting drifts in calibration,[17] offer fast response times[18] and can be interfaced to planar waveguides or standard fiber optic-based biosensors to allow internal reflection fluorescence measurements.[19,20]

Sol-gel-derived thin films can be prepared by a variety of methods including spin-casting,[21,22] dip-casting,[16,17,23,24] and aerosol spraying.[5,22,25] While such films have been successfully utilized for chemical or biosensor development, numerous drawbacks remain to be overcome. First, many of the film formation protocols (*i.e.* spin casting, aerosol spraying) are not amenable to coating the curved surface of substrates such as optical fibers, which may limit their utility for remote sensing.[26,27] Second, thin films generally require high levels of the biomolecule for sufficient signal to be generated, making it problematic for biological species such as proteins that are insoluble and/or aggregate in the alkoxysilane solution.[18] Third, high levels of alcohol are often required as a viscosity modifier to allow proper formation of a dip-cast thin film,[28] leading to denaturation of the encapsulated biomolecules.[21] Finally, thin films undergo substantial changes in structure and solvent content on a short timescale during the aging and drying process, potentially leading to extensive cracking[29,30] and dehydration of encapsulated biologicals.[5,31,32]

The primary objective of this work is to prepare and characterize sol-gel-derived thin films formed *via* the dip-casting method that cover the range of undoped, Class I, Class II and Class I/II organic-inorganic nanocomposites. A multi-step processing protocol is described that begins with the sonication of mixtures of TEOS and an

organosilane precursor in the absence of added alcohol to promote hydrolysis. A carefully chosen buffer (containing a fluorescent dye, polymer and/or protein) is then mixed with the hydrolyzed silane to promote a slow gelation process that occurs over a period of an hour or more. A substrate is cast into the silane mixture to transfer a small volume of the silane onto its surface, resulting in a thin film containing the entrapped dye, polymer and/or protein.

The physical characteristics of these composite films have been characterized using profilometry, and optical microscopy to yield information on film thickness, morphology, cracking and durability. These results are compared to previous results obtained from both monoliths and thin films that are formed without the addition of buffered aqueous solutions. The internal environment of the films, and their evolution over time, has also been examined by entrapping the dipolarity-sensitive fluorescent probe PRODAN[33] into the films. This probe has been used previously to investigate the internal environment of sol-gel derived monoliths, and thus allows for comparison of the internal environment and drying times between monoliths and thin films.[34] Studies of films containing HSA are also presented, showing that HSA remains functional and accessible to ligands when entrapped in such films. The results show that films produced using the two-step preparation method are amenable to the entrapment of biomolecules, can be tuned to optimize protein stability, and thus should be useful for the development of bioanalytical devices.

4.2 Experimental

Chemicals

PEG(MW 600), TEOS (99.999^{+}%), MTES (98%), DMDMS (98%) and TRIS were purchased from Aldrich (Milwaukee, WI, USA) and were used without further purification. HSA (essentially fatty acid free), salicylic acid and polymethacrylate fluorimeter cuvettes (transmittance Curve C) were obtained from Sigma (St. Louis, Mo, USA). Guanidine hydrochloride (GdHCl, Sequanol grade) was obtained from Pierce (Rockport, IL, USA). Sephadex G-75 fine powder was supplied by Pharmacia Biotech (Uppsala, Sweden). PRODAN was obtained from Molecular Probes (Eugene, OR, USA). Glass microscope slides (Fisher regular), which were used for casting of the thin films, were obtained from Fisher Scientific (Toronto, ON, Canada). Quartz microscope slides (for HSA studies) were obtained from Chemglass (Vineland, NJ, USA). All slides were cut to appropriate dimensions of 8 mm x 32 mm. All water was purified by reverse osmosis and deionized using a Milli-Q Synthesis A10 4-stage water purification system. All other chemicals and solvents were used of analytical grade and were used without further purification.

Procedures

Cleaning of substrates

A variety of methods were investigated for the cleaning of glass and quartz slides to maximize the adhesion of sol-gel derived thin films. The best method was found to be one that involved soaking the slides in 1.0 N NaOH for 18 to 24 hours followed by

rinsing with deionized distilled water and methanol. The substrates were then dried at room temperature under a stream of nitrogen. Clean slides generally showed contact angle for water droplets close to 0°, indicative of a hydrophobic surface. Clean slides were typically stored in a dust free container and used within 1 day of cleaning to avoid contamination. When slides were left to sit for longer than one day, the resulting films that were cast not only stuck poorly to the substrate but also contained cracks were could be detected visually by eye.

Preparation of sol-gel derived thin films

Precursor solutions contained either 100% TEOS, or co-hydrolyzed mixtures of TEOS with 20% (v/v) MTES (0.28 mole ratio) or 10% (v/v) DMDMS (0.15 mole ratio). 4.5 mL of the silane mixture was combined with 1.4 mL of distilled, deionized water and 0.1 mL of 0.1N HCl and sonicated until the mixture was visibly homogeneous. The silane solutions were used immediately for preparation of thin films.

0.5 mL of the appropriate silane solution was thoroughly mixed with an equivalent volume of buffer solution (10 to l00 mM TRIS at pH 7.2) containing 100 mM KCl, 0-10% (w/v) of PEG_{600} and either 4.5 μM of PRODAN or 35 μM of HSA and the mixture was transferred to a Teflon casting well. A clean slide mounted on a motorized dip caster (Kibron Layer-X film lift, Helsinki, Finland) with a vertically moving arm was cast into the solution at 10 $mm.min^{-1}$ and then withdrawn at rates varying from 1 to 10 $mm.min^{-1}$. The cast films were either tested immediately or suspended in air at room temperature for 10 min, and then were placed in a disposable polystyrene cuvette

that was sealed with Parafilm and stored in the dark for 72 hr at 4 °C before testing unless otherwise stated.

Purification of HSA

A plug of glass wool was placed at the tip of a 5.0 mL disposable glass pipette to create a small column for the purification of HSA. Sephadex G-75 powder was mixed with minimal buffer (TRIS; stored for 24 hr at 4 °C) and gently poured into the glass pipette, which was held on an angle to minimize the formation of bubbles within the column matrix. Several column volumes of TRIS buffer were allowed to pass through the column to ensure that it was well saturated. The void volume of the column was determined by the addition of several drops of an aqueous blue dextran solution, after which the column was again thoroughly rinsed with copious amounts of buffer. A small amount of HSA was dissolved in TRIS buffer and allowed to pass through the column, whereby 100 μL aliquots were collected after the elution of the void volume. These fractions were analyzed by UV absorbance to determine the concentration of HSA using the Trp residue (ε_{277} = 36 000 M^{-1} cm^{-1}) with Beer's Law.

Fluorescence spectroscopy.

Fluorescence spectra were collected on a SLM-Aminco 8100 spectrofluorometer. Light from a 450-W ozone-generating Xe arc lamp was passed through a double-grating excitation monochromator and then passed through a 1-cm^2 quartz cuvette containing the sample. Emission was collected at a right angle to the exciting radiation, passed through

a single grating emission monochromator and detected using a R928 PMT in a peltier-cooled housing operated in photon counting mode. A 4-nm band pass was used in both the excitation and emission paths, and no polarizers were used in cases where fluorescence spectra were collected. The sample intensity was divided by the signal from the reference channel containing a quantum counter solution of 3 g L^{-1} rhodamine B in ethanol to account for the signal fluctuations resulting from deviations in the lamp power output.

For fluorescence spectra, samples containing 35 μM HSA were excited at 295 nm and emission was collected from 305 to 450 nm in 1 nm increments at a rate of 180 nm.min^{-1} and with an integration time of 0.30 seconds. Solution samples were continuously stirred throughout the experiments and were maintained at a temperature of 20 ± 0.2 °C. Appropriate blanks were subtracted from each sample and the spectra were corrected for deviations in emission monochromator throughput and PMT response.[35]

UV-Visible absorbance

UV-visible absorbance spectra were obtained using a Cary 400BIO UV-VIS spectrophotometer (WinUV Scan Application; Varian 1999). The spectra for PRODAN or HSA were collected in 0.2 nm increments from 240 nm to 650 nm using a scan speed of 30 nm.min^{-1}, a band pass of 1.5 nm and a path length of 1 cm. In all cases, a buffer solution was collected as the reference solution, and all samples were background corrected in order to obtain the stock concentration of the desired probe or protein. The

concentrations of the solutions were determined using ε_{365} = 14 500 M^{-1} cm^{-1} for PRODAN[33] and ε_{277} = 36 000 M^{-1} cm^{-1} for HSA.[36]

Profilometry

All profilometry measurements were preformed using a Tencor Instruments (Mountain View, CA, USA) Alpha-Step 100 profilometer. The stylus was positioned over the uncoated portion of the slide in order to obtain a baseline height measurement. The stylus was moved from the uncoated region to the coated region of the slide at a rate of 6 $mm.min^{-1}$ and the film height difference was continuously monitored using a strip chart recorder with a scale of 25 000 $Å.cm^{-1}$. The results reported were an average of at least three regions per film for a minimum of three different films. Optical micrographs were acquired subsequent to profilometry to ensure that the tip did not penetrate the surface.

Optical microscopy

Micrographs were obtained using an Olympus microscope with a CCD video camera and a 10X objective. Images were obtained from films immediately after casting, after 24 hours, and after 21 days of aging. In each case, images were obtained both before and after the rehydration of the film, which was accomplished by submerging the film in water for 10 minutes. The image area in all cases is 1.1 mm x 0.8 mm (magnification factor is 400 x).

Salicylate titration of HSA

Quartz slides were coated with HSA-doped films and were placed into methacrylate fluorimeter cuvettes containing 2.0 mL of Tris buffer. The samples were titrated with 100uM salicylate in phosphate buffer at pH 7.2. Fluorescence emission spectra were collected at various levels of salicylate to monitor the quenching of Trp-214 by salicylate. The spectra were corrected for blank contributions using a solution containing salicylate but no protein, and a 10 nm window centered at 335 nm was integrated to provide intensity values for the protein at each salicylate concentration.

4.3 Results and Discussion

Preparation of thin films

The main factors that are important in development of thin biologically-doped films are the thickness of the film, its adhesion to the substrate, its resistance to cracking, the internal microenvironment and the potential for leaching of the entrapped species. Factors that were optimized to achieve useful films include substrate surface treatment prior to casting, buffer type and concentration (to control gelation times), silane type and content (to control thin film dipolarity), the presence of polymer additives and the substrate withdrawal speed. These parameters were found to have significant effects on film thickness, clarity, cracking and internal dipolarity, as described below in detail.

The adhesion of the film depended on both the method used to clean the substrate, and on the film thickness. Substrates that were cleaned using concentrated or dilute HF or H_2SO_4 did not provide good film adhesion, and introduced unwanted hazards related to

handling of these materials. On the other hand, soaking the substrates in 1N NaOH for 24 hours led to surfaces that provided good adhesion of thin films. It was also found that films greater than 1μm thick did not adhere well to any substrate regardless of the cleaning procedure used to produce durable films.

The thickness of the sol-gel derived films was highly dependent on the gelation behavior of the sol, as gelation time had a tremendous impact on the viscosity of the casting solution. The major factors affecting the rate of gelation of the hydrolyzed silane when mixed with the buffer solution were: (1) the ratio and type of organosilane present in the silane solution; (2) the concentration and molecular weight of the polymer additive; (3) the type and concentration of the buffer used; (4) the buffer pH. The gelation time increased as the amount of organosilane or polymer increased and also as the buffer pH was increased or as the buffer concentration was decreased as is shown in Table 4.1. The gelation time increased on going from TEOS to MTES to DMDMS, suggesting that steric effects partially controlled the gelation rate, and gelation time decreased dramatically when phosphate buffer was used, owing to the phosphate-based catalysis of gelation.[37] Based on the studies of the film properties, as presented below, it was determined that the optimal gelation time was in the range of 60 to 180 min. Samples with shorter gelation times were noticeably more viscous, even immediately after mixing, and produced thick films of poor quality, which often peeled away from the subtrate, making them unsuitable for protein entrapment. Accessing the longer gelation times required low ionic strength and pH values that were not compatible with the retention of protein function. The method adapted for the formation of optimal thin films involved the addition of a buffer

solution (10mM TRIS buffer, pH 7.2 with 100mM KCl) containing either 0 or 3% (v/v) PEG_{600} (higher values led to viscous casting solutions) along with the desired probe or protein, to an equal volume of the hydrated silane (containing 100% TEOS, 20% MTES or 10% DMDMS).

Thickness and morphology

Figure 4.1 shows the thickness values obtained for films composed of TEOS, 20% MTES or 10% DMDMS, with and without 3% PEG_{600}, as a function of withdrawal speed. It must be noted that the film thickness was dependent on the time elapsed between mixing the silane and the buffer and the casting of the film, with thicker films being formed as the time after mixing increased, owing to increased viscosity in the casting solution. Thus, all data is reported for films that were cast immediately after mixing of the hydrolyzed silane and buffer. As shown in Figure 4.1, film thickness increased with increased casting rates, as a result of increased drainage of the deposited solution. Inclusion of PEG_{600} at a level of 3% or less did not produce significant changes in thickness, indicating that such levels of polymer do not alter the ability to cast thin films. Inclusion of PEG_{600} at higher levels lead to much thicker films (> 1 μm, data not shown) owing to the increased level of viscosity of the polymer-doped solutions.[3] Thickness was also dependent on the type of organosilanes present, increasing in the order DMDMS > MTES ≈ TEOS, owing to lower levels of cross-linking and

Table 4.1 Gelation time of silane mixtures used to produce thin films.

Silane composition[a]	pH 4.00[b] TRIS/Phos	pH 5.50[b] TRIS/Phos	pH 7.26[b] TRIS/Phos	pH 8.5[b] TRIS/Phos	pH 10[b] TRIS/Phos
TEOS[c]	>24 hr/24hr[+]	>24 hr /16hr	**160min[b]**/4.5min	5.0min/4.0min	3.0min/2.0min
10% MTES	>24 hr/>24 hr	>24 hr/>24 hr	>24 hr/11.0min	13.0min/8.0min	6.0min/8.5min
20% MTES[c]	**>24 hr/>24 hr**	**>24 hr/>24 hr**	**120min[b]**/31min	32min/16min	13.5min/13min
40% MTES	>24 hr/>24 hr	>24 hr/>24 hr	>24 hr/60min	120min/30min	25min/40min
2% DMDMS	>24 hr/>24 hr	>24 hr/>24 hr	>24 hr/8.0min	5.5min/3.0min	3.0min/3.5min
10% DMDMS[c]	>24 hr/>24 hr	>24 hr/18hr	**90min[b]**/4.0min	11.0min/3.0min	5.5min/<2.00min
20% DMDMS	>24 hr/>24 hr	>24 hr/>24 hr	>24 hr/6.0min	7.0min/5.0min	4.0min/4.0min

[a] 10%, 20%, 40% (v/v) for MTES (0.14, 0.28, and 0.51 mole ratios) and 2%, 10% and 20% (v/v) for DMDMS (0.03, 0.15 and 0.29 mole ratios)

[b] Errors on the pH range: pH 4.00 ± 0.05; pH 5.50 ± 0.10; pH 7.26 ± 0.03; pH 8.50 ± 0.10; pH 10.00 ± 0.05, TRIS is tris buffer, Phos is phosphate buffer

[c] Boldface values show the compositions used to form the films that were studied in this paper.

correspondingly lower viscosities for the organosilane-doped films, which is consistent with the longer gelation times for such species.

In order to interpret the features that are seen in the optical micrographs of the thin films that were taken at the same time as the thickness measurements (Image 4.1), other percentages of both silane and additives were also studied by optical microscopy among other techniques as was shown in Chapter 3. All the images that are shown were obtained from the middle region of the films and predominantly show that the films are free of cracks. Cracking is known to occur in pure TEOS films, films of elevated withdrawal speeds (10 mm/min), as well as aged sols that show the outward signs of viscosity.[3] Although these films appear crack-free in the middle of the film, some cracking may be visible along the upper edge of the film, along the sides of the film support and along the bottom edge of the film. The cracking that is visible at the bottom of the film is due to the presence of a 2 – 3 mm wide thicker lip, resulting from the dipcasting technique. This area dries faster than is expected and results in the presence of small cracks.[16] However, further analysis of these films doped with probes, do not show any evidence of leaching which indicates that any reactions that are being monitored are not being monitored in solution but rather in the sol-gel derived thin film matrix.

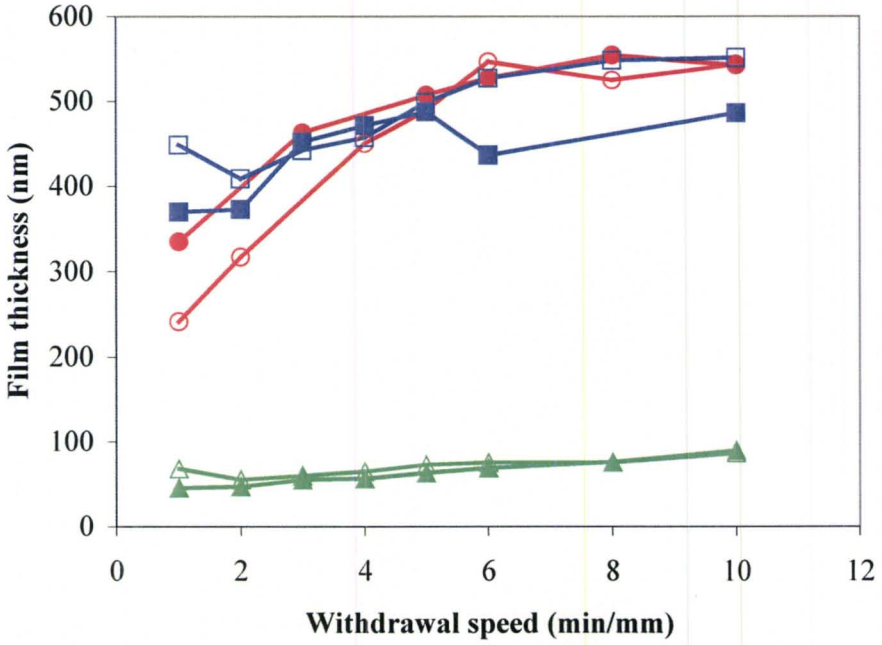

Figure 4.1: Thickness values obtained for films composed of TEOS (■), TEOS + 3% PEG_{600} (□), 20% MTES (●), 20% MTES + 3% PEG_{600} (○), 10% DMDMS (▲), 10% DMDMS + 3% PEG_{600} (△) as a function of withdrawal speed.
Typical errors are ± 30 nm.

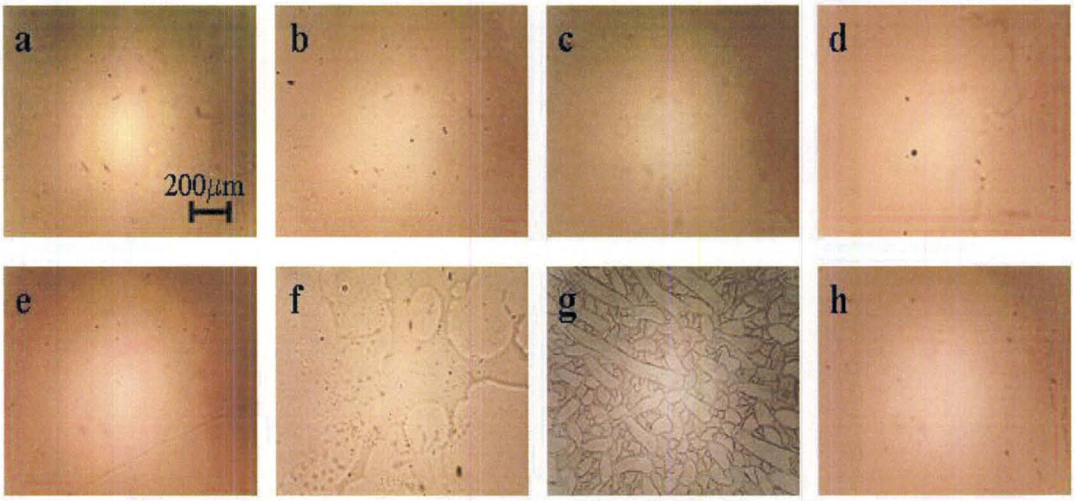

Image 4.1. Optical micrographs of thin films after casting (panels a – f) and after rehydration by immersion in water (panels g and h)/ (a) TEOS (b) TEOS +3% PEG_{600}, (c) 20% MTES, (d) 20% MTES + 3% PEG_{600}, (e) 10% DMDMS, (f) 10% DMDMS + 3% PEG_{600}, (g) rehydrated film of TEOS, (h) rehydrated film of 10% DMDMS + 3% PEG_{600}. All films were obtained at a withdrawal speed of 4 mm min^{-1} and were aged 3 days before imaging.

Some of the films, such as those shown in Images 4.1 were obtained by imaging the sol-gel derived thin films on glass supports on microscope glass slides. This type of analysis offered more features than were desired due to the appearance of features from the underlying part of the film. The optical micrographs are of films obtained at a withdrawal speed of 4 $mm.min^{-1}$ (images a –f) along with two images of films after the addition of water (images g and h). However, some of the films show minor imperfections that appear to be air bubbles trapped in the film during deposition. The most striking observation from the micrographs is the evidence for phase separation in films containing both organosilanes and polymer additives (images d and f). These films show a highly variable distribution of 'islands' and 'channels' of different composition, perhaps reflecting polymer rich or organosilane rich regions within the film. The morphology of the films observed by optical microscopy did not change as the samples were aged for up 60 days, showing that the films do not undergo macroscopic structural rearrangements during long-term aging. It should be noted that even those films that appear to be homogeneous might still show phase segregation on a scale that is below that resolution of the optical microscope as was shown in Chapter 3.

Addition of water to the films led to extensive cracking of many films. Image 4.1(g) is a representative image of a rehydrated TEOS-derived film, while Image 4.1(h) shows a rehydrated film containing 10% DMDMS. The general trends observed from the optical micrographs were as follows: (1) TEOS films tended to crack more extensively than organosilane-loaded films, suggesting that the lower dipolarity of the organosilane films prevented uptake of water and reduced hydration stress; (2) films produced at faster

withdrawal speeds (i.e. thicker films) showed more cracking than those produced at slower withdrawal speeds; addition of PEG_{600} to TEOS-derived thin films improved the resistance of the films to cracking, likely owing to the greater hydration stress during drying, and hence, a lower extent of hydration stress during rehydration; (4) aging of the films led to improved resistance to cracking, with films showing poorer stability to cracking at the early aging times (less than 10 days after casting), but improved durability as aging continued, with films over 60 days old showing no cracking. Hence, the highest quality films appeared to be those formed from TEOS with PEG_{600} or from DMDMS or MTES without PEG_{600}, as such films showed the least amount of cracking and were the most microscopically homogeneous in terms of composition.

Evolution of internal environment during film aging

Background fluorescence of the glass microscope slides

The presence of fluorescent impurities in either precursor solvents or background fluorescence of microscope slides will result in the acquisition of incorrect fluorescence data. In order to ensure that there were no fluorescence interferents from the glass substrates upon which the films were dip-cast, a series of glass microscope slides were analyzed at two different orientations (54.7° or 45°) with respect to the excitation beam. Glass microscope slides from Fisher (Regular and Finest), Corning and VWR (Select) were studied by fluorescence spectroscopy by running several excitation and emission spectra combinations at the appropriate wavelengths which would influence fluorescence data obtained from the PRODAN and SNARF-dextran fluorophores. A summary of

these results is shown in Table 4.2. Two major conclusions can be drawn from these results. First, there was a significant amount of scatter that occurs when samples are mounted at 45° with respect to the excitation beam, which results in skewed raw and corrected emission spectra of the desired fluorophores. Second, although all the glass substrates mounted at 54.7° relative the excitation beam did have lower background noise over those samples mounted at 45°, there was still significant variation in the amount of background fluorescence in the emission spectra of the four different types of microscope slides. However, Fisher 'Regular' microscope slides provided not only spectra with low amounts of background fluorescence at all the emission wavelengths (510, 470 and 640 nm) but the best reproducible results among the studied glass substrates.

Table 4.2: Background fluorescence of Fisher, VWR and Corning brands of glass microscope slides.

Cut glass microscope slides were mounted at two different angles (54.7° and 45°) with respect to the excitation beam. Since a T-format fluorimeter was used to measure the emission spectra, both the left hand side (LHS) and the right hand side (RHS) monochromators were tested during these analyses.

Property	Fisher Regular			Fisher Finest			VWR			Corning		
Holder angle (degrees)	**54.7**			54.7			54.7			54.7		
Excitation wavelength (nm)	350	**370**	**510**	350	370	510	350	370	510	350	370	510
Emission wavelength (nm)	470	**470**	**640[a]**	470	470	640[a]	470	470	640[a]	470	470	640[a]
LHS Fluorescence (± 10% a.u.)[b]	0.06	**0.02**	**0.003**	0.04	0.01	0.002	0.04	0.02	0.003	0.07	0.006	0.003
Peak maximum (± 5 nm)[c]	412	—[d]	—	412	—[d]	—	410	—[d]	—	413	—[d]	—
RHS Fluorescence (± 10% a.u.)[b]	0.04	**0.03**	**0.008**	0.03	0.02	0.009	0.07	0.02	0.01	0.04	0.02	0.008
Peak maximum (± 5 nm)[c]	411	—[d]	—	409	—[d]	—	411	—[d]	—	410	—[d]	—

Property	Fisher Regular			Fisher Finest			VWR			Corning		
Holder angle (degrees)	45			45			45			45		
Excitation wavelength (nm)	350	370	510	350	370	510	350	370	510	350	370	510
Emission wavelength (nm)	470	470	640[a]	470	470	640[a]	470	470	640[a]	470	470	640[a]
LHS Fluorescence (± 10% a.u.)[b]	0.5	2.7	0.6	/[f]	0.09	1.3	0.09	0.3	<0.001	0.2	0.2	0.001
Peak maximum (± 5 nm)[c]	—[e]	—[e]	—[e]	/[f]	—	—[e]	—[e]	—[d]	—[e]	—[e]	—[d]	—[e]
RHS Fluorescence (± 10% a.u.)[b]	0.4	0.6	0.1	0.6	0.6	/[f]	0.1	0.6	0.2	0.1	/[f]	0.03
Peak maximum (± 5 nm)[c]	—[e]	—	—	—[e]	—[e]	/[f]	—[e]	—[e]	—	—[e]	/[f]	—

[a] The emission wavelength for the RHS emission monochromator was 588 nm rather than 640 nm for the LHS emission monochromator.
[b] Fluorescence background measurements obtained at emission wavelength.
[c] Peak maximum was determined for those samples containing an observable peak in the fluorescence background.
[d] Minimal scatter in the background emission spectra due to proximity to the excitation peak.
[e] The scatter observed from the glass substrates into either emission monochromator skewed raw and corrected emission spectra.
[f] Data could not be collected.

PRODAN fluorescence

PRODAN provides information on the internal dipolarity of the solvent entrapped within the sol-gel derived materials, and also shows a characteristic emission band at *ca.* 440 nm, which is related to the formation of PRODAN aggregates when the probe exceeds its solubility limit. Figure 4.2 shows the emission spectra obtained from PRODAN within TEOS derived films over the first hour of aging. Immediately after casting (1 minute) the spectrum shows a single emission band centered at *ca.* 475 nm, indicative of a film containing a significant level of ethanol. However, the spectrum of the entrapped probe rapidly evolves (over 8.5 minutes) such that the major emission band shifts to *ca.* 530 nm, with an additional minor emission band emerging at 440 nm, consistent with the presence of small fraction of PRODAN aggregates. The emission spectrum of the casting solution, both before and after gelation, was centered at 475 nm and showed no emission band at 440 nm. Further more, none of the other films compositions resulted in the appearance of a PRODAN aggregate emission band at any time. These results suggest that (1) the rapid loss of the ethanol from the TEOS-based film immediately upon casting and the resultant decrease in PRODAN solubility, are likely responsible for the significant aggregate emission band and (2) the presence of non-polar additives such as MTES, DMDMS or PEG_{600} results in solubilization of PRODAN.

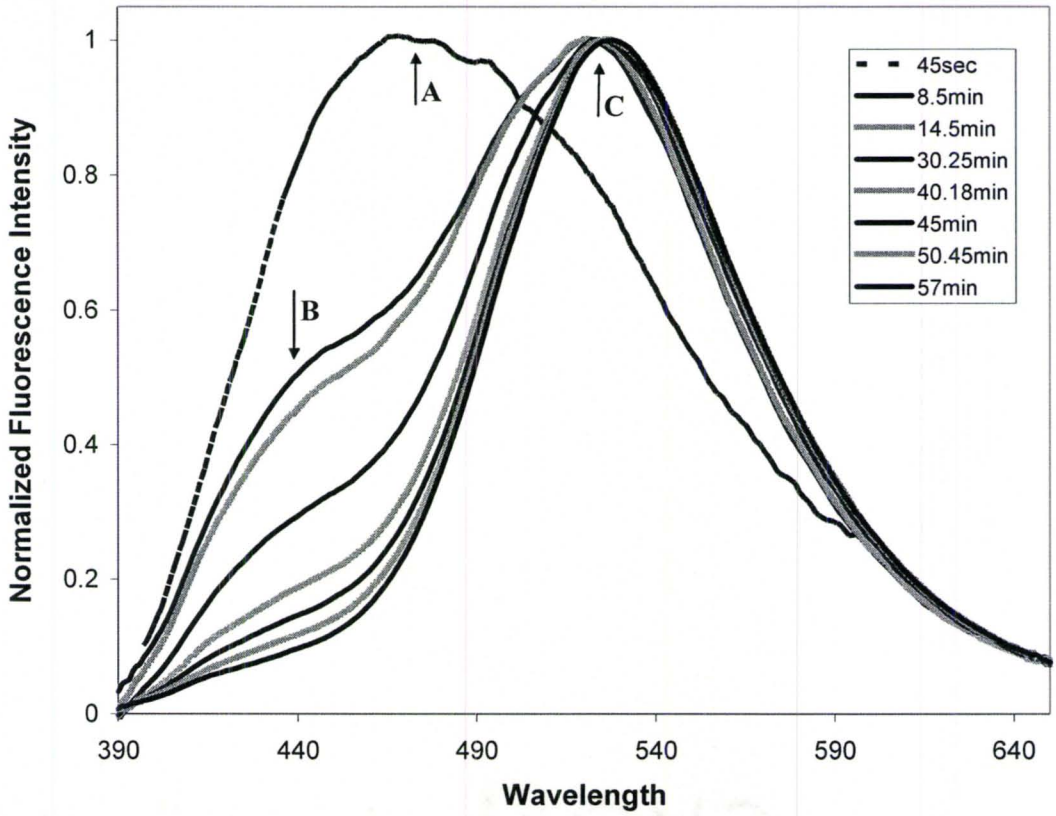

Figure 4.2: Emission spectra of PRODAN obtained from a TEOS film over its first hours of aging. The acquisition times are listed on the figure. Arrow A shows the emission at 475 nm obtained at 45 s after casting the TEOS thin film. Arrow B shows the emission peak at 440nm, indicating the presence of the PRODAN aggregate emission maximum band, which decreases with time. Arrow C shows the emission at 525 nm, which corresponds to the final location of the PRODAN spectrum in pure TEOS thin films.

As aging continued, the emission band intensity at 400 nm decreased significantly, suggesting that the probe slowly associated with the silane surface and dissociated back to the monomeric form. This is in agreement with the observation that the PRODAN aggregate band in bulk TEOS glasses slowly decreases in intensity after many months of aging. These results show that drying and aging of films are accelerated significantly relative to the same processes in the bulk glasses.

Figure 4.3 shows the evolution of the PRODAN emission maxima for each of the six films during the first five hours of aging (upper panel) and as aging continued for up to 80 days (lower panel). All samples began with similar emission maxima of 475-485 nm (reflecting similar environments for the probe), with the exception of TEOS-derived films, which had an initial emission maximum at 510 nm. Over the first 30 minutes, many of the films underwent rapid changes in emission wavelength, consisting of either a red shift in the emission wavelength, owing to the loss of ethanol (TEOS, TEOS/PEG_{600}, MTES/PEG_{600}), a blue shift in the emission maximum, owing to the loss of water from the interior of the film and/or adsorption of the probe onto the silica surface (DMDMS films with or without PEG_{600}), or no significant changes (MTES). Between one and two hours after casting, the polar films begin to show a significant blue shift, likely owing to the loss of entrapped water. The most significant shift occurs in films derived from MTES/PEG_{600}, which may reflect adsorption of the probe from the solvent phase onto methyl groups that are located on the pore wall and/or preferential partitioning of the probe into an MTES-rich phase as the water is lost. The

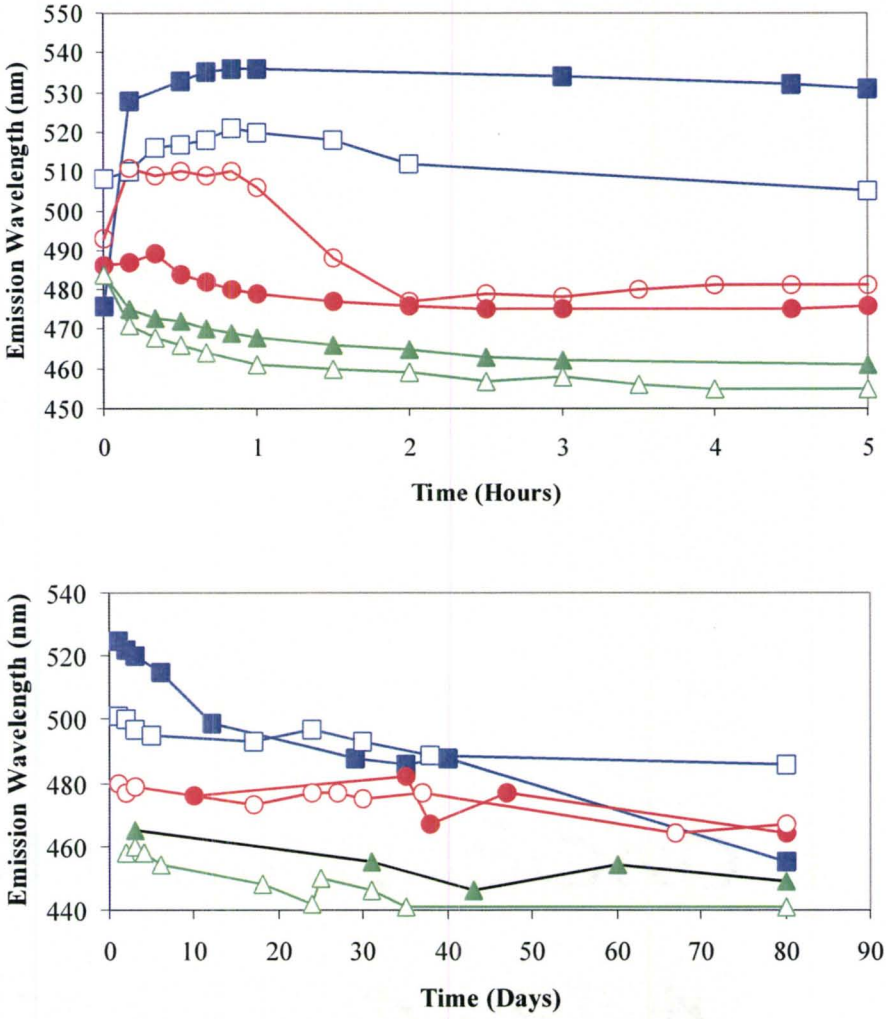

Figure 4.3: Evolution of the PRODAN emission maxima for each of the six thin films from the point of casting onto the slide over the first 5 h (upper panel) and over the remaining 80 days (lower panel). TEOS (■), TEOS + 3% PEG (□), 20% MTES (●), 20% MTES + 3% PEG (○), 10% DMDMS (▲), 10% DMDMS + 3% PEG (△). Typical errors are ± 2 nm.

film polarity begins to stabilize after two hours, and shows only minor shift in polarity over the next three months, signifying a slower change in the film properties that are consistent with the syneresis process.

The emission wavelength values five hours after casting reflect the internal polarity of the various films, with polar films (TEOS) emitting at longer wavelengths and films containing either an organosilane or polymer emitting at shorter wavelengths, consistent with a more hydrophobic environment. It is interesting to note that while MTES- and DMDMS-doped films have a similar number of alkyl groups, the dipolarity of DMDMS films was substantially lower than for MTES, suggesting that the probe may have preferentially associated with DMDMS. In each case, the addition of PEG_{600} led to decreased polarity of the internal environment, with samples containing both an organosilane and PEG_{600} being the most non-polar ($\lambda_{em} \approx 460$ nm). The significant blue shift in the PRODAN emission spectra in the presence of PEG_{600} reflects decreases in hydrogen bonding between the probe and the solvent and/or silica surface. Overall, these results show that it is possible to control the internal environment within the sol-gel derived films over a wide range, and both organosilane and polymer additives can be used for this purpose. This level of control over the internal environment is likely to be useful for optimizing the thin films to produce maximum fluorescence signaling capability or optimal protein stability.

As the films age for a further 80 days, it became clear that the films continue to evolve, as demonstrated by the continual blue shift of up to 60 nm in the emission of spectra for the different films. Such an evolution of the film dipolarity/chemistry has

been noted before by Bright and co-workers, who noted that the accessibility of entrapped pyrene to oxygen decreased over a period of one year. The final emission maximum of PRODAN in aged films ranged from 490 nm (TEOS/PEG_{600}) to *ca.* 440 nm in (10% DMDMS with or without PEG_{600}). These shifts are consistent with slow conversion of silanol groups to siloxanes, which would be expected to lower the overall dipolarity. TEOS films containing PEG_{600} do not undergo as substantial a change in polarity as the other films, suggesting that the PEG_{600} may aid water retention with the polar TEOS films, thus slowing the change in film polarity (note: TEOS/PEG_{600} films eventually evolved to show emission maxima at 460 nm over a period of 10 months). Overall, the fluorescence results suggest that the films age in two distinct stages; an initial rapid drying step, consistent with solvent loss, and a long-term evolution of the films, consistent with slower syneresis and aging of the glass. This is distinct from bulk glasses, where these two processes occur simultaneously.

While the trend of a two-stage aging process for thin films, consisting of a rapid initial change in film composition followed by a slower aging process, has been previously reported in the literature, no previous reports describe the aging of films formed by the two-step process in comparison to either identically formed bulk glasses or films formed with high levels of alcohol. In general, the aging of our films, while faster than comparable bulk glasses by approximately two orders of magnitude (hours versus months), is slower than the aging of alcohol-rich films, which have been reported to undergo aging in as little as 15 seconds. It should also be noted that the high alcohol content that was present in the previously reported thin films is not likely to be amenable

to the entrapment of biomolecules, and thus it is important to understand how biocompatible thin films age so as to optimize the stability of entrapped proteins as described below.

Characterization of entrapped HSA

Figure 4.4(A) shows the background-corrected and normalized fluorescence emission spectra of native HSA in aqueous buffer (curve A), in 1M GdHCl (curve B) and in 4M GdHCl (curve C) as compared to the emission maximum of HSA entrapped in each of the thin films in Figure 4.4(B). The emission spectra of the entrapped HSA sample are all blue shifted relative to the spectrum of native HSA in solution, and are very similar to the spectrum of HSA in 1 M GdHCl. Specific emission maximum values are shown in Table 4.3.

The blue shift suggest that the HSA may adopt a somewhat extended conformation, which results in the sequestering of the Trp residue into a hydrophobic pocket of domain II. However, previous reports show that the expanded form of HSA retains the ability to bind ligands, and thus this conformation does not necessarily reflect a denatured form of the protein. Loss of ligand binding ability generally occurs upon unfolding of domain II, which tends to correspond to a significant red shift in the emission maximum.

As shown in Figure 4.4, films prepared from either DMDMS or DMDMS/PEG_{600} showed significant emission intensity in the region between 380 and 440 nm, indicative

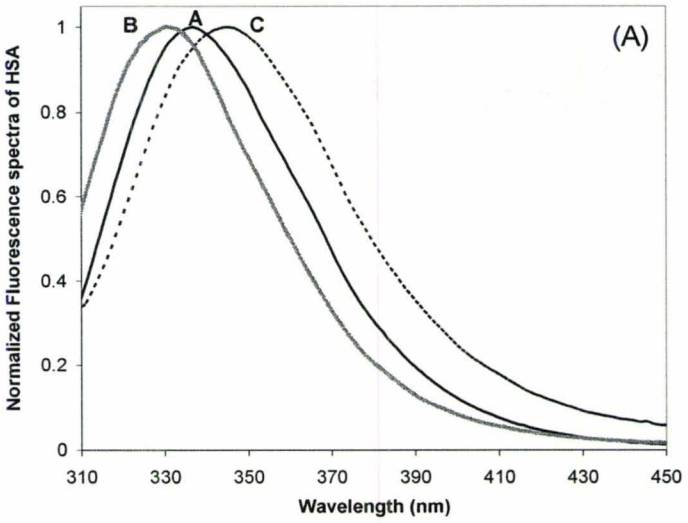

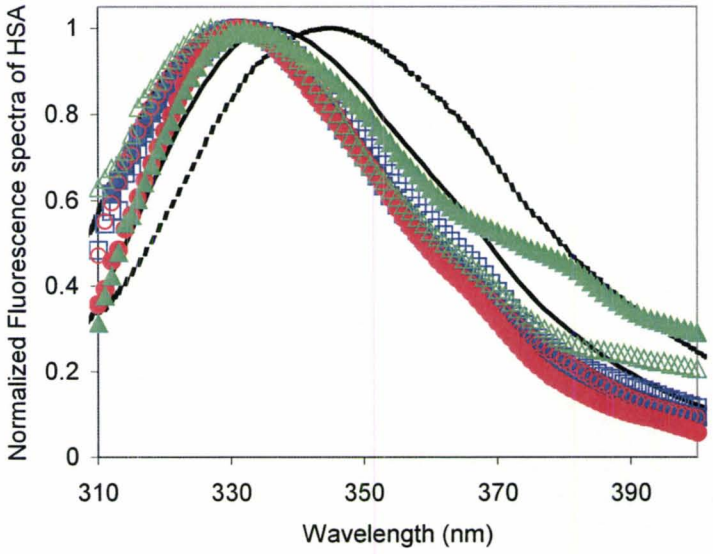

Figure 4.4: Background corrected and normalized fluorescence emission spectra obtained from HSA in solution (———, **A**), in 1 M GdHCl (·····, **B**) and in 4M GdHCl (– – – –, **C**) (panel A) and for HSA entrapped in each of the thin films: TEOS (■), TEOS + 3% PEG (□), 20% MTES (●), 20% MTES + 3% PEG (○), 10% DMDMS (▲), 10% DMDMS + 3% PEG (△) (panel B). Spectra A and C from panel A are also included to provide a basis for comparison of spectra for free and entrapped proteins.

Table 4.3: Specific maximum values related to Figure 4.4.

Environment surrounding the HSA	Emission Maximum (nm)
Native HSA	337
1 M GdHCl	330
4 M GdHCl	345
100% TEOS	331
100% TEOS/PEG	331
20% MTES	331
20% MTES/PEG	331
10% DMDMS	332
10% DMDMS/PEG	327

of a fraction of HSA which is in an aggregated form. Such films also show a somewhat larger blue shift than does HSA in TEOS or MTES-derived films, suggesting that DMDMS may have directly interacted with the Trp residue of HSA. Overall these results show that the inclusion of the MTES or polymer additives is compatible with the entrapment of HSA in a native conformation, while inclusion of the more hydrophobic DMDMS additive appears to cause the entrapped protein to undergo a significant conformational change that exposes the Trp residue to the hydrophobic additive.

To determine if the observed changes in protein conformation were related to denaturation of the entrapped protein, the ability of the entrapped protein to bind to the ligand salicylate was examined. These results were compared to those obtained for native and denatured HSA in solution, as shown in Figure 4.5. A decrease in Trp emission intensity was observed in all films including those derived form DMDMS suggesting that in all cases the entrapped protein bound to salicylate and thus retained at least partial function compared to HSA in solution. This shows that the entrapment method did not irreversibly alter the functional form of the protein. All of the curves are consistent with saturation binding, and all show saturation in the micromolar binding region.

The binding curves reveal several points that merit special attention. First, of all the entrapped protein samples appear to show higher binding to salicylate than is observed in solution. This is not likely to be due to an increase in the binding constant of the entrapped protein. Rather, it is more likely to be due to enhanced partitioning of salicylate from solution into the film *via* a solid-phase microextraction process and/or

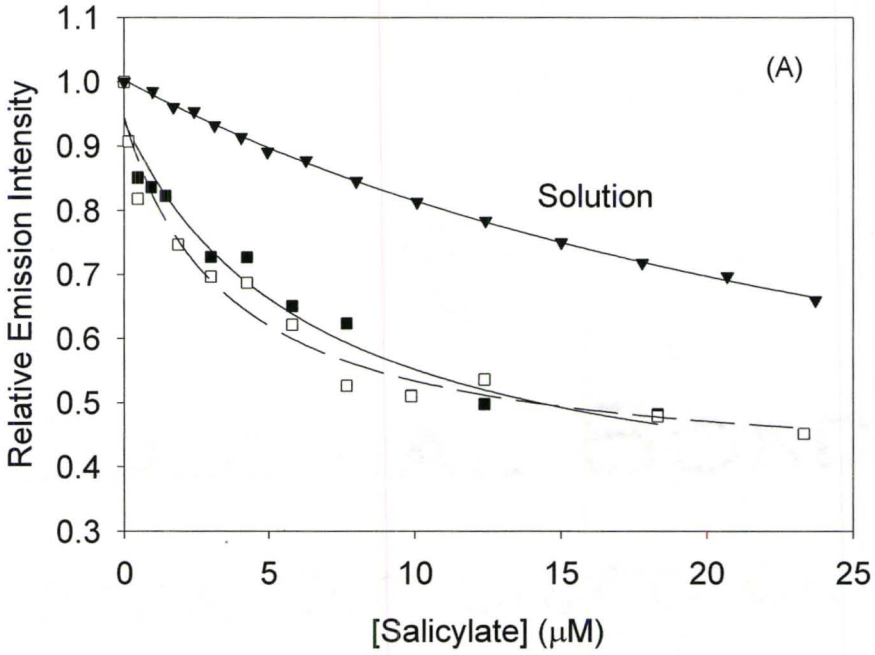
(A)
Solution
Relative Emission Intensity
[Salicylate] (μM)
1.1
1.0
0.9
0.8
0.7
0.6
0.5
0.4
0.3
0
5
10
15
20
25

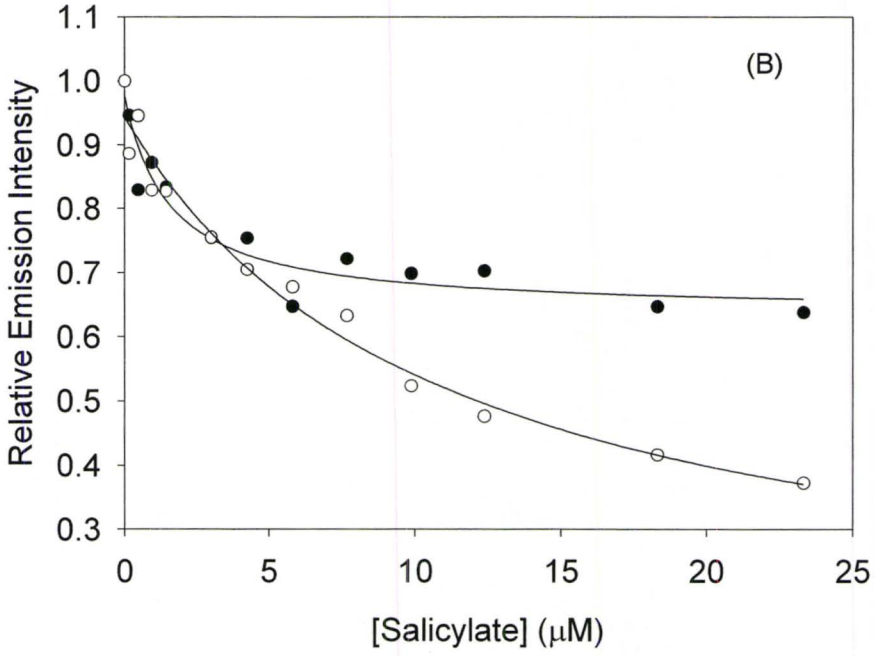
(B)
Relative Emission Intensity
[Salicylate] (μM)
1.1
1.0
0.9
0.8
0.7
0.6
0.5
0.4
0.3
0
5
10
15
20
25

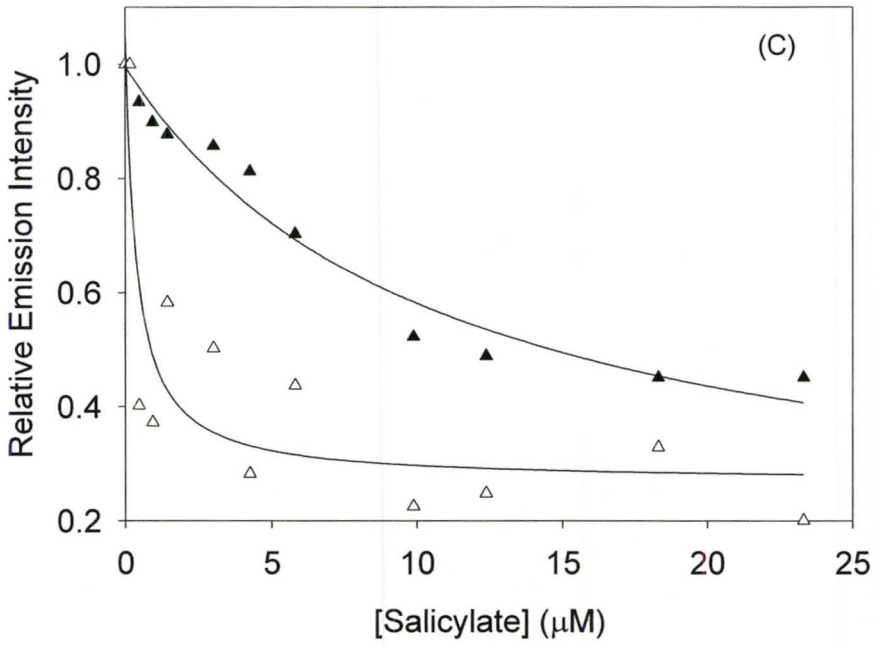

Figure 4.5: Salicylate binding to the human serum albumin in solution and when entrapped into sol-gel derived thin films. Panel (A): solution (▼), TEOS (■), TEOS + 3% PEG (□). Panel (B): 20% MTES (●), 20% MTES + 3% PEG (○). Panel (C): 10% DMDMS (▲), 10% DMDMS + 3% PEG (△). Typical errors for solution, TEOS and MTES derived thin films are ± 0.03, for DMDMS derived thin films the errors are ± 0.10.

subtle differences in the photophysics of tryptophan within each of the films, which may have led to enhanced quenching by salicylate. Second, films containing PEG_{600} appear to show a larger fluorescence response than do films without PEG_{600}; however, this again reflects enhanced quenching of the Trp residue in the presence of PEG_{600}, which was noted to decrease the intensity of Trp fluorescence from HSA in solution. Third, the film derived from DMDMS/PEG_{600} shows an unusually shaped binding curve and extremely high levels of quenching of Trp, which may reveal that HSA is in such films is denatured, thus exposing the Trp residue and leading to direct interactions between the Trp residue and the salicylate.

4.4 Conclusions

Overall the results clearly show that it is possible to prepare high quality films and to entrap functional HSA within such films using the two-step sol-gel processing method involving sonication of precursors followed by addition of a buffered solution containing the protein. This is in agreement with other results obtained from the Brennan research group, which show that such films are capable of maintaining the activity of entrapped lipase for detection of glycerol tributyrate. The PRODAN results offer insight into the rapid drying and slow aging processes that occur within these films. The consecutive nature of the drying and aging processes in thin films is very different from that of monolithic blocks, where these two processes occur simultaneously. The rapid evolution of these films suggests that it should be possible to use the films only hours after

formation. Unfortunately, the slow process observed in these films, which continues over periods of months, may lead to difficulties with long-term drift in the calibration of analytical instruments.

Acknowledgements:

We would like to thank the Natural Sciences and Engineering Research Council of Canada for financial support of this work. We would also like to acknowledge Mike Rakic and Adam Bryant for technical assistance, and Professor Harald Stöver and Professor Adrian Kitai for providing access to optical microscopy and profilometry equipment. JDB holds the Canada Research Chair in Bioanalytical Chemistry at McMaster University.

4.5 References

1. Braun, S.; Rappoport, S.; Zusman, R.; Avnir, D. and M. Ottolenghi. *Mater. Lett.* **10** (1990): 1.

2. Hench, L.L. and J.K. West. *Chem. Rev.* **90** (1990): 33.

3. Brinker, C.J. and G.W. Scherer. *Sol-Gel Science: The Physics and Chemistry of Sol-Gel Processing*, Academic Press, San Diego, 1991.

4. Turniansky, A.; Avnir, D.; Bronshtein, A.; Aharonson, N. And M. Alstein. *J. Sol-Gel Sci. Technol.* **7** (1996): 135.

5. Narang, U.; Prasad, P.N.; Bright, F.V.; Kumur, A.; Kumur, N.D.; Malhotra, B. M.; Kamalasanan, M.N. and S. Chandra. *Chem. Mater.* **6** (1994): 1596.

6. Caruso, R.A. and M. Antonietti. *Chem. Mater.* **13** (2001): 3272.

7. Baker, G.A.; Pandey, S.; Maziarz, E.P., III and F.V. Bright. *J. Sol-Gel Sci. Technol.* **15** (1999): 37.

8. Baker, G.A.; Jordon, J.D. and F.V. Bright. *J. Sol-Gel Sci. Technol.* **11** (1998): 43.

9. Lesot, P.; Chapuis, S.; Bayle, J.P.; Rault, J.; Lafontaine, E.; Campero, A. and P. Judeinstein. *J. Chem. Mater.* **8** (1998): 147.

10. Keeling-Tucker, T.; Rakic, M.; Spong, C. and J.D. Brennan. *Chem. Mater.* **13** (2000): 3965.

11. Reetz, M.T.; Zonta, A. and J. Simplekamp. *Biotechnol. Bioeng.* **49** (1996): 527.

12. Brennan, J.D.; Hartman, J.S.; Illnicki, E.I. and M. Rakic. *Chem. Mater.* **11** (1999): 1853.

13. Wittouck, N.; De Schryver, F. and I. Snijkers-Hendrickx. *J. Sol-Gel Sci. Technol.* **8** (1997); 895.

14. Avnir, D.; Braun, S.; Lev, O. and M. Ottolenghi. *Chem. Mater.* **6** (1994): 1605.

15. Guglielmi, M.; Colombo, P.; Peron, F. and L.M.D. Esposti. *J. Mater. Sci.* **27** (1992): 5052.

16. Nishida, F.; McKiernan, J.M.; Dunn, B.; Zink, J.I.; Brinker, J.C. and A.J. Hurd. *J. Am. Ceram. Soc.* **78** (1995): 1640.

17. Huang, M.H.; Soyez, H.; Dunn, B.S. and J.I. Zink. *Chem. Mater.* **12** (2000): 231.

18. Flora, K.K. and J.D. Brennan. *Analyst* **124** (1999): 1455.

19. Butler, T.M.; MacCraith, B.D. and C. McDonagh. *J. Non-Cryst. Solids* **224** (1995): 249.

20. Rughini, G.C. and S.J. Pelli. *J. Sol-Gel Sci. Technol.* **8** (1997): 1991.

21. Dunawila, D.D.; Torgerson, B.A.; Chang, C.K. and K.A. Berglund. *Anal. Chem.* **66** (1994): 2739.

22. Narang, U.; Prasad, P.N.; Bright, F.V.; Ramanathan, K.; Kumar, N.D.; Malhotra, B.D.; Kamalasanan, M.N. and S. Chandra. *Anal. Chem.* **66** (1994): 3139.

23. Dave, B.C.; Soyez, H.; Miller, J.M. Dunn, B.; Valentine, J.S. and J.I. Zink. *Chem. Mater.* **7** (1995): 1431.

24. Dave, B.C.; Miller, J.M.; Dunn, B.; Valentine, J.S. and J.I. Zink. *J. Sol-Gel Sci. Technol.* **8** (1997): 629.

25. Jordan, J.D.; Dunbar, R.A. and F.V. Bright. *Anal. Chim. Acta* **332** (1996): 83.

26. Rogers, K.R. and E.J. Poziomek. *Chemosphere* **33** (1996): 1151.

27. Chang, A.-C.; Gillespie, J.B. and M.B. Tabacco. *Anal. Chem.* **73** (2001): 467.

28. Dunbar, R.A.; Jordan, J.D. and F.V. Bright. *Anal. Chem.* **68** (1996): 604.

29. Uchida, N.; Ishiyama, N.; Kato, Z. and K.J. Uematsu. *J Mater. Sci.* **29** (1994): 5188.

30. Panusa, A.; Flamini, A. and N. Poli. *Chem. Mater.* **8** (1996): 1202.

31. Wang, R.; Narang, U.; Prasad, P.N. and F.V. Bright. *Anal. Chem.* **65** (1993): 2671.

32. Lundgren, J.S. and F.V. Bright. *Anal. Chem.* **68** (1996): 3377.

33. Weber, D. and F.J. Farris. *Biochemistry* **18** (1979): 3075.

34. Flora, K.K. and J.D. Brennan. *J. Phys. Chem. B.* **105** (2001): 12003.

35. Zheng, L.; Reid, W.R. and J. D. Brennan. *Anal. Chem.* **69** (1997): 3940.

36. Picó, G. A. *Int. J. Biol. Macromol.* **20** (1997): 63.

37. Matijevic, E. *Acc. Chem. Res.* **14** (1981): 22.

Chapter 5: Reagentless pH-Based Biosensing using a Fluorescently-Labelled Dextran Co-entrapped with a Hydrolytic Enzyme in Sol-Gel Derived Nanocomposite Films

The following chapter has been accepted in the scientific journal *Analytica Chimica Acta* under the following citation:

Gulcev, Makedonka D.; Goring, Gillian L. G.; Rakic, Michael and John D. Brennan "Reagentless pH-Based Biosensing using a Fluorescently-Labelled Dextran Co-entrapped with a Hydrolytic Enzyme in Sol-Gel Derived Nanocomposite Films" *Analytica Chimica Acta* **457(1)** (2002): 47-59.

This manuscript was a combined effort between Mike Rakic, Makedonka Gulcev and Gillian Goring. The components dealing with urease assays were performed by Makedonka Gulcev with some assistance from Anna Zavodni. Mike Rakic had done some early exploration work on this concept in his thesis, where proof of concept was the ability to entrap lipase within a sol-gel thin film and see the presence of hydrolysis of glycerol tributyerate. The figure (Figure 5.5) showing the time trace of entrapped lipase with a high concentration of GTB was part of his proof of concept from his thesis. Gillian Goring performed the titration curves for the two fluorophores, SNARF-1 (free and bound to dextran ligand) and fluorescein (free and bound to dextran ligand). The initial draft of the thesis was prepared by Gillian Goring and Makedonka Gulcev with input from Dr. John D. Brennan and was submitted to *Analytica Chimica Acta* for publication.

5.0 Abstract

We report on the development of reagentless fluorescence-based sensing films utilizing hydrolytic enzymes co-entrapped with polymers that are labelled with pH sensitive fluorophores. Aqueous solutions of a hydrophilic enzyme (urease) or a lipophilic enzyme (lipase) containing fluorescein or carboxy-seminaphtharhodafluor-1 (SNARF-1), either free or conjugated to a dextran polymer backbone, were mixed with hydrolyzed alkoxysilane solutions and cast onto planar surfaces to form thin, biologically active sol-gel derived films (*ca.* 500 nm thick). The films also contained various additives, such as methyltriethoxysilane, dimethyldimethoxysilane, polyethylene glycol or polyvinyl alcohol, to optimize the activity of the entrapped enzymes. The photostability, leaching, pK_a and pH response of the entrapped probes were characterized, as was the performance of the entrapped enzymes, and an optimal set of processing conditions was obtained for each different sensing film. In general, the results indicated that SNARF-labelled dextran was the most useful pH sensitive dye owing to insensitivity to leaching and photobleaching. Furthermore, it was observed that the pK_a and pH response of this probe was insensitive to preparation conditions. The performance of the co-entrapped enzymes was highly dependent on the type and level of additive, but in all cases it was possible to obtain active enzymes with good performance characteristics. Reagentless sensing films for urea and glyceryl tributyrate are demonstrated based on the detection of enzyme-mediated pH changes from films coated onto planar substrates.

5.1 Introduction

In the past few years, several reports have appeared describing biosensors based on biorecognition elements that were entrapped into sol-gel processed glasses derived from tetraethylorthosilicate (TEOS) or tetramethylorthosilicate (TMOS)[1,2,3,4,5,6,7,8,9,10,11,12,13,14,15,16,17,18]. The encapsulation protocol generally involved hydrolysis of the alkoxysilane precursors using acidic or basic catalysts, followed by the addition of a buffer solution containing the protein of interest to promote gelation. In most cases, low temperature aging over a period of several days or weeks resulted in a durable, optically clear material that was suitable for optical sensor development [19]

The development of fluorescence-based biosensors generally relies on the ability to place both a biorecognition element and a fluorescent reporter group in close proximity to an inorganic transducer. A key advantage of sol-gel derived matrixes is the ability to entrap multiple species within a confined space. Recently, several reports have described the successful entrapment of multi-enzyme systems within a single sol-gel derived matrix. Examples include the co-immobilization of glucose oxidase and horseradish peroxidase for glucose sensing,[20] the entrapment of a three-enzyme system[21] for catalysis of reactions to form CO_2 from methanol, and the entrapment of a six enzyme mixture produce a multi-step biosynthesis of α(2,6)sialyl- *N*-acetyllactosamine from *N*-acetyllactosamine and *N*-acetylmannosamine.[22] In each of these cases, the ability to co-immobilize multiple species with good control over the spatial distribution of the various dopants resulted in an increase in the rate of product formation, and thus better overall performance.

A second advantage of sol-gel processed materials is the ability to tune the material properties so as to optimize the performance of the entrapped biomolecules.[23,24,25,26,27] Examples include the entrapment of atrazine chlorohydrolase into methyltrimethoxysilane-based materials,[28] immobilization of lipase into polymer-doped materials formed from organically modified silanes,[29,30,31,32] entrapment of lipase and human serum albumin in organically modified silicates (ORMOSILS),[33] co-immobilization of glucose oxidase and horseradish peroxidase in the presence of a graft copolymer of polyvinylimidazole and polyvinylpyridine[34,35] and the entrapment of acetylcholinesterase and butyrylcholinesterase in the presence of polyethylene glycol.[36] In each case, the addition of organosilane precursors or polymers resulted in improved function for the entrapped protein as compared to that obtained in unmodified glasses, with typical activity enhancements being on the order of 4-20 fold.[23,24,25,26,27,28,29,30,31,32]

In this study, we have employed sol-gel-processing methods to develop biosensors based on the co-entrapment of hydrolytic enzymes and pH sensitive fluorescent probes into submicron thick silica films. Acidic or basic products that are generated by the enzymes are detected *via* changes in the emission of the pH sensitive dye, resulting in a sensing film that requires the addition of no extra reagents (aside from the analyte) to generate a signal. Both a hydrophilic enzyme (urease) and a lipophilic enzyme (lipase) were examined to allow us to investigate the effects of organosilane precursors and polymer additives on enzyme performance, and to see if optimal compositions could be obtained for each type of enzyme. The reactions catalyzed by these enzymes, and the resultant products, are shown in Scheme 5.1. The detection of pH

shifts resulting from product formation was accomplished using the pH sensitive fluorescent probes fluorescein and seminaphtharhodafluor-1 (SNARF-1). These probes were used in the free form, or were bound to a high molecular weight dextran backbone to determine if this modification could prevent leaching.[37] Fluorescein and SNARF-1 report pH in different ways: the former producing a pH dependent intensity change,[38] and the latter producing a change in the ratio of intensities at two emission wavelengths as a function of pH.[39] Overall, our results show that the film composition has significant effects on both the pH sensitive dyes and the entrapped proteins. However, careful choice of organosilane precursors, polymer additives, and the pH sensitive dye allow one to optimize both the activity of the entrapped enzymes and the overall sensitivity of the sensing films.

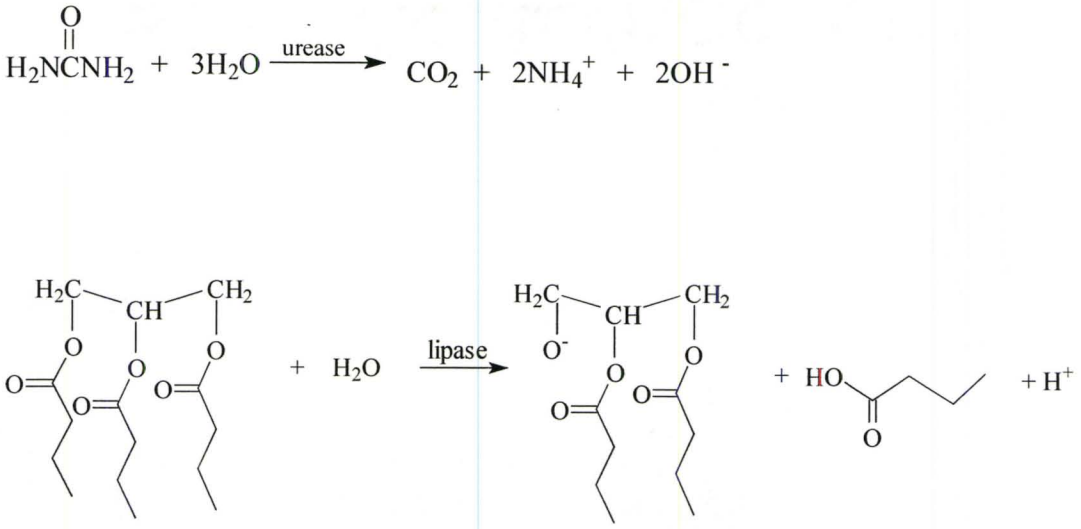

Scheme 5.1: The reactions catalyzed by urease and lipase.

5.2 Experimental

Chemicals

Tetraethylorthosilicate (TEOS, 98%), methyltriethoxysilane (MTES, 98%), dimethyldimethoxysilane (DMDMS, 98%), polyvinyl alcohol (PVA, MW 9000-13,000, 87% hydrolyzed) and polyethylene glycol (PEG 400 or 600) were purchased from Aldrich (Oakville, ON) and were used without further purification. Urease (E.C. 3.5.1.5, type IX from Jack Beans, 50,000 units.g^{-1} solid), lipase (E.C. 3.1.1.3, from *Candida rugosa*, 300,000 units.mg^{-1} protein), urea and glyceryl tributyrate (GTB) were from Sigma (Oakville, ON). 5-(and-6)-carboxy seminaphtharhodafluor-1 (SNARF-1), SNARF-dextran (SD, MW 70,000), fluorescein and fluorescein-dextran (FD, MW 70,000) were obtained from Molecular Probes (Eugene, Oregon). Glass microscope slides (cut to dimensions of 7 mm x 25 mm) were obtained from Fisher Scientific (Toronto, ON). All water was purified by reverse osmosis and deionized using a 4-stage Milli-Q water purification system. All other chemicals and solvents used were of analytical grade and were used without further purification.

Procedures

Preparation of sol-gel derived films: Solutions containing 20% (mol:mol) MTES or 10% (mol:mol) DMDMS in TEOS were hydrolyzed using a H_2O:Si molar ratio of 4:1 under acid-catalyzed conditions, as described elsewhere.[33] A volume of 0.1 mL of the hydrolyzed silane solution was added to an equivalent volume of a buffer solution (10 mM Tris, 100 mM KCl, pH 7.0) that contained 10 – 50 μM of the appropriate

fluorophore or fluorophore-dextran conjugate, and *ca.* 2.0 $mg.mL^{-1}$ of the appropriate enzyme, if present. In some cases, the buffer solution also contained 3% (w/v) of PEG 400, PEG 600 or PVA. The contents were mixed for one minute (using a vortex mixer) and 70 μL of the solution was transferred onto a glass slide that was previously cleaned by soaking in 1.0 M KOH for 24 hours, followed by rinsing with copious amount of distilled, deionized water drying under a stream of N_2. The slide was spun at 2000 rpm for 1 minute to produce a thin film. The films were then aged in air at 4 °C for at least 12 hours before testing. The thickness of the films was determined using an alpha-step 500 surface profilometer. All samples were prepared and tested in triplicate.

Fluorescence spectroscopy: Silane coated glass slides were mounted in a teflon holder in a 1 cm^2 polymethacrylate cuvette at an angle of 45° with respect to the excitation beam, such that the excitation radiation was reflected away from the emission PMT.[18] The coated slides were present in a Tris buffer solution maintained at a temperature of 20 ± 0.2°C, using an SLM 8100 spectrofluorimeter described elsewhere.[18] Samples containing SNARF were excited at 510 nm with emission collected from 550 nm to 800 nm, while fluorescein-doped samples were excited at 460 nm with emission collected from 480 nm to 650 nm. All spectra were collected in 1 nm increments at a rate of 3 $nm.sec^{-1}$ and were corrected for wavelength-dependent anomalies in the emission monochromator throughput and PMT response.

Leaching and photobleaching studies: Fluorophore-doped films were incubated in cuvettes containing 2.0 mL of a buffer solution for 12 hours. The emission spectra of these solutions were then collected to examine probe leaching. Photobleaching studies were done using samples that showed no leaching, to eliminate contributions to intensity decreases resulting from loss of the probe. The samples were continuously irradiated at their maximum excitation wavelength and the fluorescence intensity at the emission wavelength maximum was monitored for 15 minutes. The total loss of intensity after 15 minutes of irradiation is reported.

pH response studies: The pH response of the free and entrapped fluorophores was tested by placing the sample into solutions containing 0.1 M Tris buffer adjusted to pH values ranging from 4.0 to 10.5. Fluorophore-doped films were equilibrated for 10 minutes before a scan was collected (note: longer equilibration times did not alter the results). For fluorescein-doped samples, the integrated intensity was plotted against pH, while for SNARF, the ratio of emission maxima at 588 nm and 620 nm, obtained by integrating a 20 nm window centered on each peak, was plotted against pH. Alternatively, the emission intensity was collected at 520 nm (fluorescein) or simultaneously at 588 nm and 620 nm (T-format detection for SNARF) as a function of time for response time studies.

Reagentless sensing: Silane-coated slides containing SNARF-dextran and the appropriate enzyme were suspended from the top of a cuvette containing 1.5 mL of buffer. The sample was excited at 510 nm and emission was detected by obtaining a full

emission spectrum, or by simultaneously monitoring the emission intensity at 588 nm and 620 nm using T-format detection. Once a constant signal was obtained, the appropriate substrate solution was added to the cuvette to obtain a final substrate concentration of 50 – 300 mM for urea, or 60 – 400 mM for glyceryl tributyrate. The emission ratio was measured as a function of time and the slope of the response curve was plotted against substrate concentration to generate a concentration-response curve.

5.3 Results and Discussion

Optimization of signals from entrapped probes

Three key factors determine the utility of entrapped fluorophores for optical pH sensing. These are the signal-to-noise level for detection of the probe in the thin films, the retention of the probe within the films (which relates to the stability of intensity-based signals), and the photostability of the probe, which can alter intensity-based signals. Entrapment of various levels of fluorescein-dextran (FD) and SNARF-dextran (SD) into thin films revealed that the limits-of-detection for the two probes were 0.1 μM and 1.0 μM, respectively. In order to produce high quality emission spectra, we typically used 10 μM FD and 45 μM SD in all samples. At these levels, the signal-to-noise ratios were 300:1 and 100:1, respectively (using 4 nm bandpasses on both the excitation and emission monochromators). These concentration levels were also selected so that the emission signal was at least a factor of 50 higher than the background, eliminating the need for subtraction of blanks.

Table 5.1 shows the extent of leaching and photobleaching for free and dextran-linked versions of both fluorescein and SNARF. It is clear that the both of the dispersed probes leached extensively from TEOS-derived films, even with polymer doping, with as much as 30% of the entrapped probe leaching from the films after 12 hours. These results suggest that the probes were located in the solvent phase of the film, and thus were free to diffuse throughout the matrix. On the other hand, incorporation of organosilanes markedly reduced the extent of leaching for both of the probes, consistent with the hydrophobic probes associating with the alkyl chains present at the pore surfaces. This result clearly demonstrates that leaching of probes can be controlled relatively well by incorporation of hydrophobic groups into the polar silica glasses, in agreement with previous studies by Collinson et al.[40] and MacCraith and co-workers.[41]

Films that contained dextran-linked fluorophores showed no leaching whatsoever, regardless of the film composition, provided that the films were aged for a minimum of 12 hours before testing to allow the films to fully dry.[42,43,44] These results are in agreement with previous studies by Bright and coworkers,[37] but are contrary to recent results reported by Saavedra et al.[45] The latter results suggested that significant leaching of FD (70,000 MW) occurred from bulk glasses derived from TMOS. However, these glasses were aged for only 48 hrs, and thus would be expected to have a relatively open pore structure.[46] In contrast, our films are almost completely dry after 12 hours of aging,[42,43,44] and thus are likely to have a more highly crosslinked structure that would result in full retention of the probe. Overall, the attachment of the probes to a high

Table 5.1. Properties of entrapped pH-sensitive probes. All values are given after aging the films for 24 hours in a sealed scintillation vial, unless otherwise stated.

Sample	% Leaching after 12 hrs[a] (S/SD/F/FD)	% Photo-bleaching (SD/FD)[b,c]	pK_a (± 0.2) (SD/FD)	Change in Signal (%) (SD/FD)[d]	Analytical Range (ΔpH) (SD/FD)[e]	Response Time (s)[f] (SD/FD)
Solution	-	9/35	7.2/6.0	1.43/94	3.9/5.0	5/5
TEOS	30/0/18/0	6/29	7.5/8.0	0.97/82	4.1/3.4	95/107
20% MTES	1/0/3/0	5/6	7.5/8.3	0.78/70	3.0/3.0	73/140
10% DMDMS	4/0/2/0	3/18	7.8/7.5	0.53/84	3.4/3.5	76/216
TEOS-PEG 600[c]	12/0/16/1	3/14	7.8/5.1	0.87/75	3.8/5.0	84/58
20% MTES-PEG 600	2/0/3/0	7/16	8.1/5.1	0.77/67	2.8/4.0	96/80
10% DMDMS-PEG 600	4/0/3/0	3/9	7.4/6.3	0.39/82	3.2/4.5	30/119
TEOS-PVA[d]	13/0/20/0	5/22	8.2/5.5	0.78/91	3.6/5.0	86/105
20% MTES-PVA	2/0/2/0	5/17	8.1/5.1	0.75/84	3.0/5.0	51/207
10% DMDMS-PVA	3/0/3/0	2/27	8.0/6.1	0.43/75	3.6/5.5	111/84

a) S = SNARF, SD =SNARF-dextran, F = fluorescein, FD = fluorescein dextran, typical relative standard deviation (RSD) for leaching data is ± 10%, b) photobleaching was done only for dextran linked probes to avoid contributions from leaching, c) values refer to photobleaching after 15 minutes irradiation time d) the first number gives the changes in emission ratio for SD, the second gives the total percentage change in intensity for FD for a pH shift from 4.0 to 10.0, e) the limit of detection for the upper and lower pH values was determined using a S/N ratio of 3, and the number reported is the difference in these values, the RSD for SD samples is ± 0.2, RSD for FD samples is ± 0.5, f) typical errors are on the order of ± 10s.

molecular weight backbone of neutral charge proved to be an effective means to eliminate leaching of the probe from thin films, and thus provided a stable intensity-based signal. Furthermore, this method did not require the incorporation of hydrophobic species (although this was still possible), meaning that a wider range of glass compositions could be employed for sensor development. Thus, fluorescently labelled dextran species were used for all further studies.

The data in Table 5.1 indicates that the photostability of the probes was a more serious problem, with both fluorescein-dextran and SNARF-dextran showing substantial photobleaching over a period of 15 minutes, although the SNARF probe was more photostable than the fluorescein probe (2-7% signal loss for SD, 6-29% signal loss for FD). The incorporation of organosilanes or polymers into the films did not alter the extent of photobleaching, within error. This result suggested that the major cause of photodegradation was likely the inability of the probes to diffuse within the matrix, coupled with the fact that the films were not deoxygenated, potentially leading to photo-oxidation.[18] As shown below, this led to serious problems with sensor reversibility and reproducibility for fluorescein-based sensors. One potential method to overcome this difficulty is to use a pulsed excitation source in conjunction with gated detection. However, such instrumentation was not utilized in the present study since the ability to detect pH changes by monitoring a ratio of intensities for the two emission peaks of SNARF removed any deviations that were related to degradation of the probe.

Analytical behavior of entrapped pH-sensitive fluorescent probes

The use of entrapped optical probes for sensing of pH changes has been examined extensively, and it has been noted that entrapment can in many cases alter the pK_a of the probe,[37,47] the sensitivity of the probe to pH changes[37] and the analytical range for pH sensing.[48] Figure 5.1 shows typical pH response profiles for (A) SNARF-dextran and (B) fluorescein-dextran in solution and in sol-gel derived films prepared from pure TEOS (which typically gave good response characteristics) and from DMDMS containing 3% (v/v) PVA (as an example of a sample with relatively poor response characteristics). As shown in Figure 1A, SNARF showed a decrease in the intensity of the peak at 588 nm (acidic form) and an increase in the intensity of the peak at 640 nm (basic form) as pH increased, resulting in the ratio (I_{588}/I_{640}) decreasing as pH became more basic. Incorporation of the probe into sol-gel derived thin films caused the apparent pK_a (obtained by determining the inflection point in the pH-based titration curves) to increase by up to 1.0 pH unit as compared to the solution pK_a of 7.8. This result suggests that the probe sensed a more acidic environment within the glass. The shift in the pK_a value to more basic pH values may reflect the association of the positively charged probe with the negatively charged silicate surface, leading to protonation of the probe. It should be noted that the pK_a is still fairly close to the physiologically relevant pH value (pH 7.4), making it useful for enzyme-based studies.

The data in Table 5.1 also reveal that entrapment causes the SNARF probe to have lower sensitivity to pH, as judged by the smaller change in the emission ratio over

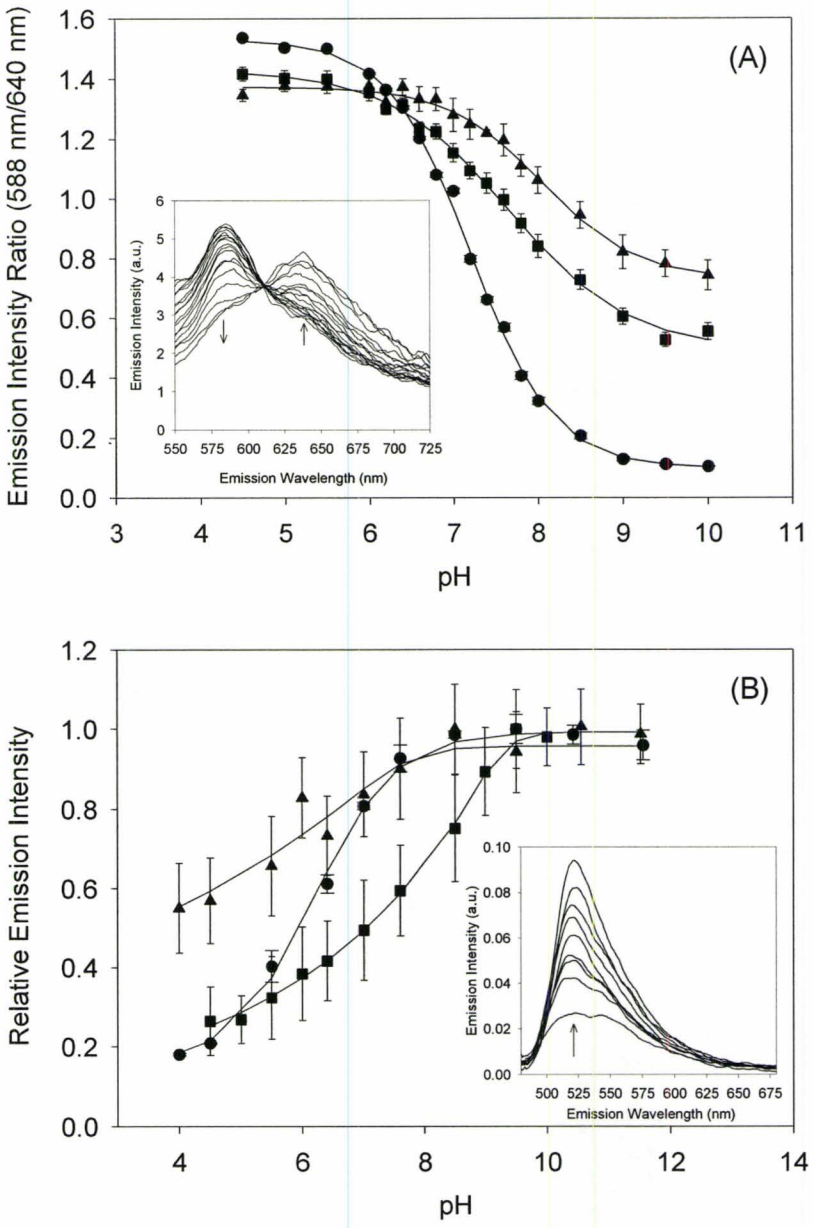

Figure 5.1. Typical pH response profiles for (A) SNARF-dextran and (B) fluorescein-dextran in solution (●) and in sol-gel derived films prepared from pure TEOS (■) and from DMDMS containing 3% (v/v) PVA (▲). The error bars for SD in solution are within the symbols. The lines are intended only as a guide for the eye. The inset figures show the spectra obtained from TEOS derived films, the arrows show the direction of the peak intensity changes on shifting the pH to more basic conditions.

the pH range from 4.5. to 10.0. For example, the probe is 33% less sensitive when entrapped in a TEOS derived glass than in solution, while the probe loses over 75% of its sensitivity to pH shifts when entrapped in DMDMS-PVA glasses. In general, probes within TEOS-derived samples were the most sensitive to pH changes, followed by probes within MTES and then DMDMS. Addition of polymers tended to produce slight decreases in the sensitivity of the entrapped probe to pH, perhaps reflecting polymer-probe interactions that produced photophysical changes in the probes (i.e., alterations in quantum yield of the basic and/or acidic forms). Probes entrapped within TEOS-derived samples also showed the largest analytical ranges, followed by probes entrapped in DMDMS and MTES. Addition of polymer had no statistically significant effect on the analytical ranges for the three types of films. Overall, the data show that the addition of organosilane species alters the pH response behaviour of the probe significantly, while addition of polymers tends to have a smaller overall effect. The results suggest that TEOS-based films are best for pH sensing when using SNARF as the pH-sensitive dopant.

The pH response of fluorescein was more sensitive to film composition than was found for SNARF. The emission intensity increased as pH became more basic, consistent with the conversion from the monoanionic form (Φ = 0.37) to the dianionic form (Φ = 0.93) of the probe [19]. In this case, the pK_a value of the probe ranged from 5.1 to 8.0, depending on film composition (pK_a in solution is 6.0). In general, the probe showed higher pK_a values (more acidic microenvironment) when present in neat TEOS and organosilane films and had a lower pK_a value (more basic environment) upon

entrapment into polymer-doped films. Fluorescein showed very large pK_a shifts when entrapped in either TEOS or MTES, but had a pK_a value similar to that in solution when entrapped in DMDMS. The shifts to lower pK_a values could be problematic, as they cause the sensitivity of the probe to shift to a range that is quite far from the physiologically relevant pH range, where the enzyme assays were performed.

The sensitivity of entrapped fluorescein to pH was similar to that observed in solution, suggesting that the quantum yields of the acidic and basic form of the probe did not shift significantly with film composition. The total signal change, defined as $(F_{max} - F_{min})/ F_{max}$ x 100%, ranged from a low of 67% (MTES-PEG) to a high of 91% (TEOS-PVA), with the probe in solution having the highest sensitivity (94%). However, the analytical range of the probe also tended to shift with film composition, with sensing films derived from polymer-free samples showing smaller ranges (3-3.5) and PVA doped films showing the largest range (5.0-5.5), similar to that observed in solution (5.0).

Perhaps most important for pH sensing was the relative error of the pH measurement. For SNARF, there was typically a variation of at most a few percent in the emission ratio for a given pH value (note the small error bars on the SD titration curves). However, for fluorescein, relative errors of up to 15% were typical in films, likely owing to a superposition of photobleaching and pH driven changes in quantum yield. Hence, the use of changes in peak ratios to monitor shifts in pH appears to produces a more robust signal and thus a more reliable sensing strategy.

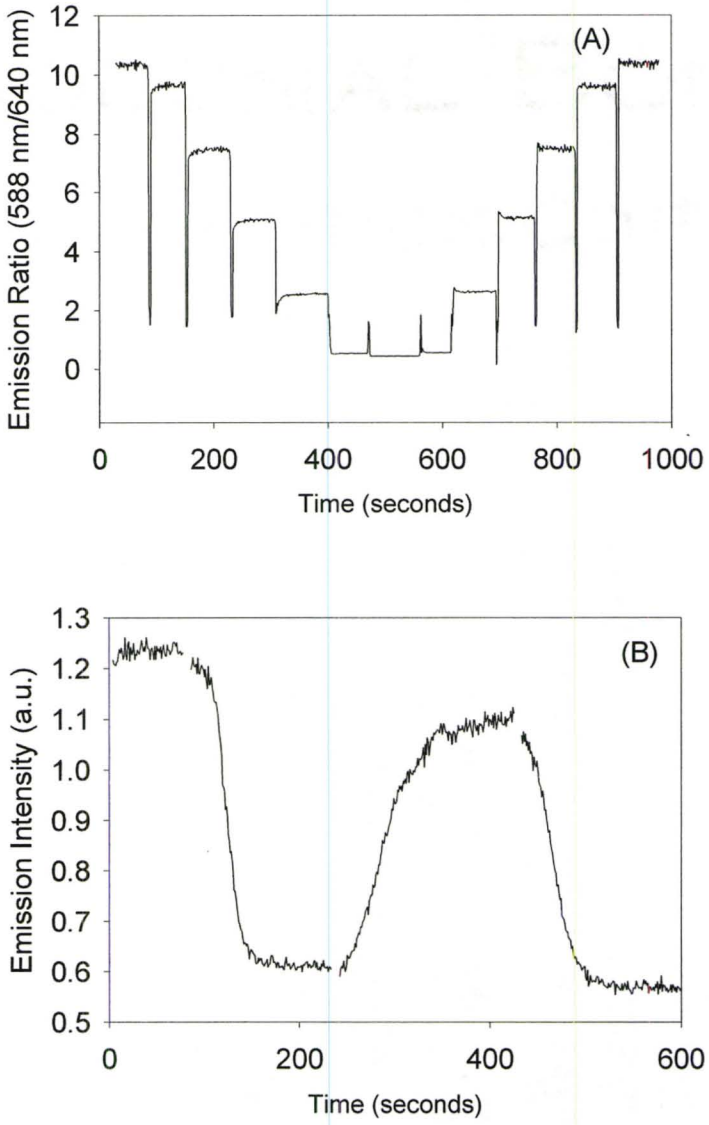

Figure 5.2. pH response as a function of time during addition of acid or base to SNARF-dextran (Panel A) and fluorescein-dextran (Panel B) in TEOS derived films. In Panel (A), the response refers to the successive addition of six 10 μL aliquots of 0.1 M NaOH (0-500 s), resulting in decreases in the emission ratio, or 0.1 M HCl (500-1000 s), resulting in increases in the emission ratio. In Panel (B), the response refers to the addition of one aliquot of 50 μL of 0.1 M HCl, followed by 50 μL of 0.1 M NaOH, and finally 50 μL of 0.1 M HCl. Note: the dips in intensity shown in panel A are due to closing of the shutters in the instrument during addition of reagents, and are not part of the actual response of the probe.

Figure 5.2 shows the pH response obtained upon addition of acid or base to SNARF-dextran (panel A) and fluorescein-dextran (panel B) entrapped in TEOS derived films containing 3% PVA. These films were chosen as they showed reasonable sensitivity to pH changes, and, as shown below, good responses from entrapped enzymes. In general, the response times were quite rapid for all samples (< 2 min, see Table 5.1), as expected given that the films were on the order of 500 nm thick. However, it was noted that the response was fastest in the more polar films (TEOS < MTES < DMDMS), and that the addition of PEG improved response times while PVA had no effect on response times relative to undoped films.

The ratio of emission intensities for entrapped SNARF-dextran as a function of pH (Figure 5.2A) shows the ratio of emission intensities for entrapped SNARF-dextran decreased with increasing pH. It must be noted that the gain on the detectors for peaks at 588 nm and 640 nm was adjusted to expand the range of peak ratios from 0 – 10. The pH-dependent responses are consistent with those obtained from solution based studies. The pH response was fully reversible, and was sensitive to small changes in pH while being immune to changes in emission intensity resulting from photodegradation of the probe. The signals obtained from SD were completely reversible, and the films could be cycled through numerous pH shifts with no degradation in performance. The reproducibility in the response with pH is excellent, with the relative standard deviation (RSD) of the response being on the order of 1% or less. The response of entrapped fluorescein to addition of acid and base was much less reproducible. As shown in Figure 4.2B, there was a continual loss in signal intensity as time elapsed, presumably owing to

photodegradation of the probe. This clearly indicated that the pH response from fluorescein-doped films was not reversible, since the baseline intensity continually decreased with exposure of the film to light. This signal loss also caused reproducibility to be compromised, with the some samples having relative differences in signal of up to 15% for sensing of pH between cycles (one cycle consists of a shift from pH 10 to pH 4, and back to pH 10). These results clearly indicated that fluorescein-based films were not suitable for pH sensing applications, since the signal did not remain stable over time.

Reagentless sensing using enzymes co-entrapped with SNARF-dextran

Effect of film composition on enzyme performance: Given that SNARF-dextran provided a more reliable indication of pH shifts than fluorescein-dextran, SNARF-dextran was used for all enzyme-based sensing studies. Figure 5.3 shows the relative activity of lipase in the presence of saturating levels of glyceryl tributyrate for each of the nine different films compositions, as measured using SNARF-dextran that was entrapped in each of the films. Panel A shows actual measured data, while panel B shows activity data that has been corrected for both film thickness (to account for differences in amount of enzyme present) and for probe sensitivity to shifts in pH to provide insights into how additives alter enzyme performance.

In general, the activity of lipase was somewhat improved when PEG was present, and was significantly improved when PVA was present. The effects of polymer additives and organosilanes on lipase behaviour has been widely studied[29,30,31,32,33] and it has

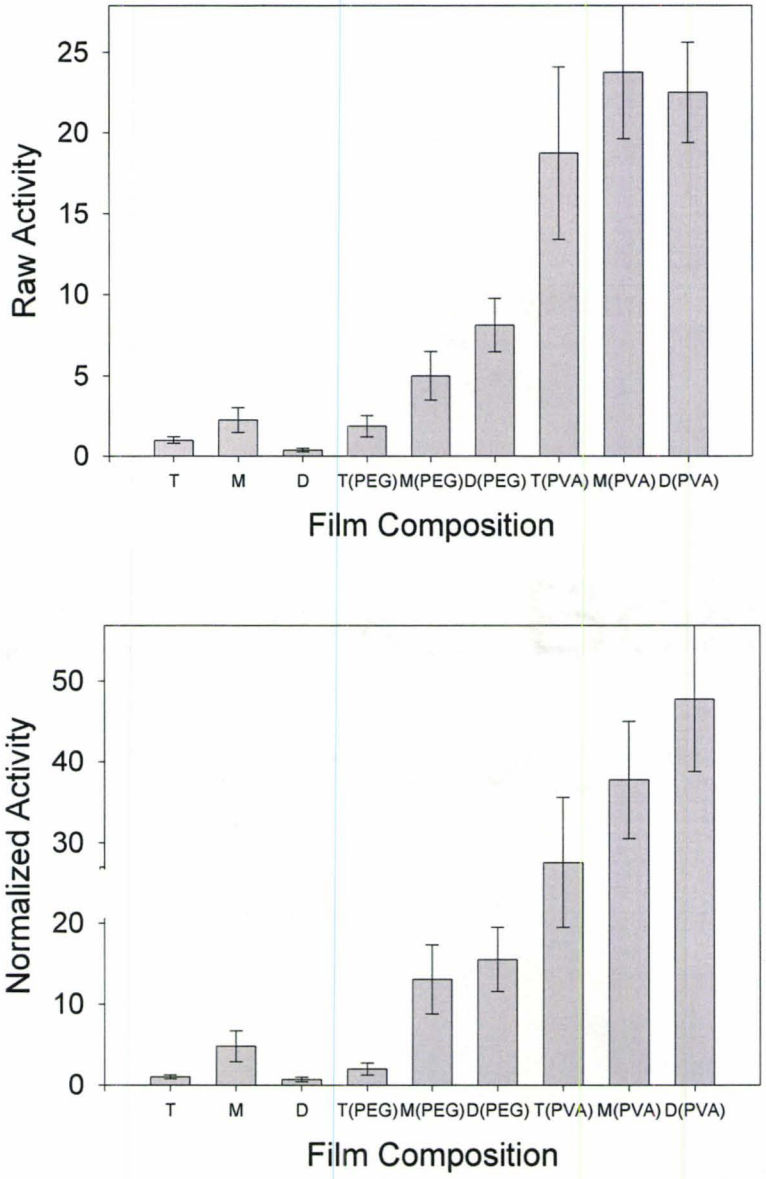

Figure 5.3. Relative activity of entrapped lipase in the presence of saturating levels of glyceryl tributyrate for each of the nine different films compositions, as measured using SNARF-dextran loaded films. Panel A shows the results for the raw data, while panel B shows activity data that has been corrected for both film thickness and probe sensitivity to pH. Film compositions are as follows: T(100% TEOS), M (20% MTES), and D(10% DMDMS), where X(PEG) is X silane with 3% PEG and X(PVA) is X silane with 3% PVA.

previously been noted that both PEG[33] and PVA[29] can lead to significant enhancements in the activity of the protein. Lipase is an interfacially active protein,[49,50,51,52,53] and thus operates most efficiently when entrapped into organic-inorganic nanocomposite materials. As shown in Panel B, significant enhancements are observed in the normalized activity of lipase in composite films such as DMDMS-PVA relative to polar materials such as TEOS (ca. 50-fold), confirming the interfacial activation of lipase. It should be noted that the increased activity of PVA-loaded samples as compared to PEG-loaded samples is in contradiction to previously reported results from our group using lipase entrapped in bulk glasses.[33] The differences likely reflect the very different evolution of films vs. bulk glasses,[54] and suggest that optimal compositions for sol-gel-based bulk materials may not be identical to optimal compositions for films.

The raw data (Panel 5.3A) shows the overall sensitivity of the lipase-sol-gel composite films, and is a combination of pH sensitivity, enzyme activity and film thickness (enzyme amount). In this case, the MTES-PVA sample shows the highest overall sensitivity (although the activity is effectively identical to that obtained in the DMDMS-PVA sample, within error). This result is predominantly based on the much higher sensitivity of SD to pH changes in such films, and the good activity of lipase within MTES-PVA composites. The result suggests that detection of GTB with entrapped lipase-SD mixtures is best accomplished using a composite film composed of MTES doped with PVA, which gives both good pH sensitivity, and good enzyme activity.

Figure 5.4 shows the relative activity of urease in the presence of saturating levels of urea (Panel 5.4A) and the corrected activity data (Panel 5.4B) for each of the nine different films compositions, measured using SD entrapped in the films. In this case, the enzyme showed maximum activity in the more polar TEOS derived films, as might be expected given that the enzyme is water soluble and the analyte is polar. Addition of organosilane precursors lowered the measured activity markedly, regardless of whether there was any polymer additives incorporated into the film. Panel 5.4B shows the direct effect of film composition on enzyme behaviour, after accounting for differences in pH sensitivity and amount of enzyme. These results indicate that the inclusion of MTES does not alter the apparent enzyme activity, rather it is the lower pH sensitivity of SD and the decrease in film thickness that produces the lower overall measured activity in such films. The results also show that PEG has no statistically significant effect on the enzyme behaviour, regardless of which organosilane is used to form the film. On the other hand, both DMDMS and PVA are somewhat deleterious to enzyme function (or they reduce the penetration of urea into the film), which is exactly opposite to the findings for lipase. Overall, the results clearly show that tuning of the film properties is essential for optimizing the sensitivity of the sensing film to the analyte of interest. In general, more polar films are most suitable for polar analytes and soluble proteins, and more hydrophobic films are most suitable for non-polar analytes and lipophilic proteins.

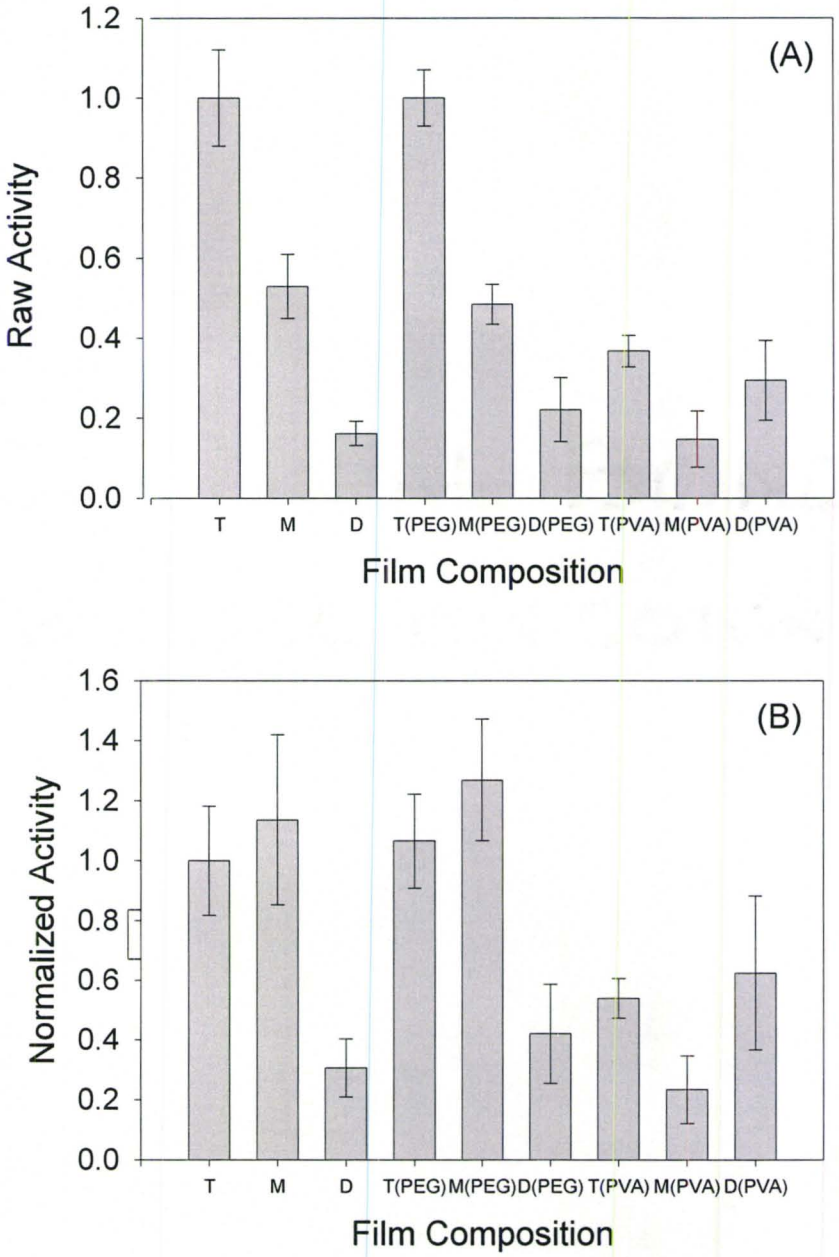

Figure 5.4. Relative activity of the urease as a function of film composition. Panel (A) is the raw data, Panel (B) is the corrected data. Film compositions are as follows: T(100% TEOS), M (20% MTES), and D(10% DMDMS), where X(PEG) is X silane with 3% PEG and X(PVA) is X silane with 3% PVA.

Reagentless sensing using coated slides:

Figure 5.5 shows the time-dependent change in the ratio of emission intensities upon addition of 0.10 M of GTB to MTES-PVA films containing SNARF-dextran that is co-entrapped with lipase. It is clear that the initial baseline is stable and that the response time is relatively fast, showing no lag before the change of slope. The slight jump in emission ratio immediately upon substrate addition reflects differential scattering into the two channels of the T-format detection system. It is clear that the new slope stabilizes rapidly (about 1 min), thus allowing for relatively rapid measurements of GTB. The value of the slope is somewhat lower than is obtained in solution (*ca.* 25% as large, as shown in Figure 5.3), and the response does not reach a plateau even after 1000 minutes. This likely reflects the slow kinetics for diffusion of the hydrophobic substrate within the glass.[18]

Figure 5.6 shows the calibration plot for the response obtained with varying concentrations of glyceryl tributyrate in an MTES-PVA based film. The response curve is linear in concentration of GTB, and provides a sensitivity corresponding to a change of 0.01 in the ratio of emission intensities per 50 mM change in GTB, and a LOD of approximately 20 mM (based on a signal-to-noise ratio of 3). These numbers are somewhat large owing to the buffering effects of both the solution (10 mM Tris) and the glass itself. These numbers likely also reflect the relatively poor partitioning of the emulsified analyte into the glass. Work on optimizing the signal is currently underway using different buffer types and levels, and the effects of partitioning via solid phase

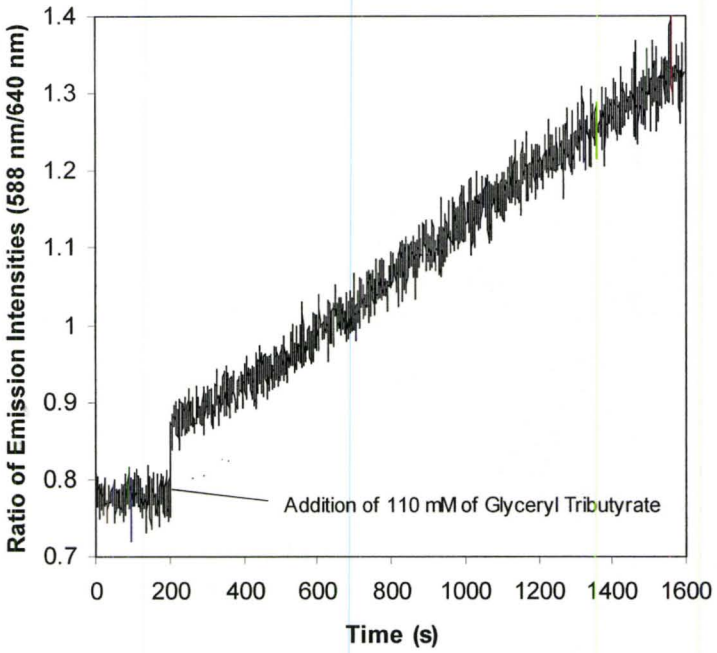

Figure 5.5. Time-dependent change in the ratio of emission of SNARF-dextran co-entrapped with lipase in a MTES-PVA film upon the addition of 110 mM GTB.

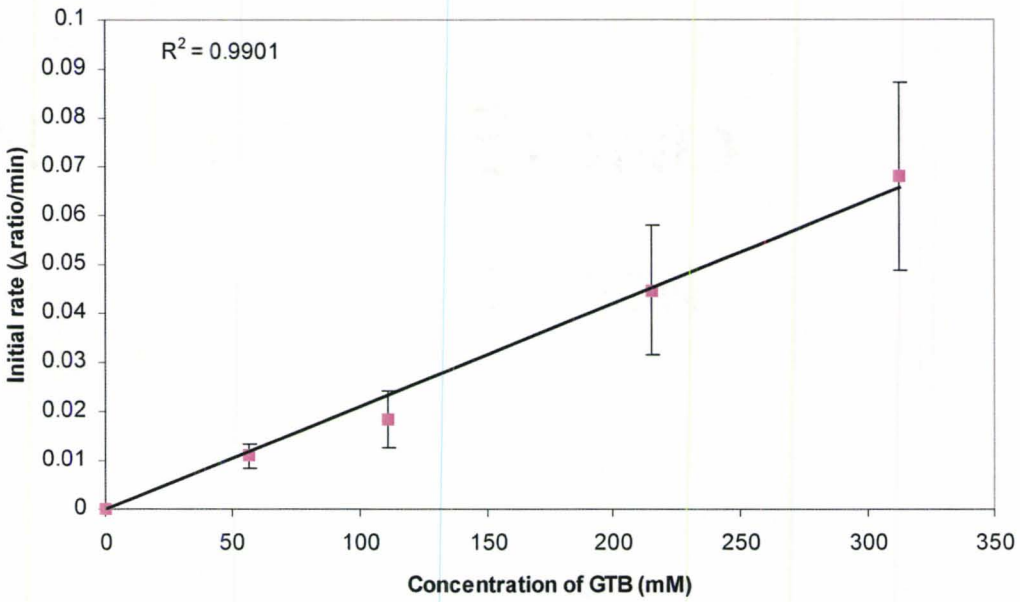

Figure 5.6. Calibration plot for a MTES-PVA based film containing lipase and SNARF-dextran upon addition of varying concentrations of glyceryl tributyrate.

microextraction is being examined by comparing the response from GTB to that obtained using a soluble variant of the analyte. These results will be reported elsewhere.

Figure 5.7 shows the calibration plot for the response of SD entrapped in a urease-doped TEOS-PEG based film as a function of urea concentration. The ratio of basic (640 nm) over acidic (588 nm) peak intensities is reported in this case so that the signal increases with increasing concentration of substrate. In this case, the signal is initially linear (over the range from 0 – ~20 mM urea), and then begins to show a non-linear response beyond ~30 mM urea, likely owing to saturation of the enzyme with the substrate. The changes in emission ratio per unit time were obtained by recording the slope during only the first minute after the addition of substrate, (at which point the slope was stable), providing a relatively rapid response. Based on the calibration plot, a limit-of-detection on the order of 1 mM is obtained for urea, with a dynamic range of ~30 mM. These values are in agreement with those obtained using other electrochemical[55] and optical[56] sensors for urea.

5.4 Conclusions

Reagentless fluorescence-based sensing films that are suitable for the determination of pH, urea or glyceryl tributyrate concentration have been developed based on co-entrapment of a fluorescently-labelled polymer and a hydrolytic enzyme in a sol-gel derived glass. It was determined that linkage of the fluorophore to a high molecular weight polymer backbone completely eliminated leaching, while use of a ratiometric signal from a dual-emission probe eliminated signal variations arising from

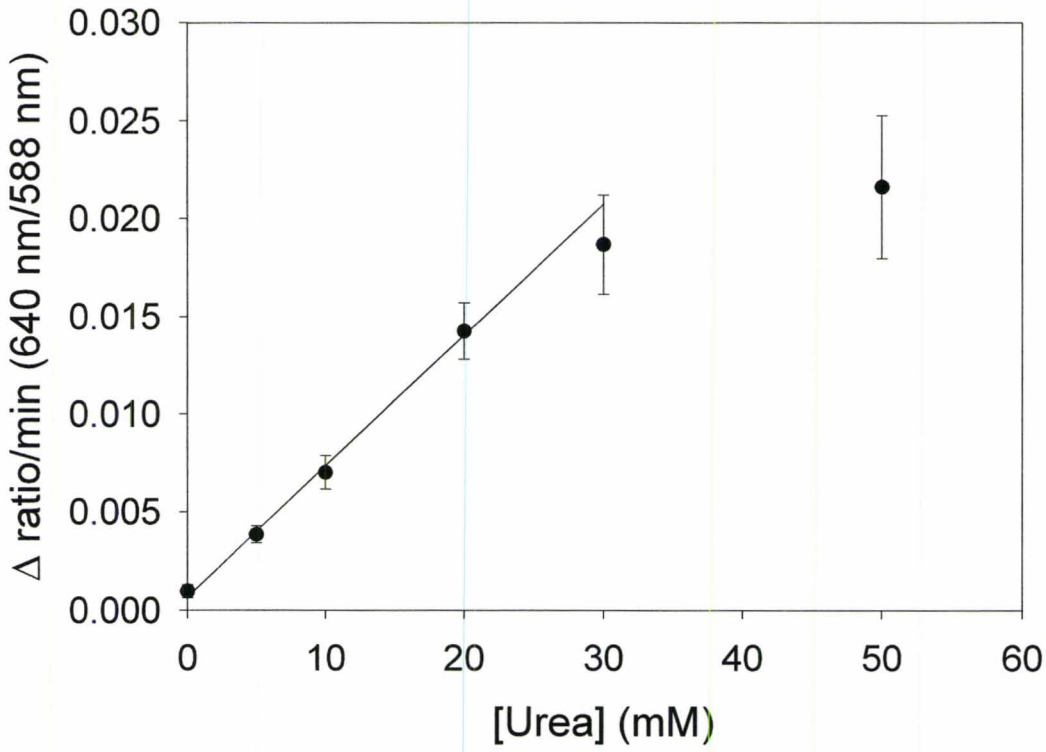

Figure 5.7. Calibration plot for a TEOS-PEG based film containing urease and SNARF-dextran upon addition of varying concentrations of urea.

photodegradation of the probe. Together, these improvements led to a highly stable and reproducible fluorescence signal that, in optimal cases, was capable of measuring a pH change of as little as 0.10 units over the range from 6.5 to 9.5 in under one minute. The sensitivity to pH could be adjusted by varying either silane precursors or polymer additives, although optimal pH sensitivity was obtained from TEOS derived films without polymer present.

The addition of a hydrolytic enzyme (urease or lipase) to the matrix resulted in the production of biologically selective films, which were used for biosensing of urea and glyceryltributyrate based on the detection of acidic or basic products related to the enzyme-substrate reactions. The ability to co-immobilize the pH indicator along with the protein led to rapid response times while avoiding the possibility of altering the protein behaviour as a result of covalent attachment of the probe. An important finding from this work was that the overall performance of the entrapped enzyme could be optimized to a significant degree by addition of both organosilane precursors and polymer dopants. In fact, lipase-doped films prepared from DMDMS with dispersed PVA had a normalized activity that was almost 50-fold higher than was obtained for TEOS based films, and, accounting for differences in pH sensitivity and enzyme loading in the different films (as manifested by different film thicknesses), a measured response that was ~25-fold higher than was obtained from TEOS alone. These results clearly show that substantial tuning of the response can be achieved by carefully adjusting the sol-gel immobilization protocols to suit the particular biomolecule and analyte of interest.

While the new biofilms show promise for reagentless sensing applications, more work is needed to both understand and optimize the signal. Firstly, the enzyme behaviour in the films must be more carefully examined, and factors such as the Michaelis constant and turnover number must be measured to better understand how the various additives altered enzyme performance. Furthermore, the accessibility of the enzyme must be determined (via quenching studies) to determine if the higher sensitivity of PVA-doped films is due to improved enzyme activity or enhanced accessibility. Finally, methods must be developed to account for drifts in pH that are not related to enzyme-substrate reactions, including the use of multi-analyte sensing configurations with one sensor for pH, and the other for analyte. Efforts are continuing in these areas, and will be reported in due course.

Acknowledgements

We wish to thank the Natural Sciences and Engineering Research Council of Canada for financial support of this work. We also thank Ms. Anna Zavodni for technical assistance in acquiring some of the fluorescence spectra.

5.6 References

1. Narang, U.; Jordan, J.D.; Bright, F.V. and P.N. Prasad. *J. Phys. Chem.* **98** (1994): 8101.

2. Lundgren, J.S. and F.V. Bright. *Anal. Chem.* **68** (1996): 3377.

3. Jordan, J.D.; Dunbar, R.A. and F.V. Bright. *Anal. Chem.* **67** (1995): 2436.

4. Wang, R.; Narang, U.; Prasad, P.N. and F.V. Bright. *Anal. Chem.* **65** (1993): 2671.

5. Narang, U.; Prasad, P.N.; Bright, F.V.; Ramanathan, K.; Kumar, N.D.; Malhotra, B.D.; Kamalasanan, M.N. and S. Chandra. *Anal. Chem.* **66** (1994): 3139.

6. Ellerby, L.M.; Nishida, C.R.; Nishida, F.; Yamanaka, S.A.; Dunn, B.; Valentine, J.S. and J.I. Zink. *Science* **225** (1992): 1113.

7. Wu, S.; Ellerby, L.M.; Cohan, J.S.; Dunn, B.; El-Sayed, M.A.; Valentine, J.S. and J.I. Zink. *Chem. Mater.* **5** (1993): 115.

8. Miller, J.M.; Dunn, B.; Valentine, J.S. and J.I. Zink. *J. Non-Cryst. Solids* **202** (1996): 279.

9. Yamanaka, S.A.; Dunn, B.; Valentine, J.S. and J.I. Zink, *J. Am. Chem. Soc.* **117** (1995): 9095.

10. Dave, B.C.; Soyez, H.; Miller, J.M.; Dunn, B.; Valentine, J.S. and J.I. Zink. *Chem. Mater.* 7 (1995): 1431.

11. Yamanaka, S.A.; Nishida, F.; Ellerby, L.M.; Nishida, C.R.; Dunn, B.; Valentine, J. S. and J.I. Zink. *Chem. Mater.* **4** (1992): 495.

12. Dave, B.C.; Dunn, B.; Valentine, J.S. and J.I. Zink. *Anal. Chem.* **66** (1994); 1120A.

13. Braun, S.; Rappoport, S.; Zusman, R.; Avnir, D. and M. Ottolenghi. *Mater. Lett.* **10** (1990); 1.

14. Braun, S.; Shtelzer, S.; Rappoport, S.; Avnir, D. and M. Ottolenghi. *J. Non-Cryst. Solids* **147** (1992): 739.

15. D. Avnir. *Acc. Chem. Res.* **28** (1995): 328.

16. Edmiston, P.L.; Wambolt, C.L.; Smith, M.K. and S.S. Saavedra, *J. Coll. Int. Sci.* **163** (1994): 395.

17. Wambolt, C.L. and S.S. Saavedra. *J. Sol-Gel Sci. Tech.* **7** (1996): 53.

18. Zheng, L.; Reid, W.R. and J.D. Brennan. *Anal. Chem.* **69** (1997): 3940.

19. Avnir, D.; Braun, S.; Lev, O. and M. Ottolenghi. *Chem. Mater.* **6** (1994): 1605.

20. Coche-Guérente, L.; Cosnier, S. and P. Labbé. *Chem. Mater.* **9** (1997): 1348.

21. Obert R. and B.C. Dave. *J. Am. Chem. Soc.* **121** (1999): 12192.

22. Gill I. and A. Ballesteros. *J. Am. Chem. Soc.* **120** (1998): 8587.

23. Chen, Q.; Kenausis, G.L. and A. Heller. *J. Am. Chem. Soc.* **120** (1998): 4582.

24. Heller, J. and A. Heller. *J. Am. Chem. Soc.* **120** (1998): 4586.

25. Baker, G.A.; Jordan, J.A. and F.V. Bright. *J. Sol-Gel Sci. Technol.* **11** (1998): 43.

26. Baker, G.A.; Pandey, G.A.; Maziarz III, E.P. and F.V. Bright. *J. Sol-Gel Sci. Technol.* **15** (1999): 37.

27. Lesot, P.; Chapuis, S.; Bayle, J.P.; Tault, J.; Lafontaine, E.; Campero A. and P. Judeinstein. *J. Mater. Chem.* **8** (1998): 147.

28. Kauffmann C. and R.T. Mandelbaum. *J. Biotechnol.* **62** (1998): 169.

29. Reetz, M.T.; Zonta A. and J. Simpelkamp. *Biotech. Bioeng.* **49** (1996): 527.

30. Reetz, M.T.; Zonta, A.; Simpelkamp, J. and W. Konen. *Chem. Commun.* (1996): 1397.

31. Reetz, M.T.; Zonta, A. and J. Simpelkamp. *Agnew. Chem. Int. Ed. Engl.* **34** (1995): 301.

32. Kuncova, G.; Guglielmi, M.; Dubina, P. and B. Safar. *Collect. Czech. Chem. Commun.* **60** (1995): 1573.

33. Brennan, J.D.; Hartman, J.S.; Ilnicki, E.I. and M. Rakic. *Chem. Mater.* **11** (1999): 1853.

34. Wang, B.; Li, B.; Deng Q. and S. Dong. *Anal. Chem.* **70** (1998): 3170.

35. Wang, B.; Li, B.; Wang, Z.; Xu, G.; Wang Q. and S. Dong. *Anal. Chem.* **71** (1999): 1935.

36. Altstein, M.; Segev, G.; Aharonson, N.; Ben-Aziz, O.; Turniansky A. and D. Avnir. *J. Agric. Food Chem.* **46** (1998): 3318.

37. Baker, G.A.; Watkins, A.N.; Pandey S. and F.V. Bright. *Analyst* **124** (1999): 373.

38. Sjöback, R.; Nygren, J. and M. Kubista. *Spectrochim. Acta A* **51** (1995): L7.

39. Whitaker, J.E.; Haugland, R.P. and F.G. Prendergast. *Anal. Biochem.* **194** (1991): 330.

40. Makote, R. and M.M. Collinson. *Anal. Chim. Acta* **394** (1999): 195.

41. Butler, T.M.; MacCraith, B.D. and C. McDonagh. *J. Non-Cryst Solids* **224** (1998): 249.

42. Huang, M.H.; Dunn, B.S.; Soyez H. and J.I. Zink. *Langmuir* **14** (1998): 7331.

43. Huang, M.H.; Dunn B.S. and J.I. Zink. *J. Am. Chem. Soc.* **122** (2000): 3739.

44. Chia, S.; Urano, J.; Fuyuhiko, T.; Dunn B. and J.I. Zink. *J. Am. Chem. Soc.* **122** (2000): 6488.

45. Skrkla, P.J.; Saavedra, S.S. and N.R. Armstrong. *Appl. Spectrosc.* **53** (1999): 785.

46. Brinker, C.J. and G.W. Scherer. Sol-Gel Science: The Physics and Chemistry of Sol-Gel Processing, Academic Press, San Diego, 1990.

47. Dunn, B. and J.I. Zink. *Chem. Mater.* **9** (1997): 2280.

48. Lam, M.H.W.; Lee, D.Y.K.; Man, K.W. and C.S.W. Lau. *J. Mater. Chem.* **10** (2000): 1825.

49. Turner, N.A.; Needs, E.C.; Khan J.A. and E.N. Vulfson. *Biotechnol. Bioeng.* **72** (2001): 108.

50. Grochulski, P.; Li, Y.; Schrag, J.D.; Bouthillier, F.; Smith, P.; Harrison, D.; Rubin B. and M. Cygler. *J. Biol. Chem.* **268** (1993): 12843.

51. Dodson, G.G.; Lawson, D.M. and F.K. Winkler. *Faraday Disc.* **93** (1992): 95.

52. Shirai K. and R.L. Jackson. *J. Biol. Chem.* **257** (1982): 1253.

53. Chapus, C.; Semeriva, M.; Bovier-Lapierre C. and P. Desnuelle. *Biochemistry* **15** (1976): 4980.

54. Nishida, F.; McKiernan, J.M.; Dunn, B.; Zink, J.I.; Brinker, C.J. and A.J. Hurd. *Am. Ceram. Soc.* **78** (1995): 1640.

55. Ogura, K.; Nakaoka, K.; Kakayama, M.; Kobayashi M. and A. Fujii. *Anal. Chim. Acta* **384** (1999): 219.

56. Xie, X.; Suleiman A.A. and G.G. Guilbault. *Talanta* **38** (1991): 1197.

6.0 Conclusions and Future Work

6.1 Conclusions

The entrapment of biomolecules within organic/inorganic nanocomposite derived materials by the sol-gel method has proven to be a viable route for the development of biosensor and biocatalysts. In this thesis, a series of organic-inorganic nanocomposite materials were prepared by a two-step sol-gel processing method that was suitable for the entrapment of biomolecules and cast as thin films on surfaces. Both non-bonding polymer additives (Class I dopants) and covalently bound organosilane additives (Class II dopants) were investigated as modifiers of the internal chemical environment of films. Furthermore, processing conditions (separate or co-hydrolysis of silanes) was investigated as a means to control the homogeneity of films. Using a series of microscopic imaging methods, it was determined that methylsilanes could be used to prepare largely homogeneous materials, while dimethylsilanes or longer chain butylsilanes generally led to phase separated materials. The addition of Class I additives such as PEG can improve the homogeneity in some materials, likely due to coating of silica sol particles which reduces microscopic phase separation. However, this is not a generic effect. Employment of co-hydrolylsis of silanes, on the other hand, provided more homogeneous materials than were obtained from separate hydrolysis of silane constituents, allowing for a good degree of control over the final homogeneity of films with various additives.

Further analysis of the co-hydrolyzed films was performed to characterize their thickness, homogeneity and changes in the internal polarity during drying and aging.

Using the polarity sensitive dye PRODAN, it was determined that the alcohol hydrolysis byproducts evaporate within the first few minutes after film casting, with further changes in the internal chemical environment occurring over ca. three days. This demonstrated that thin films tended to evolve much more rapidly than bulk glasses. However, these thin films did continue to evolve slightly over a period of at least three months owing to continued condensation reactions within the film. Therefore, even though the film structure is fixed as the film is removed from the casting well, the formation of siloxane bonds continues to occur. This suggests that the properties of entrapped proteins may also change slowly over time, making long-term calibration of sensors difficult.

The immobilization of the well-known model protein, HSA, within the different thin films provided a means to correlate the ligand binding activity of the protein to the polarity of the protein environment. The tryptophan emission spectrum of HSA indicated that the protein adopted a partially denatured "expanded" conformation upon entrapment, which was most prevalent in the highly hydrophobic DMDMS modified films. However, by monitoring the reaction between salicylate and HSA by fluorescence spectroscopy, it was determined that the protein was functional and accessible within all silica materials, and appeared to show higher binding to salicylate than was observed in solution, reflecting enhanced partitioning of salicylate from solution into the film *via* a solid-phase microextraction process.

A series of organically modified films were then used as a platform for biosensor development. Aqueous solutions of a hydrophilic enzyme (urease) or a lipophilic enzyme (lipase) containing fluorescein or carboxy-seminaphtharhodafluor-1 (SNARF-1),

either free or conjugated to a dextran polymer backbone, were mixed with hydrolyzed alkoxysilane solutions containing organosilane additives and cast as thin films. The results indicated that SNARF-labelled dextran was the most useful pH sensitive dye owing to insensitivity to leaching and photobleaching. Furthermore, it was observed that the pK_a and pH response of this probe was insensitive to preparation conditions. The performance of the co-entrapped enzymes was highly dependent on the type and level of additives, but in all cases it was possible to obtain active enzymes with good performance characteristics. Reagentless sensing films for urea and glyceryl tributyrate were demonstrated based on the detection of enzyme-mediated pH changes from films coated onto planar substrates.

Overall, the studies presented in this thesis show that it is possible to prepare organically modified silica films that contain a range of covalently and non-covalently bound additives using a two-step processing method. By utilizing methyl or dimetylsilanes in conjunction with co-hydrolysis of silanes, it is possible to prepare homogeneous materials that are suitable for optical sensor development. Inclusion of such additives allows for the tuning of the internal environment of the film over a wide range, which leads to enhanced ligand binding and catalytic activity for entrapped proteins.

6.2 Future work

The studies presented in this thesis focused on characterization of sol-gel derived thin films and on the function of ligand binding proteins and enzymes within such films. While there are clearly correlations between the film properties and the function of

proteins, there are several other studies which could provide more detailed insights into the nature of the thin films, the behavior of entrapped proteins and their utility for sensor development. For example, more detailed analysis of the nature of the phase separation within thin films could be done using chemically modified tips to perform chemical force microscopy, which may provide a method to observe chemical heterogeneity at the nanoscale in such materials. Further studies are also needed to determine how the different materials affect partitioning of analytes into the films. Further examination of the partitioning of small molecules between solution and the film, and between the surface of the material and the pore solvent, are needed to develop an understanding of why some proteins showed enhanced activity relative to solution. Studies of the accessibility, conformational dynamics and thermodynamic stability of proteins within different Ormosils are also important, as these may provide insights into the processes by which proteins denature upon entrapment. Finally, the development of a true biosensor remains to be done; such a system could utilize a thin protein-doped film on an optical fiber to produce a remote sensing device. Alternatively, these materials could be further assessed as a platform for the development of protein microarrays or bioselective solid phase extraction media.